NASA Contractor Report 4346, Part I

Effects of Engine Emissions From High-Speed Civil Transport Aircraft: A Two-Dimensional Modeling Study, Part I

Malcolm K. W. Ko, Debra K. Weisenstein,
Nein Dak Sze, Jose M. Rodriguez,
and Curtis Heisey

CONTRACT NAS1-18460
MARCH 1991

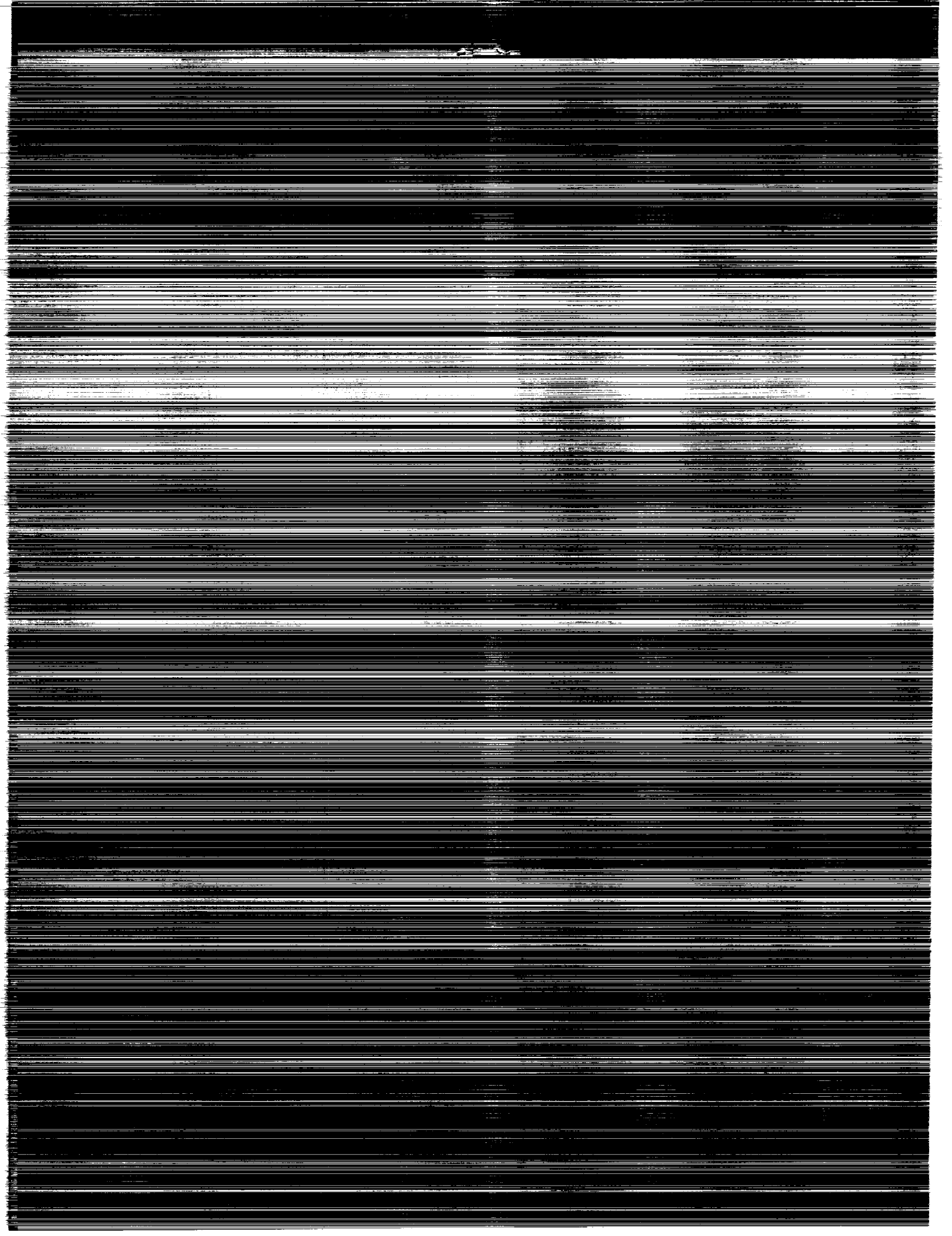

NASA Contractor Report 4346, Part I

Effects of Engine Emissions From High-Speed Civil Transport Aircraft: A Two-Dimensional Modeling Study, Part I

Malcolm K. W. Ko, Debra K. Weisenstein,
Nein Dak Sze, Jose M. Rodriguez,
and Curtis Heisey
Atmospheric and Environmental Research, Inc.
Cambridge, Massachusetts

Prepared by
Atmospheric and Environmental Research, Inc.
under Subcontract 89-6209-D1417
to ST Systems Corporation
for Langley Research Center
under Contract NAS1-18460

National Aeronautics and
Space Administration
Office of Management
Scientific and Technical
Information Division

1991

TABLE OF CONTENTS

EXECUTIVE SUMMARY

The AER two-dimensional chemistry-transport model is used to study the effect on stratospheric ozone (O_3) from operations of supersonic and subsonic aircraft. The study is based on six emission scenarios provided to AER. Our study showed that:

- the O_3 response is dominated by the portion of the emitted nitrogen compounds that is entrained in the stratosphere. The entrainment is a sensitive function of the altitude at which the material is injected.

- the O_3 removal efficiency of the emitted material depends on the concentrations of trace gases in the background atmosphere. Evaluation of the impact of fleet operations in the future atmosphere must take into account the expected changes in trace gas concentrations from other activities.

Areas for model improvements for future studies are also discussed.

I. Introduction

Engine emissions from High Speed Civil Transport (HSCT) aircraft operating in the stratosphere are expected to perturb the chemical composition of the atmosphere. Projected emissions include nitrogen oxides, water vapor, carbon monoxide, carbon dioxide, sulfur dioxide, and unburned hydrocarbons. Changes in the atmospheric concentrations of these compounds will in turn perturb ozone.

The amount of emissions from a high speed aircraft will depend on the engine characteristics and on the speed and altitude of flight. Aircraft engines are characterized by an emission index (EI) specifying the amount of nitrogen oxides emitted per kilogram of fuel. Current engine designs have a range of EI of 5 to 50 grams of NO_2 per kilogram of fuel. Emissions from a fleet of aircraft will also be a function of flight frequency on the most traveled routes. The HSCT emissions used in this modeling study were based on either a cruise speed of Mach 2.4 with a cruise altitude of 60000 ft or a cruise speed of Mach 3.2 and a cruise altitude of 79000 ft.

Projected emissions of nitrogen oxides ($NOX = NO + NO_2$) from fleets of supersonic and subsonic aircraft could become comparable to or larger than the natural atmospheric source of NOX. Stratospheric NOX concentrations within flight corridors could be dominated by the NOX emissions from HSCT aircraft. Since catalytic destruction of ozone by nitrogen oxides accounts for a large fraction of the O_3 loss in the middle to lower stratosphere, the impact on ozone of HSCT aircraft emissions could be significant. At the same time, the partitioning of the nitrogen species depends on the concentrations of other radical species such as OH, which will be affected by water vapor, CO and hydrocarbons emissions.

Apart from local chemistry, the actual impact of emissions also depends on the location of injection and the transport circulation. Since emission products may be transported many thousands of kilometers between regions of varying chemistry, only a multi-dimensional chemistry-transport model can provide an assessment of the impact on ozone. The present modeling study, which was designed around six emission scenarios provided by Boeing and McDonnell-Douglas, used the AER Two-Dimensional Chemistry-Transport model. A

description of the model is given in the appendix. The study represents an attempt to provide a first order assessment of the impact of engine emissions on stratospheric ozone using a currently available model. The purpose is to examine the sensitivity of the O_3 response, identify limitations in the present model formulation and explore ways to improve on the model predictions.

The 2-D model provides information on the steady state seasonal and latitudinal response of O_3 on a global scale. Implicit in the 2-D treatment is the assumption that within the few weeks that it takes for the emitted material to become zonally-mixed, there is no special chemistry that transforms the trace gases in the exhaust plume. The zonal-mean latitudinal and vertical distributions of the emissions from the six scenarios and how they are treated in the model will be discussed in section II. The model calculated response for each of the cases is discussed in section III.

A discussion of some of the uncertainties in the approach is given in section IV, including the results from a number of sensitivity studies. We performed a number of simulations to determine the sensitivity of the model response to the altitude at which the materials are injected. We found that, in the model, material injected below 18 km is rapidly transported to the troposphere and as a result has less impact on stratospheric O_3. In contrast, a much larger percentage of the material injected above 18 km is entrained in the stratosphere. The sensitivity of the results suggest that models with finer vertical resolution and more sophisticated physics may be necessary to examine the problem associated with stratospheric and tropospheric exchange.

Atmospheric perturbations due to HSCT emissions will not occur in isolation, as other natural and anthropogenic causes are also altering atmospheric trace gas concentrations. The increase of CO_2 is well documented. Nitrous oxide (N_2O) and methane (CH_4) are estimated to have been increasing at 0.25% per year and 1% per year, respectively, in the past decade or longer. Past increases in concentrations of the chlorofluorocarbons (CFCs) are well documented and their future trends will depend on future industrial production and the current atmospheric burden. Changes in the concentrations of these gases will also affect the ozone content of the atmosphere. It is well recognized that the net effect on ozone from simultaneous changes in these gases is not additive. It is important to evaluate the effect of HSCT's

within the projected range of trace gas concentrations for the future atmosphere. In our study, we found that the O_3 impact from the engine emissions could change depending on the future state of the atmosphere.

Current efforts to treat temperature and circulation feedbacks in two-dimensional models are still at a research stage. The effects of increasing levels of CO_2 on temperature and circulation in the future atmosphere cannot be assessed with reasonable reliability. We will provide estimates of the CO_2 effects on temperature based on the AER Interactive 2D model currently under development.

Recent studies associated with the Antarctic ozone phenomenon have focused attention on the possible importance of heterogeneous reactions occurring on ice particles in the global stratosphere (Rodriguez et al., 1988). We will discuss the possible effect of heterogeneous reactions on ozone if the water vapor emissions from the aircraft engines were to result in enhanced formation of ice particles.

Finally, in section V, we will discuss a number of improvements that could be made in the approach of future modeling studies.

II. Model Input for Engine Emissions

A. Approach

Exhaust products emitted from the engines of High Speed Civil Transport aircraft will include nitrogen oxide (NO), nitrogen dioxide (NO_2), water vapor (H_2O), carbon dioxide (CO_2), carbon monoxide (CO), sulfur dioxide (SO_2), and unburned hydrocarbons. Once emitted, the photochemically active trace gases will react chemically to adjust to their environment. Nitrogen oxide and nitrogen dioxide are quickly transformed to N_2O_5 and then to HNO_3. Since we are interested in the long term impact of NO and NO_2 after they are zonally mixed, they are input to the model as NOY, or total odd nitrogen. Total odd nitrogen is treated as a long-lived specie and transported within the model. Local chemical conditions determine how NOY is partitioned among NO, NO_2, NO_3, N_2O_5, HNO_3, HO_2NO_2, and $C\ell NO_3$.

Emission of CO is included in the model directly as a local production term. Unburned hydrocarbons are assumed to take the form of methane (CH_4). There are large uncertainties in the kinetic data for long-chain hydrocarbons. Using CH_4 as a proxy is probably adequate to account for the effects of hydrocarbons on CH_2O and on OH. However, reactions from long-chain hydrocarbons can lead to formation of PAN-type molecules which may act as a temporary reservior for the nitrogen species.

Water vapor is treated as a fixed species by the model and is not calculated. We used the given water vapor emissions to increase the background water vapor concentration by running a transport model with a background H_2O of 2 ppmv in the stratosphere and adding the prescribed emissions. With mixing ratios fixed in the troposphere, model transport disperses the emissions, and H_2O comes to a new equilibrium profile. The water vapor in excess of 2 ppm was then added to the baseline water vapor to obtain a new water distribution for each case.

Sulfur dioxide emissions and carbon dioxide emissions were not included in this model assessment. Carbon dioxide is chemically inert in the lower stratosphere. Emissions of CO_2 from aircraft are too small to enhance the local concentration of CO_2. Its long-term effects on the global burden of CO_2 could be assessed in the context of other fossil fuel use. The emission of

CO_2 from all aircraft operations constitutes a few percent of the contribution from total fossil fuel use. There are large uncertainties in our knowledge of the natural sulfur budget in the stratosphere. Aircraft emissions of SO_2 could be as large as 25% of the natural budget. The effect from gas-phase reactions associated with the emitted SO_2 is expected to be small. However, its effect on the global sulfate layer is unknown. Changes in the sulphate layer could result in global climate changes and possible perturbation to the chemical cycles if heterogeneous chemistry occurs on the sulphate particles.

B. Emissions for the Six Scenarios

Six different emission scenarios were examined in the present study. Scenarios B7, B8, and B10 were provided by the Boeing Corporation to represent projected engine emissions from both subsonic and supersonic fleets of aircraft operating in the year 2015. The Boeing scenarios are for supersonic aircraft operating at Mach 2.4 at a maximum altitude of 18 km or 60000 ft. Scenarios A3, A4, and A5 were provided by the McDonnell-Douglas Corporation. These scenarios represent supersonic aircraft only operating at Mach 3.2 up to a maximum altitude of 24 km or 79000 ft. Emissions from the aircraft are sorted into latitude and altitude bins per dimensions of the model grid (approximately 3.5 km in the vertical and 9.5° in latitude) for input into the 2-D model. This is done under the assumption that there is no transformation of the material in the exhaust plume until it becomes zonally well-mixed. The emissions are assumed to be uniform in time and are introduced into the model at a constant rate throughout the year.

Emissions of NOY, CO, CH_4, and H_2O are listed by altitude for Scenarios B7, B8, and B10 in Table 1. Scenario B7 represents emissions at 3 altitudes: 26000 ft, 37000 ft, and 60000 ft. Scenario B8 has emissions at 26000 ft, 37000 ft, and 58500 ft, however, due to model resolution (3.5 km in the vertical), modeled emissions occur at identical altitudes. Scenario B10 represents a variation in flight plans from B7, using airspeeds of Mach 1.5 overland and Mach 2.4 for overwater cruise. B10 has emissions at 4 altitudes (26000 ft, 37000 ft, 46000 ft, and 60000 ft). Emissions at 26000 ft and 60000 ft are the same for Scenarios B7 and B10. Both Scenario B7 and B10 use the Pratt and Whitney low emission engine with EI of 5, while Scenario B8 uses the GE low emission engine with EI of 9. Due to the different engine

characteristics, Scenario B8 has double the NOY emissions, larger CO emissions, and smaller hydrocarbon emissions at 60000 ft than Scenario B7. At 37000 ft, NOY emissions of B7 and B8 are comparable, but CO and and hydrocarbon emissions are much greater for Scenario B8.

Table 2 shows emissions of NOY, CO, CH_4, and H_2O by altitude for Scenarios A3, A4, and A5. All three scenarios are based on the Pratt and Whitney Duct Burning Turbofan engine using TSJF fuel. Scenario A3 used an EI of 39.5 for cruise and an EI of 8.1 for climb. A4 used an EI of 12.1 for cruise and 8.1 for climb. A5 used an EI of 5.2 for cruise and 2.67 for climb. Emissions of CO, CH_4, and H_2O are similar for all three cases, but total NOY emissions vary by a factor of 5. As expected from the emission indices, Scenarios A3 and A4 have similar NOY emissions at all levels but the highest level, where A3 has three times the emissions of A4. Scenario A5 NOY emissions are smaller than A4 at all levels.

Total NOY emissions from the McDonnell-Douglas scenarios are smaller than the Boeing NOY emissions since they do not include the contribution from the subsonic fleet. Emissions at the highest altitude (22 km) account for 91%, 76%, and 81% of the total NOY emissions for Scenarios A3, A4, and A5, respectively. Comparison of the NOY emissions above 18 km shows that there is a factor of 6 spread among the six scenarios. It is interesting to note that the emissions of CO, CH_4 and H_2O above 18 km are uniformly smaller in the McDonell-Douglas cases.

The latitudinal distribution of emissions is shown in Figures 1, 2, and 3 for Scenarios B7, B8, and B10, as interpolated onto the AER model grid in 9.5 degree latitude bands and 3.5 km height bands. Note that the largest emissions occur in the northern hemisphere mid-latitudes where the largest number of flight will take place. There are no emissions south of 50°S at the 60000 ft level, and only minor emissions at lower levels from 50°S to 70°S. In the northern hemisphere, however, emissions extend all the way to the pole. Emissions in the 33°N to 62°N latitude bands account for 60% of the total NOY emissions for the Boeing scenarios.

The latitudinal distribution of emissions from Scenarios A3, A4, and A5 are shown in Figures 4, 5, and 6, respectively. Emissions extend only from 40°S to 60°N, maximizing at 40°N to 50°N. There is a minor secondary peak in emissions in the southern hemisphere low latitudes. The emissions of NOY in

the 33°N to 62°N latitude bands account for 60% of the total NOY emissions of Scenario A3 and approximately 50% of the total NOY emissions of Scenarios A4 and A5.

The histograms of emissions (Figures 1-6) also show the relative amounts of emissions at each level for each latitude band. Emissions are shown in units of molecules per second emitted into a grid box. The change in mixing ratio of a trace gas will be a function of emissions and of the ambient air density, since emissions are distributed through an area of roughly constant volume but varying air density. Therefore, a given quantity of emissions expressed as molecules per second emitted at a given latitude and level will have a larger impact on the trace gas mixing ratio the higher the altitude of injection.

Table 3 compares total emissions from Scenarios B7, B8, B10, A3, A4, and A5 with the natural source strength and global burden of NOY, CO, CH_4, and H_2O. This provides a rough estimate of the expected impact in lieu of a model calculation. Table 3 indicates that the stratospheric NOY budget will be significantly perturbed, as emissions of NOY are comparable to the natural source. CO and CH_4 should be perturbed only slightly. The H_2O emissions represent 8% (for Scenarios A3, A4, and A5) and 40% (for Scenarios B7, B8, and B10) of the natural stratospheric production by oxidation of CH_4.

III. O_3 Response to Engine Emissions

We will assess the combined impact of the emissions of NOY, CH_4, CO, and H_2O on ozone and compare that to the impact of NOY alone. We begin the discussion with a description of the expected effects of each of the emitted gases on the O_3 budget. We then present results of the calculated changes in NOY, CH_4, CO, H_2O, and O_3 based on Scenario B7. Our results showed that the O_3 response is dominated by the NOY emissions, in particular by the amount of NOY that is entrained in the stratosphere. The results for the rest of the scenarios will then be presented, discussing only the calculated changes in NOY and O_3.

A. Effects of Trace Gas Emissions on O_3

The local concentration of ozone in any region of the stratosphere is set by a balance between local photochemical production and loss and transport into and out of the region. Except for near the poles, O_3 is in photochemical equilibrium above 35 km. In the tropical lower stratosphere, the O_3 concentration is a result of the balance between local photochemical production and transport out of the region. On the other hand, O_3 at high latitudes is determined by photochemical removal balancing transport into the region (Ko, et al, 1989). Injection of HSCT exhaust products into the lower stratosphere will enhance the photochemical removal rate of O_3. This will have a larger effect on the O_3 concentration at mid and high latitudes than at tropical latitudes.

Photochemical removal of O_3 in the lower stratosphere is achieved by a number of catalytic cyles mediated by nitrogen, chlorine and hydroxyl radicals. Each catalytic cycle promotes the reaction of atomic oxygen (O) with O_3 or the self-reaction of O_3 to form molecular oxygen (O_2). The nitrogen catalytic cycle is responsible to 50-80% of the net sink for odd oxygen in the middle to lower stratosphere in the present day atmosphere (see, e.g. Wofsy and Logan, 1985; Crutzen and Schmailzl, 1985; Jackman et al., 1986). The hydroxyl cycle dominates the ozone loss mechanisms below about 20 km. The chlorine cycle is a major factor at 40 km.

The nitrogen catalytic cycle occurs via reactions with oxides of nitrogen through the following reactions:

$$NO + O_3 = NO_2 + O_2$$
$$NO_2 + O = NO + O_2$$

net: $$O + O_3 = 2\ O_2$$

Because this is a catalytic cycle, small amounts of NOX can have a significant impact on ozone which exists at concentrations 1000 times greater. The potency of the cycle depends on the amount of total odd nitrogen present and the portion that is found in the form of NO and NO_2. The partitioning of the nitrogen species depends on local concentrations of other radical species such as OH. Thus, the emitted trace gases can perturb O_3 either by increasing the NOY content in the stratosphere or by changing the partitioning of the NOY species.

Removal of O_3 via reactions with OH and HO_2 and the chlorine species are less efficient than the nitrogen catalyzed cycle unless the atmosphere is highly denitrified due to occurrence of heterogeneous reactions. Although the aircraft engines do not emit OH or chlorine species, engine emissions can still affect the hydroxyl and the chlorine catalyzed cycles since there is strong coupling among the various species. The efficiency of the chlorine catalyzed cycle depends on the proportion of odd chlorine found as HCℓ. This is controlled by the local concentration of OH.

The hydroxyl radicals are primarily produced by reaction of $O(^1D)$ with water. However, reactions initiated by oxidation of CH_4 can also produce OH depending on the ambient concentration of the nitrogen species. The reactions with HCℓ, HNO_3 and HNO_4 are the major removal pathway for OH in the lower stratosphere. Thus, the CH_4, H_2O and nitrogen emissions could alter the local concentration of OH.

Finally, oxidation of CH_4 in the presence of nitrogen species can lead to production of O_3 through the smog producing reactions which are expected to be important in the troposphere.

B. Model Results

The natural source of total odd nitrogen (NOY) in the stratosphere is the reaction of N_2O with $O(^1D)$ and has a magnitude of approximately $8x10^{26}$ molecules per second. Removal includes reaction of N with NO in the upper stratosphere and washout of HNO_3 in the troposphere. NOY concentrations in the lower stratosphere are quite sensitive to transport, since both the production rate and the photochemical removal rates are small there.

The change in NOY concentration in ppb produced by the emissions of Scenario B7 is show in Figure 7. Maximum changes in NOY occur at northern mid-latitudes at 13 km and 20 km, where the maximum emissions occur. The model's transport circulation largely determines the impact of emissions at various latitudes and altitudes. Emissions into the tropical region are carried upward and poleward by the winds, dispersing globally. Emissions in the mid- and high-latitudes are carried downward towards the troposphere and concentrated by moving into regions of higher air density. NOY which reaches the troposphere is removed rapidly by washout. Thus there is minimal impact below 8 km.

NOY concentrations increased by 2 to 3 ppb at 13 km and 45°N, where the background concentration was 2 ppb. At 20 km and 45°N, the concentration increased by 2 ppb, where the background concentration was 6 ppb. The NOY emissions for Scenario B7 above 18 km is 25% of the natural stratospheric source of NOY. As most of the natural production occurs at a higher altitude, local NOY concentrations have changed by as much as 150%. The greatest NOY perturbation occurs in the winter and spring, due to the greater strength of the downward circulation at high latitudes in winter.

Since the values given in Table 3 indicate that the CO emissions are about three order of magnitude smaller than the global source, no significant perturbation is expected on the global burden. On the other hand, the emissions are comparable to the local removal rate (OH + CO). Figure 8 shows the change in CO mixing ratio for Scenario B7. The CO concentration has increased by 2 ppb (about 4-5%) in the northern hemisphere lower stratosphere. It has decreased in the upper stratosphere and troposphere due to the enhanced OH concentration produced by emission of water vapor.

Again, no change in global burden is expected in the case of CH_4 since the emission is five order of magnitude smaller than the global source. The

change in CH_4 mixing ratio is shown is Figure 9. CH_4 has decreased everywhere despite the injection of CH_4 in the lower stratosphere. The CH_4 concentration in the mid-latitude lower stratosphere is controlled by a balance between transport and photochemical removal by reaction with OH. The calculated result is a response to the increase in OH produced by emission of water vapor.

Water vapor is not a computed specie in the model, but is held fix for all seasons. The baseline water vapor is based on LIMS observations (Remsberg, et al., 1984) for the stratosphere and on prescribed relative humidity for the troposphere. The increase in water vapor concentration calculated for Scenario B7 is shown in Figure 10. The water vapor increased by 1 ppm in the northern hemisphere at 20 km, about a 20% increase. At high altitudes, it increased by 0.3 ppm, about 6%. This produced an OH change of 2-5% in the middle to upper stratosphere.

The change in local concentration of ozone due to HSCT emissions of NOY, CO, CH_4, and H_2O for Scenario B7 is show in Figure 11. Ozone has decreased by 2-4% at 15 km in the northern hemisphere and by 1% in the middle and upper stratosphere globally. The tropical troposphere shows an ozone increase due to the "self-healing effect", i.e., increased production of ozone due to enhanced uv penetration when the overhead ozone column decreases. The area of ozone increase in the northern hemisphere low altitudes is caused by the very large injection of odd nitrogen in this region, which enhances the production of O_3 in the troposphere by smog reactions.

Figure 12 shows the change in ozone column as a function of latitude and time of year for Scenario B7. Because total ozone column is a measure of the amount of ultraviolet radiation that can reach the earth's surface, it is an indicator of the impact on the biosphere. Ozone depletion due to Scenario B7 ranges from 0.3% at the equator to 2% at the north pole in spring and 1% at the south pole in southern spring. Mid-latitude ozone changes are 0.5% to 0.9% in the southern hemisphere and 1-2% in the northern hemisphere. The change in the total ozone column can be related to the local change at 15 km in mid-latitudes and at 25 km in tropical latitudes. The regions of ozone increase at lower altitudes make only a small contribution to the total column because the ozone mixing ratio there is very small.

In order to compare the ozone impact of NOY emissions alone with the

impact of NOY, CO, CH_4, and H_2O emissions together, we ran the model with only the NOY emissions from Scenario B7. The ozone column change for this case is shown in Figure 13. It can be seen by comparing Figure 13 with Figure 12 that NOY is primarily responsible for the O3 depletion calculated for Scenario B7. The case with NOY alone shows a slightly larger ozone depletion at high northern latitudes, indicating that the addition of CO, CH_4, and H_2O makes ozone slightly less sensitive to the NOY increase.

Having established that the primary response of O_3 is from the NOY emissions, we will limit the discussion of the results from the rest of the scenarios to changes in NOY and O_3. It should be noted, however, that the other emissions are included in all the calculations unless explicitly stated otherwise.

The NOY perturbation due to emissions from Scenario B8 is show in Figure 14. Scenario B8 has twice the NOY emissions of Scenario B7 at the 18-22 km level, and the maximum change of 3 ppb in NOY now occurs at 19 km. The perturbation in NOY has also increased in the tropical middle stratosphere, from 0.5 ppb to 1 ppb. The ozone change for Scenario B8 is show in Figure 15. The local ozone decrease is 3-4% at 15 to 20 km in the northern hemisphere. Ozone in the middle stratosphere has decreased by 2%. Also, the zone of self-healing is reduced in area compared to the results for Scenario B7.

Figure 16 shows the change in column ozone for this case. The ozone percentage decrease is approximately double that for B7. Maximum impact is 4.4% near the north pole in spring and fall. Northern hemisphere mid-latitudes show an ozone decrease of 2-4%, while southern hemisphere mid-latitudes show a 1-1.5% decrease. The model-predicted change in column ozone using emissions of NOY only from Scenario B8 is show in Figure 17. Maximum ozone depletion is 5% near the north pole in fall and 2.5-4% for the northern mid-latitudes. Again we see that addition of CO, CH_4, and H_2O decreases the impact of NOY on ozone.

The change in NOY concentration for Scenario B10 is shown in Figure 18. The impact is quite similar to that of Scenario B7, as the emissions are almost the same. The local ozone change for Scenario B10 is shown in Figure 19. The ozone depletion above 40 km is slightly greater than for Scenario B7, but otherwise the impact is nearly the same. Figure 20 shows the column ozone change for B10. It is nearly identical to the B7 column ozone change.

The NOY difference for Scenario A3 is show in Figure 21. The increase in NOY is 8 ppb at 22 km in the northern hemisphere. Emissions for the McDonnell-Douglas scenarios occur as high as 22-24 km, which allows for a longer stratospheric residence time and more opportunity for global dispersal. The NOY increase is as much as 3 ppb in tropical and southern latitudes. The local ozone change, shown in Figure 22, is as much as 16% between 15 and 20 km in the northern hemisphere. Southern hemisphere ozone change was as much as 4% from 15 to 25 km. The region of ozone increase is now confined to equatorial latitudes, because the NOY emissions below 18 km for Scenario A3 were only 5% of those for Scenario B7. Subsonic aircraft emissions were not included in the McDonnell-Douglas scenarios. The ozone column change, shown in Figure 23, is 12-15% at northern high latitudes, 2% near the equator, and 2-5% in the southern hemisphere.

The NOY change for Scenario A4 is shown in Figure 24. Maximum change is only 2-3 ppb at 22 km. Figure 25 shows the change in ozone mixing ratio for Scenario A4. There is a 4% decrease in ozone between 15 and 20 km at northern latitudes. The ozone column difference for this case, shown in Figure 26, ranges from 0.5% at the equator to 3.5% at high northern latitudes and 1.4% at high southern latitudes.

The NOY mixing ratio difference, the O_3 mixing ratio difference, and the O_3 column difference for Scenario A5 are shown in Figures 27, 28, and 29, respectively. The NOY maximum increase is only 1 ppb. The ozone decreased by 2% in the northern hemisphere lower stratosphere and by 1.5% in the upper stratosphere. The ozone column change was 0.25% at the equator and 1.75% maximum. NOY emissions for this scenario were half of that for Scenario A4, and the ozone column difference was proportionally smaller.

IV. Uncertainties and Sensitivity Studies

A. Sensitivity to Injection Altitude

In order to explore the sensitivity of ozone to the altitude at which the emissions are injected and to determine the limitation of the vertical resolution in the present model, we ran four additional cases using Scenarios B8 and B10. Case 1 used only the emissions at the lower two altitudes (8-12 km and 12-14 km) of Scenario B8. Case 2 used only the emissions at the upper altitude (18-22 km) of B8. Results from cases 1 and 2 can be considered as estimates representing the individual effects from subsonic and supersonic operations respectively. For Case 3 we shifted the B10 emissions from the top level (18-22 km) to the next lower model level (14-18 km). In Case 4 we doubled the B10 emissions at the two upper altitudes (14-18 km and 18-22 km). In all cases, the water vapor emissions were not modified. This accounts for the consistency of the calculated O_3 changes in the upper stratosphere.

Figure 30 shows the change in NOY from Case 1. The maximum change in NOY was 1-2 ppb, and outside the area of emissions was only 0.1 ppb. In contrast, Scenario B8 (Figure 14) showed a maximum change of 3 ppb over a wider area with a 1 ppb change at all latitudes. The change in ozone cross-section, shown in Figure 31, shows a 1-2% depletion in the middle and upper stratosphere and an ozone increase of 4-8% in the northern hemisphere below 15 km. The ozone column shows little change, varying from -0.25% to +0.25%, as shown in Figure 32. The stratospheric ozone depletion was compensated by tropospheric ozone increases at some altitudes and seasons.

The results for Case 2 are shown in Figures 33, 34, and 35, for NOY, O_3, and O_3 column changes. Using emissions from only the 18-22 km level of Scenario B8, we see that the NOY distribution differs from Scenario B8 (Figure 14) only below 15 km in the northern hemisphere. This indicates that low-level emissions have mainly a local impact, while emissions higher than 18 km can disperse globally. Ozone changes are similar to those from Scenario B8 (Figure 15) except for the region below 15 km. The ozone column change is quite similar to that of Scenario B8 (Figure 16) indicating that the lower

altitude regions have only a small impact on the column when stratospheric depletion is significant. High northern latitudes showed a slightly smaller ozone column decrease than did Scenario B8.

In Case 3, emissions from Scenario B10 were shifted from the 18-22 km level to the 14-18 km level. The NOY response, shown in Figure 36, was much smaller than that from B10 (Figure 18). As seen in Figure 37, the ozone showed only a 1% change in the 15 to 25 km region except in spring when there was a 2% decrease. The ozone column change, shown in Figure 38, shows both increases and decreases. Maximum depletion was 0.75% at the north pole in spring. The results of cases 1, 2, and 3 indicate that emissions below 18 km do not have a great impact on the ozone column.

Case 4 represents a doubling of the B10 emissions at the 18-22 km and 14-18 km levels. Figure 39 shows the change in NOY, which is roughly double the change for B10 (Figure 18) in the middle stratosphere. Ozone changes, shown in Figure 40, are as much a 4% locally. As seen in Figure 41, the ozone column change is approximately double that of Scenario B10 (Figure 20). The ozone response was approximately linear with the emissions at the 18-22 km level for the given mix of exhaust gases and the given background atmosphere.

Our results showed that the O_3 response is proportional to the amount of NOY entrained in the stratosphere which is very sensitive to the altitude at which the injection occurs. Given that the present model has a vertical resolution of 3.5 km and that the exchange between the stratosphere and troposphere is parameterised to simulate only the large scale behavior, a more careful consideration of the stratospheric-tropospheric exchange process is called for.

B. Sensitivity to Background Trace Gas Concentrations

Concentrations of several important trace gases are known to be increasing in the earth's atmosphere. In order to test the response of ozone to HSCT emissions in the future atmosphere, we have performed five additional sets of model calculations using emissions from Scenario B7 in all cases. Each set of calculations contained a baseline future atmosphere with one or more trace gases perturbed, as predicted for the year 2060, and a case with

HSCT emissions included on this background. The five model experiments were:

Experiment I: 20% increase in N_2O
Experiment II: Doubling of CH_4
Experiment III: CFC's increased, yielding CℓY concentration of 6 ppbv
Experiment IV: Doubling of CO_2 simulated by an imposed temperature change
Experiment V: Combined effect of changes in Experiments I through IV.

For each experiment, we show four figures: Panel (a) shows the response of the present-day O_3 column to B7 emissions. This is identical to Figure 12 and is included in each case for reference purposes. Panel (b) shows the change in the ozone column of the future atmosphere as a percent of the background ozone in the present day atmosphere. Panel (c) shows the change in ozone column expressed as a percentage of the present day ozone when the emissions from Scenario B7 are included in the future atmosphere . Panel (d) is the same as Panel (c) but expressed as a percentage of the future ozone background. Note that panel (a) and (d) provide a measure of the O_3 removal efficiency of the emissions in the present-day and future atmospheres respectively.

Results from Experiment I, with N_2O increased by 20%, are shown in Figure 42. Panel (b) shows a 1-3% decrease in ozone from the present day to the future background cases. Since N_2O is a precursor of NOY, ozone depletion would be expected from the increase in NOY content. Increasing N_2O by 20% produced a larger ozone change than B7 HSCT emissions produced in the present atmosphere. The future atmosphere with B7 emissions shows an ozone decrease of 1-5% from the present day baseline (panel (c)) and 0.25-2.25% from the future baseline (panel (d)). Comparing Panel (a) and Panel (d) shows that ozone is more sensitive to HSCT emissions when the background NOY is larger. This can be explained in terms of the role of OH in determining the partitioning between NOX and HNO_3. With a higher NOY content in the future atmosphere, the OH concentration is lower. Thus, a larger portion of the NOY introduced by HSCT emissions remains in the form of NOX resulting in a larger efficiency in removing O_3.

The results of Experiment II are shown in Figure 43. The effect of a doubling of CH_4 is to increase the ozone column by 1.25-2.5% (panel (b)), with

local ozone changes of about 8% in the tropical troposphere and also at 40 km at high latitudes. With the addition of B7 emissions, the ozone column is still greater at all latitudes than the present day baseline (panel (c)). Compared with the future baseline, HSCT emissions decreased ozone at mid- and high-latitudes and cause little change in the tropics (panel (d)). We see that ozone is less sensitive to aircraft emissions with a background atmosphere containing twice the CH_4 of the present-day atmosphere. It should be noted that in this simulation, the H_2O distribution is kept fixed at the present day value. Since oxidation of CH_4 will lead to production of H_2O in the stratosphere, the effect of water feedbacks from the CH_4 increase should be included in future studies.

The ozone response to Experiment III is shown in Figure 44. Increasing the odd chlorine content of the model atmosphere reduced the ozone column by 3-7%. Ozone is depleted by as much as 40% at 40 km and high latitudes. Adding NOY to a high-chlorine atmosphere helps to sequester a larger fraction of the total odd chlorine in the form of $C\ell NO_3$, and decrease the O_3 removal efficiency of the chlorine cycle. Panel (d) shows that ozone increased in southern and tropical latitudes and decreased in high latitudes when B7 emissions were added to this future atmosphere. The nitrogen emitted is less efficient in removing O_3 because, compare to the present day atmosphere, a larger portion of the emitted NOY is in the form of $C\ell NO_3$.

The atmospheric burden of CO_2 is steadily increasing due to the burning of fossil fuels, deforestation, and other anthropogenic activities. An increase in the burden of CO_2 is expected to cool the stratosphere and raise the earth's surface temperature. A cooler stratosphere will result in a decrease in the O_3 removal efficiency of the chemical cycles leading to an increase in O_3 in the stratosphere. Figure 45 shows the assumed change in temperature from a doubling of CO_2 used in the model calculation. The cooling in the stratosphere is calculated from the AER 2-D interactive model (Schneider et al, 1989). A surface warming of 4°K is imposed in the model based on results from GCM simulations. A change in the radiative properties of the atmosphere would also likely produce a change in the atmospheric circulation, but that effect was not considered here.

Figure 46 shows the change in ozone produced in the model by imposing the given temperature change. The stratospheric temperature decrease produced a

local ozone increase of up to 12%. The ozone column increased by 1 to 4%. The response with B7 emissions was a consistent reduction in ozone column from the future atmosphere baseline, but with a slightly smaller magnitude than for the present-day atmosphere.

Experiment V used a future atmosphere containing 20% more N_2O, double CH_4, 6 ppb of odd chlorine, and perturbed temperature. The ozone response shows a complex pattern of increases at some latitudes and heights and decreases at others. The column ozone response, shown in Figure 47, shows increases of 0.5% near the equator and decreases of 2% near the poles for this future atmosphere. HSCT emissions from Scenario B7 imposed on this atmosphere cause an additional increase in column ozone in the tropics and an additional decrease in mid-latitudes.

C. Heterogeneous Chemistry

The calculations presented in this report include only gas-phase reactions. Recent developments connected with the Antarctic ozone hole phenomenon indicate that heterogeneous reactions of gas-phase molecules with trace gases in solid or liquid phase could play a major role in the chemistry of the stratosphere (Solomon et al., 1986; McElroy et al., 1986; Rodriguez et al., 1988). Laboratory measurements now exist for the following reactions:

$$C\ell NO_3 + H_2O\ (s) \rightarrow HOC\ell + HNO_3(s,g) \quad (1)$$

$$C\ell NO_3 + HC\ell\ (s) \rightarrow C\ell_2 + HNO_3(s,g) \quad (2)$$

$$N_2O_5 + H_2O\ (s) \rightarrow 2HNO_3\ (s,g) \quad (3)$$

$$N_2O_5 + HC\ell\ (s) \rightarrow C\ell NO_2 + HNO_3\ (s,g) \quad (4)$$

In the above, the (s) denotes that the species is incorporated in either a solid or liquid phase. The active chlorine products are released into the gas phase, while the nitric acid usually remains in the solid phase (Molina et al., 1987; Tolbert et al., 1987, 1988; and Leu, 1988a,b). However, it is possible that this nitric acid is also released into the gas phase under

saturation conditions. Laboratory measurements now exist for (1) -(4) primarily for ice surfaces (Molina et al., 1987; Tolbert et al., 1987, 1988a; Leu, 1988a,b). Preliminary laboratory results, however, indicate that reactions (1) -(3) could occur at very fast rates on sulfuric acid solutions, with the rate depending on the water content of the surface (Tolbert et al., 1988b; Worsnop et al., 1988; Mozurkewich and Calvert, 1988).

The above reactions have two main effects: a) Reactions (1), (2) and (4) repartition the inorganic chlorine species, decreasing the relative abundance of $HC\ell$. b) Reactions (1) to (4) convert short-lived species in the NO_x family to nitric acid, which has a longer lifetime. This process would be particularly efficient at high latitudes during winter through reactions (3) and (4).

We can anticipate the following possible impacts of including heterogeneous chemistry in our calculations:

1. The water injected by the aircrafts could condense locally and provide sites for heterogeneous activity. Such effects could be particularly important, since the heterogeneous reaction rates measured in the laboratory increase dramatically with water content of the surface. Information is needed as to the condensation nuclei emitted by the aircraft, and the possibility of condensing water on these nuclei.

2. The SO_2 injected by the exhaust gases could enhance the aerosol loading in the Junge layer, in a manner similar to that encountered in a volcanic eruption. Such enhancements could also increase the rate of heterogeneous reactions.

3. Reactions (1) to (4) introduce two competing effects: Conversion of NO_x to HNO_3 would dampen the catalytic removal of O_3 by the nitrogen cycles, and thus <u>decrease</u> the estimated ozone losses from NO_x injection. At the same time, a decrease in NO_x would increase the ratio of $C\ell O$ to $C\ell NO_3$, thus enhancing the effectiveness of chlorine catalytic cycles. These cycles could also be enhanced by the conversion of $HC\ell$ to other forms of chlorine by reactions (1), (2) and (4). The net effect on O_3 would depend on the nitrogen and chlorine content in the atmosphere.

We stress that detailed calculations of the impact of heterogeneous reactions are hampered at present by large uncertainties still existing in the

rates of reactions (1) - (4). Assessment of the effects of heterogeneous reactions would thus require a careful consideration of specific scenarios, a calculation of possible enhancements in aerosol loading and/or water cloud formation, and sensitivity studies covering a range of possible rates for proposed heterogeneous reactions.

V. Concluding Remarks

The ability to model the atmosphere is limited by our understanding of the atmospheric processes, by the skill in converting this knowledge into a computer model, and by available computer technology. We have presented the model-calculated response of ozone to six HSCT emission scenarios along with the results of a number of sensitivity studies using an existing 2-D model of the atmosphere. We have included the effects of NOY, CO, CH_4, and H_2O emissions on atmospheric ozone. We did not include the effect of SO_2 or CO_2 emissions, but these should produce only a small or negligible effect for studies that exclude heterogeneous reactions and dynamic feedbacks. Our results showed that the model calculated response of O_3 is dominated by the amount of NOY that is entrained in the stratosphere. The entrainment is sensitive to the altitude at which the emission is injected, and very possibly, on model treatment of the stratospheric-tropospheric exchange processes and the vertical resolution of the model.

Prediction of the impact of HSCT is coupled to the future states of the atmosphere. Our simulations showed that the O_3 removal efficiency of the emitted material depends on the trace gas concentrations in the background atmosphere.

Two-dimensional models are appropriate for examining the response of O_3 once the emitted materials become zonally-mixed. It may be necessary to use other models to determine the zonal-mean inputs from given emissions if additional transformation may occur in the exhaust plume. We have identified several areas where refinement of the model may clarify and/or alter the calculated O_3 response. These include :

Entrainment of NOY

There is a need to examine the entrainment of the emitted NOY using a model with a finer vertical resolution near the tropopause. As a first step, it may be sufficient to examine the response of NOY alone in a sub-model rather than running the model with full chemistry in the finer grid. The sensitivity of NOY entrainment to seasonally dependent emissions should also be examined. Consideration of the diabatic circulation would suggest that material emitted in winter would stand a better chance of being transported to

the troposphere. The eddy treatment in 2-D models may be a real limitation in this aspect. The study could benefit from comparison with 3-D model results and observational data from the Stratospheric and Tropospheric Exchange Program.

The role of long-chain hydrocarbons and PAN chemistry

In the present study, the unburned hydrocarbons are input to the model as CH_4. Long-chain hydrocarbons can be oxidized to aldehydes which can combine with NO_2 to form PAN-like molecules. Formation of Pan-like molecules would moderate the O_3 impact from the emitted NO_2. The stratospheric concentration of C_2H_6 is less than 1 ppbv, about three order of magnitude smaller than that of CH_4. Thus, the emitted hydrocarbons could have a larger impact if introduced to the model as C_2H_6 A version of the AER 2-D model developed this past year includes C_2H_6 and PAN chemistry. This version of the model would be used in future studies.

The role of heterogeneous chemistry on aerosol and ice particles

Heterogeneous reactions can affect the outcome of the model simulations in at least three aspects. First, reactions occurring on the aerosols and/or ice particles in the exhaust plume can modify the trace gas compositions before they are dispersed. Second, reactions occurring on the global aerosol layer could alter the sensitivity of the response of global O_3 to the aircraft emissions. Third, emissions from aircraft could enhance and/or modify the chemical compositions of the aerosols and change the O_3 response. While the first aspect is beyond the scope of a 2-D model study, the second and third could be studied in the context of 2-D models augmented by microphysics describing aerosol formations. At present, there are large uncertainties in the kinetic data on heterogeneous reactions, in particular on their dependence on temperature and chemical composition of the aerosol particles. While it is premature to use the model results for assessment purposes, it is prudent to incorporate parametrization of these reactions in the model.

Temperature and dynamics feedback

Studies using the AER 2-D models showed that changes in temperature of a few degrees in the lower stratosphere can cause a change in the diabatic circulation which will in turn modify the calculated O_3 column abundance by about 2-3%. The change in temperature could be a result of the change in wave-forcing in the atmosphere or a change in the radiative properties of the lower stratosphere. Thus, any climatic or radiative impact from HSCT could affect O_3 via the temperature and circulation. The current program at AER in developing the interactive 2-D model would be very helpful in this aspect.

Tropospheric O_3

The primary goal of the present study is to identify the response of stratospheric O_3 to the engine emissions. Although the necessary chemistry for the troposphere is included in the present model study, improvement should be made on the boundary conditions for various trace species. There is a need to ascertain the extent to which 2-D models can capture the O_3 response in spite of the more pronounced zonal asymmetry in the troposphere.

References

Crutzen, P.J., and V. Schmailzl (1983) Chemical budgets of the stratosphere. Planet. Space Sci., 31, 1009-1032.

Jackman, C.H., R.S. Stolarski, and J.A. Kaye (1986) Two-dimensional monthly average ozone balance from limb infrared monitor of the stratosphere and stratospheric and mesospheric sounder data. J. Geophys. Res., 91, 1103-1116.

Ko, M. K. W., K. K. Tung, D. K. Weisenstein, and N. D. Sze (1985) A zonal-mean model of stratospheric tracer transport in isentropic coordinates: Numerical simulations for nitrous oxide and nitric acid. J. Geophys. Res., 90, 2313-2329.

Ko, M. K. W., M. B. McElroy, D. K. Weisenstein, and N. D. Sze (1986) Lightning: A possible source of stratospheric odd nitrogen. J. Geophys. Res., 91, 5395-5404.

Ko, M.K.W., N.-D. Sze, and D.K. Weisenstein (1989) The roles of dynamical and chemical processes in determining the stratospheric concentration of ozone in one-dimensional and two-dimensional models. J. Geophys. Res., 94, 9889-9896.

Leu, M.-T. (1988a) Laboratory studies of sticking coefficients and heterogeneous reactions important in the Antarctic stratosphere. Geophys. Res. Lett., 15, 17-20.

Leu, M.-T. (1988b) Heterogeneous reactions of N_2O_5 with H_2O and $HC\ell$ on ice surfaces: implications for Antarctic ozone depletion. Geophys. Res. Lett., 15, 851-854.

McElroy, M.B., R.J. Salawitch, S.C. Wofsy, and J.A. Logan (1986) Antarctic ozone: reductions due to synergistic interactions of chlorine and bromine. Nature, 321, 759.

Molina, L.J., T.L. Tso, L.T. Molina, and F.C.Y Wang (1987) Antarctic stratospheric chemistry of chlorine nitrate, hydrogen chloride and ice: release of active chlorine. Science, 238, 1253.

Mozurkewich, M., and J.G. Calvert (1988) Reaction probability of N_2O_5 on aqueous aerosols. J. Geophys. Res., 93, 15889-15896.

NASA/JPL (1987) Chemical Kinetics and Photochemical Data for Use in Stratospheric Modeling, Evaluation Number 8. JPL Publication 87-41.

Remsberg, E. E., J. M. Russell, III, L. L. Gordley, J. C. Gille, and P. L. Bailey (1984) Implications of the stratospheric water vapor distribution as determined by the Nimbus 7 LIMS experiment. J. Atmos. Sci., 41, 2934-2945.

Rodriguez, J.M., M.K.W. Ko, and N.D. Sze (1988) Antarctic chlorine chemistry: possible global implications. Geophys. Res. Lett., 15, 257-260.

Schneider, H.R., M.K.W. Ko, N.D. Sze, G.-Y. Shi, and W.-C. Wang (1989) An evaluation of the role of eddy diffusion in stratospheric interactive two-dimensional models. J. Atmos. Sci., 46, 2079-2093.

Solomon, S., R.R. Garcia, F.S. Rowland, and D.J. Wuebbles (1986) On the depletion of Antarctic ozone. Nature, 321, 755.

Tolbert, M.A., M.J. Rossi, R. Malhotra, and D.M. Golden (1987) Reaction of chlorine nitrate with hydrogen chloride and water at Antarctic stratospheric temperatures. Science, 238, 1258.

Tolbert, M.A., M.J. Rossi, and D.M. Golden (1988a) Heterogeneous chemistry related to Antarctic ozone depletion chemistry: reactions of N_2O_5 with H_2O and $HC\ell$ on ice surfaces. Science, 240, 1018-1021.

Tolbert, M.A., M.J. Rossi, and D.M. Golden (1988b) Heterogeneous interactions of chlorine nitrate, hydrogen chloride, and nitric acid with sulfuric acid surfaces at stratospheric temperatures. Geophys. Res. Lett., 15, 847-850.

WMO/NASA (1986) Atmospheric Ozone: Assessment of Our Understanding of the Processes Controlling Its Present Distribution and Changes. World Meteorological Organization Report #16, Geneva.

Wofsy, S. C., and J. A. Logan (1982) Recent developments in stratospheric photochemistry. In Causes and Effects of Stratospheric Ozone Reduction: An Update. National Academy Press, Washington, D.C. 1982.

Worsnop, D., M. Zahniser, C. Kolb, L. Watson, J. Van Doren, J. Jayne, and P. Davidovits (1988) Mass accommodation coefficient measurements for HNO_3, $HC\ell$, and N_2O_5 on water, ice and aqueous sulfuric acid droplet surfaces. (Abstract) In: Polar Ozone Workshop, Abstracts. Proceedings of the Polar Ozone Workshop held in Snowmass, Colorado, U.S.A., May 9-13, 1988. NASA Conference Publication 10014.

Table 1.
Emissions of NOY, CO, hydrocarbons (as CH_4), and water vapor for Boeing Scenarios B7, B8, and B10 in molecules per second at each model altitude level.

Model Level	ht (km)	NOY Emissions (molecules/sec) B7	B8	B10
3	8-12	1.36×10^{26}	1.36×10^{26}	1.36×10^{26}
4	12-14	1.10×10^{27}	1.13×10^{27}	1.08×10^{27}
5	14-18			4.41×10^{25}
6	18-22	1.99×10^{26}	4.05×10^{26}	1.99×10^{26}
Total		1.435×10^{27}	1.67×10^{27}	1.46×10^{27}

Model Level	ht (km)	CO Emissions (molecules/sec) B7	B8	B10
3	8-12	1.29×10^{25}	1.25×10^{25}	1.29×10^{25}
4	12-14	4.02×10^{26}	1.94×10^{27}	9.05×10^{25}
5	14-18			5.15×10^{25}
6	18-22	1.35×10^{26}	3.56×10^{26}	1.35×10^{26}
Total		5.50×10^{26}	2.31×10^{27}	2.90×10^{26}

Table 1. (continued)

Model Level	ht (km)	CH_4 Emissions (molecules/sec) B7	B8	B10
3	8-12	4.60×10^{24}	4.60×10^{24}	4.60×10^{24}
4	12-14	8.58×10^{25}	1.76×10^{26}	3.13×10^{25}
5	14-18			8.99×10^{24}
6	18-22	2.35×10^{25}	8.88×10^{24}	2.35×10^{25}
Total		1.14×10^{26}	1.89×10^{26}	6.84×10^{25}

Model Level	ht (km)	H_2O Emissions (molecules/sec) B7	B8	B10
3	8-12	2.13×10^{28}	2.13×10^{28}	2.13×10^{28}
4	12-14	1.93×10^{29}	1.97×10^{29}	1.63×10^{29}
5	14-18			3.29×10^{28}
6	18-22	8.62×10^{28}	9.82×10^{28}	8.62×10^{28}
Total		3.01×10^{29}	3.16×10^{29}	3.03×10^{29}

Table 2.
Emissions of NOY, CO, hydrocarbons (as CH_4), and water vapor for McDonnell-Douglas Scenarios A3, A4, and A5 in molecules per second at each model level.

Model Level	ht (km)	NOY Emissions (molecules/sec) A3	A4	A5
1	1-4	2.20×10^{25}	2.19×10^{25}	8.56×10^{24}
2	4-8	8.40×10^{24}	8.37×10^{24}	3.26×10^{24}
3	8-12	7.40×10^{24}	7.37×10^{24}	2.88×10^{24}
4	12-14	8.95×10^{24}	8.91×10^{24}	3.47×10^{24}
5	14-18	4.75×10^{24}	4.73×10^{24}	1.85×10^{24}
6	18-22	4.24×10^{24}	4.22×10^{24}	1.65×10^{24}
7	22-24	5.63×10^{26}	1.72×10^{26}	9.40×10^{25}
Total		2.27×10^{26}	1.89×10^{26}	1.16×10^{26}

Model Level	ht (km)	CO Emissions (molecules/sec) A3	A4	A5
1	1-4	2.72×10^{26}	2.74×10^{26}	2.61×10^{26}
2	4-8	1.04×10^{26}	1.04×10^{26}	9.94×10^{25}
3	8-12	9.14×10^{25}	9.21×10^{25}	8.75×10^{25}
4	12-14	1.10×10^{26}	1.11×10^{26}	1.06×10^{26}
5	14-18	5.87×10^{25}	5.91×10^{25}	5.62×10^{25}
6	18-22	5.23×10^{25}	5.28×10^{25}	5.01×10^{25}
7	22-24	4.16×10^{25}	2.23×10^{25}	4.27×10^{25}
Total		7.30×10^{26}	7.15×10^{26}	7.03×10^{26}

Table 2. (continued)

Model Level	ht (km)	CH_4 Emissions (molecules/sec) A3	A4	A5
1	1-4	1.80×10^{24}	1.89×10^{24}	1.60×10^{24}
2	4-8	6.86×10^{23}	7.23×10^{23}	6.11×10^{23}
3	8-12	6.04×10^{23}	6.36×10^{23}	5.38×10^{23}
4	12-14	7.30×10^{23}	7.69×10^{23}	6.50×10^{23}
5	14-18	3.87×10^{23}	4.08×10^{23}	3.46×10^{23}
6	18-22	3.46×10^{23}	3.64×10^{23}	3.08×10^{23}
7	22-24	5.28×10^{23}	5.29×10^{23}	5.77×10^{23}
Total		5.08×10^{24}	5.32×10^{24}	4.63×10^{24}

Model Level	ht (km)	H_2O Emissions (molecules/sec) A3	A4	A5
1	1-4	6.45×10^{27}	6.45×10^{27}	6.45×10^{27}
2	4-8	2.46×10^{27}	2.46×10^{27}	2.46×10^{27}
3	8-12	2.17×10^{27}	2.17×10^{27}	2.17×10^{27}
4	12-14	2.62×10^{27}	2.62×10^{27}	2.62×10^{27}
5	14-18	1.39×10^{27}	1.39×10^{27}	1.39×10^{27}
6	18-22	1.24×10^{27}	1.24×10^{27}	1.24×10^{27}
7	22-24	3.39×10^{28}	3.39×10^{28}	3.39×10^{28}
Total		5.02×10^{28}	5.02×10^{28}	5.02×10^{28}

Table 3.
Summary of total emissions for each scenario,
including the natural source strength and the global burden.

(Units are molecules/sec for emissions and natural source strength and molecules for global burden)

	NOY*	CO	CH_4	H_2O
B7	1.99×10^{26}	5.50×10^{26}	1.14×10^{26}	3.01×10^{29}
B8	4.05×10^{26}	2.31×10^{27}	1.89×10^{26}	3.16×10^{29}
B10	1.99×10^{26}	2.90×10^{26}	6.84×10^{25}	3.03×10^{29}
A3	5.67×10^{26}	7.30×10^{26}	5.08×10^{24}	5.02×10^{28}
A4	1.76×10^{26}	7.15×10^{26}	5.32×10^{24}	5.02×10^{28}
A5	9.57×10^{25}	7.03×10^{26}	4.63×10^{24}	5.02×10^{28}
Natural Source	8×10^{26}†	6×10^{29}	3.8×10^{29}	3×10^{29}†
Global Burden	6×10^{34}†	8.5×10^{36}	1.8×10^{38}	5.7×10^{37}†

*Only emissions above 18 km are included.

†Only the stratospheric components of the source and burden are included.

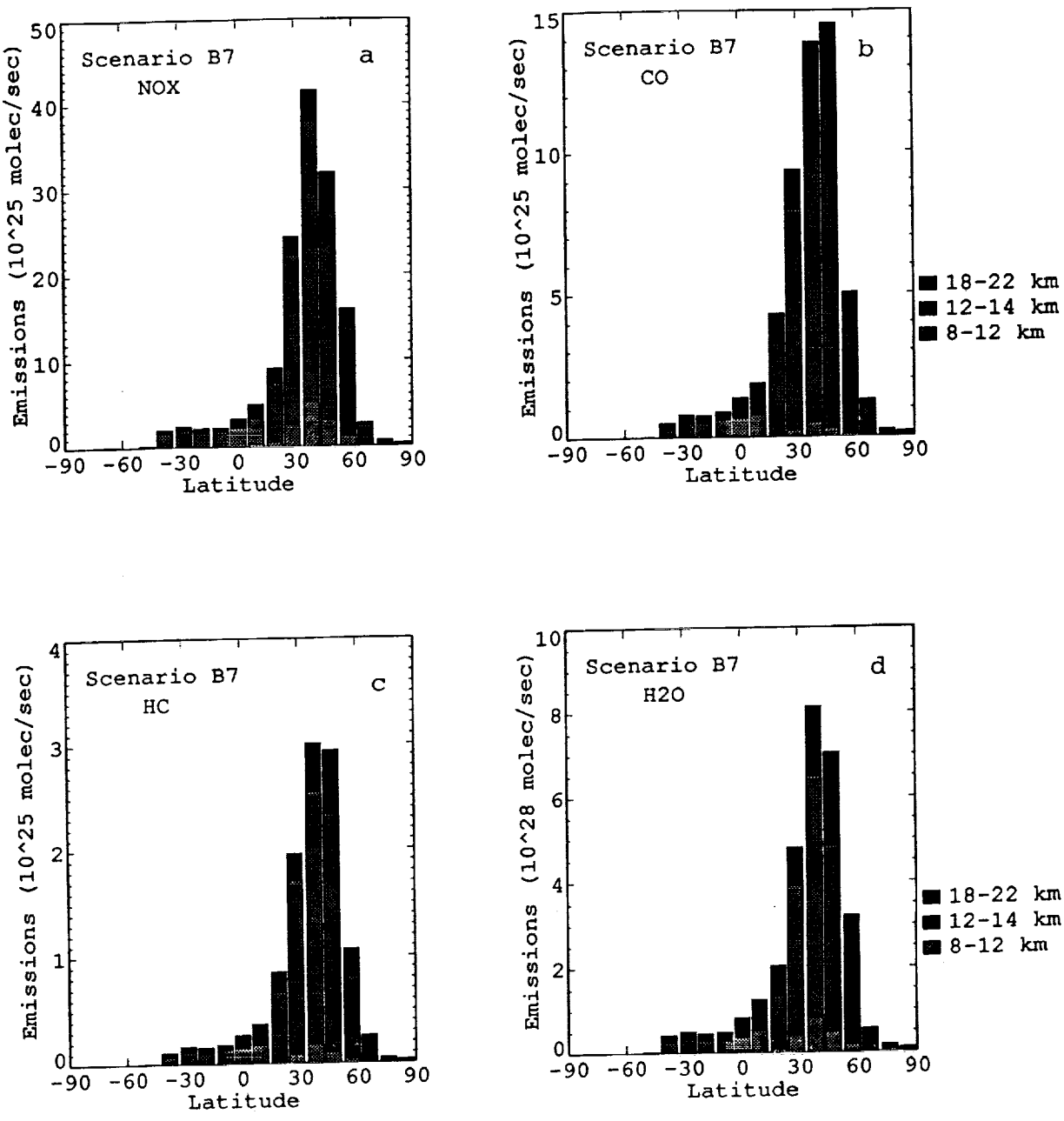

Figure 1. Emissions of (a) NOY, (b) CO, (c) hydrocarbon as CH_4, and (d) water vapor for Scenario B7 as a function of latitude. The height of the bar represents total emissions for the 9.5 degree latitude band in molecules per second. Shadings within bars represent the contribution to emissions from difference model altitude levels.

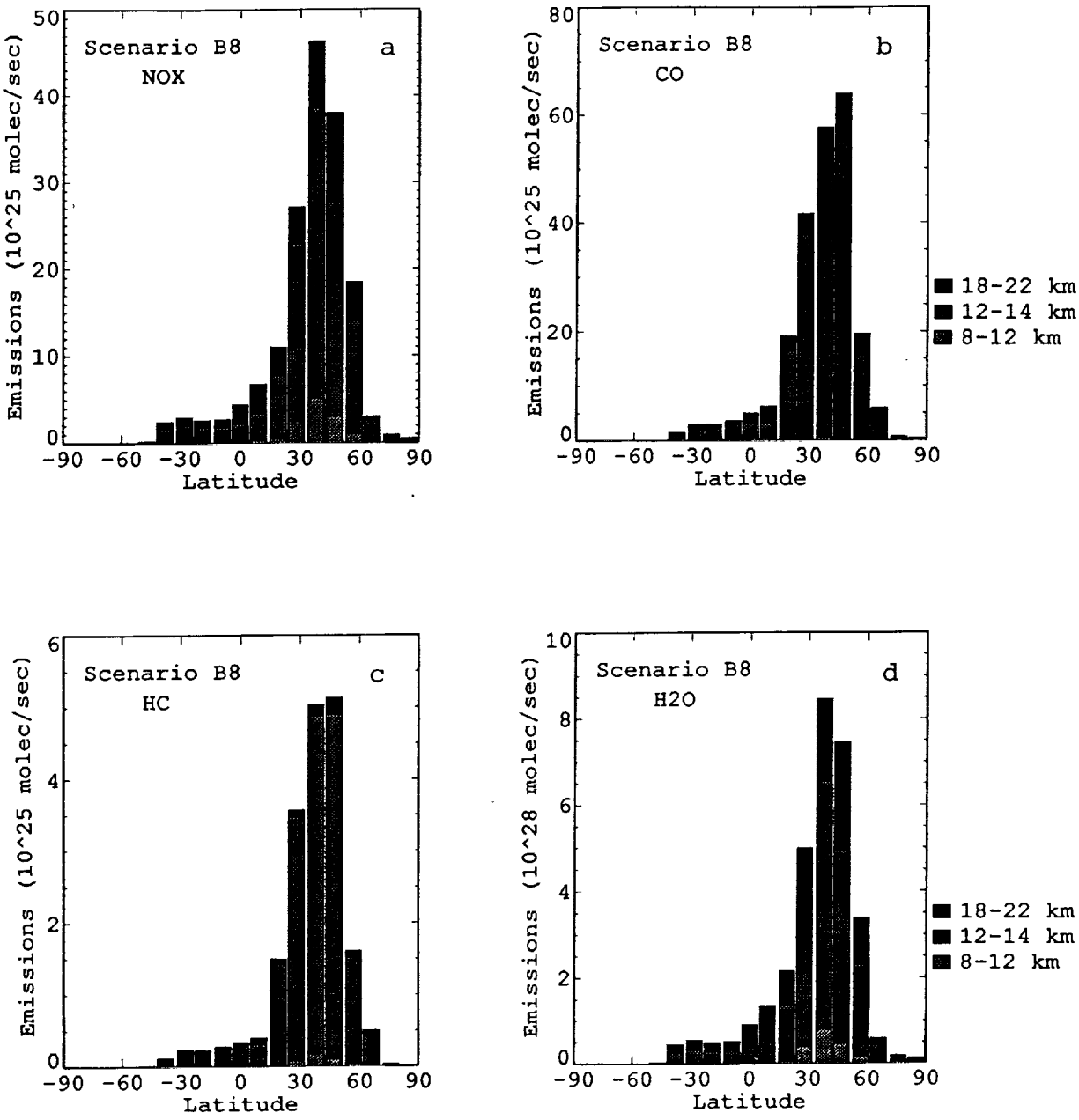

Figure 2. Emissions of (a) NOY, (b) CO, (c) hydrocarbon as CH_4, and (d) water vapor for Scenario B8 as a function of latitude. The height of the bar represents total emissions for the 9.5 degree latitude band in molecules per second. Shadings within bars represent the contribution to emissions from difference model altitude levels.

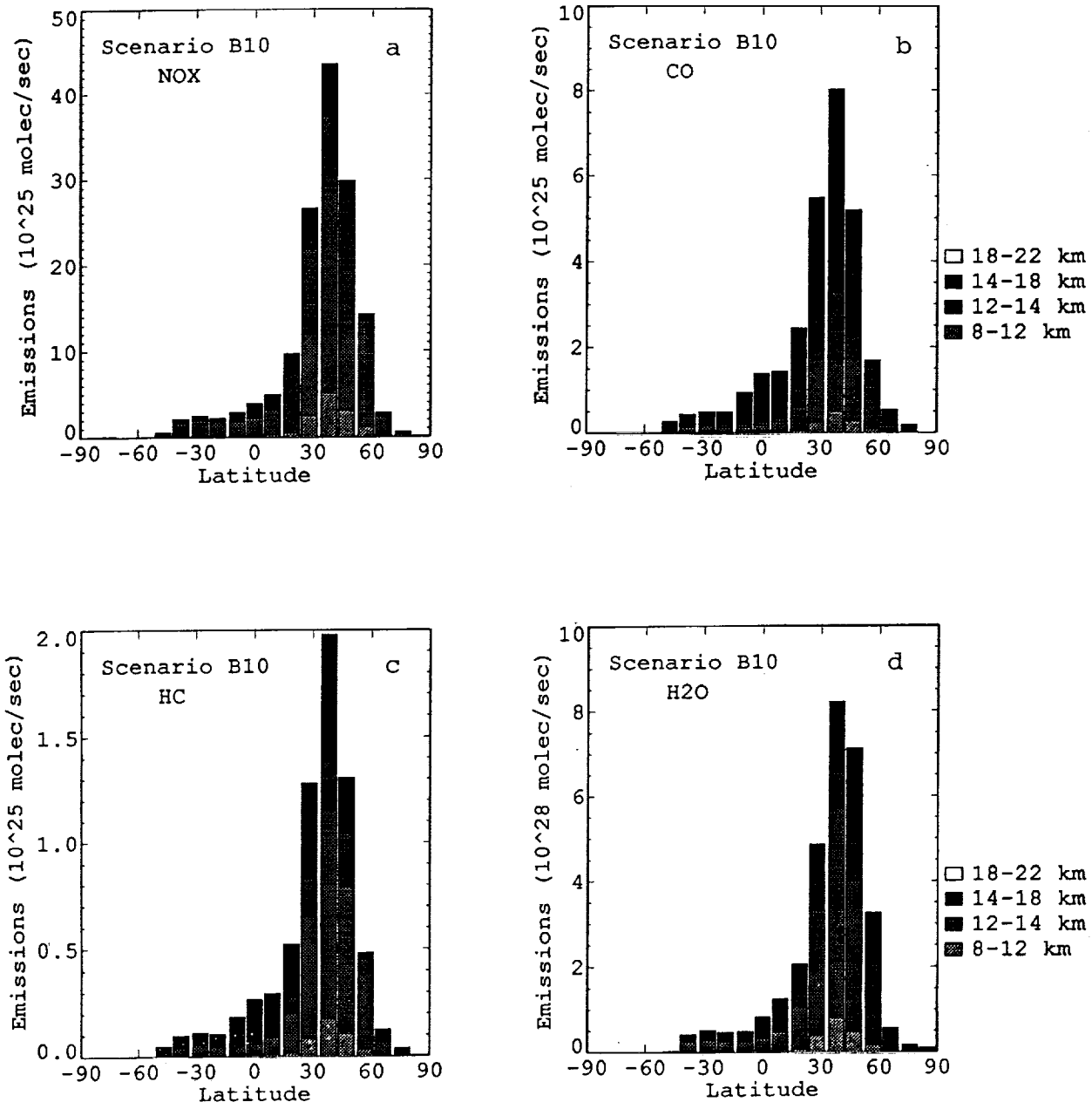

Figure 3. Emissions of (a) NOY, (b) CO, (c) hydrocarbon as CH_4, and (d) water vapor for Scenario B10 as a function of latitude. The height of the bar represents total emissions for the 9.5 degree latitude band in molecules per second. Shadings within bars represent the contribution to emissions from difference model altitude levels.

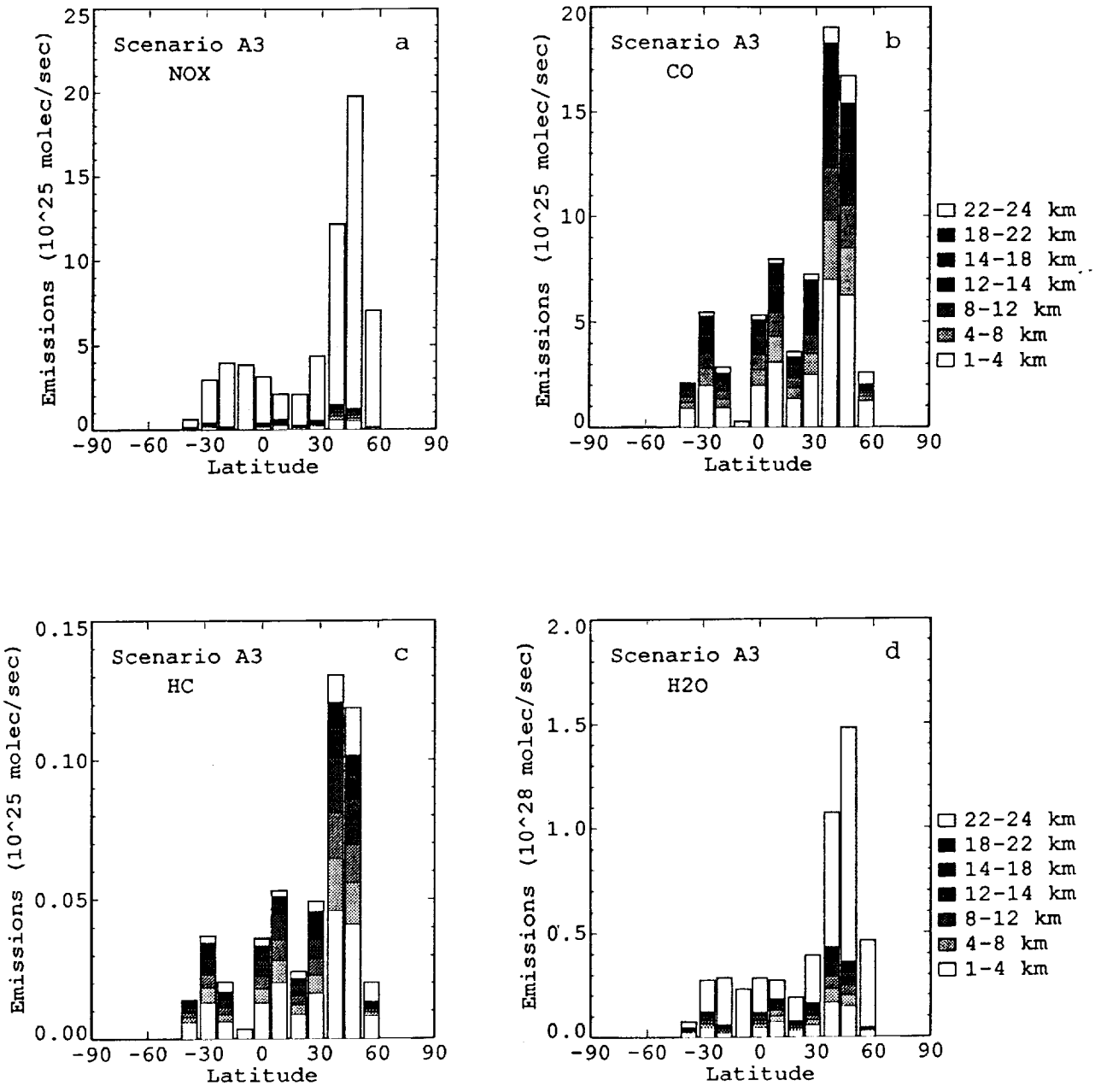

Figure 4. Emissions of (a) NOY, (b) CO, (c) hydrocarbon as CH_4, and (d) water vapor for Scenario A3 as a function of latitude. The height of the bar represents total emissions for the 9.5 degree latitude band in molecules per second. Shadings within bars represent the contribution to emissions from difference model altitude levels.

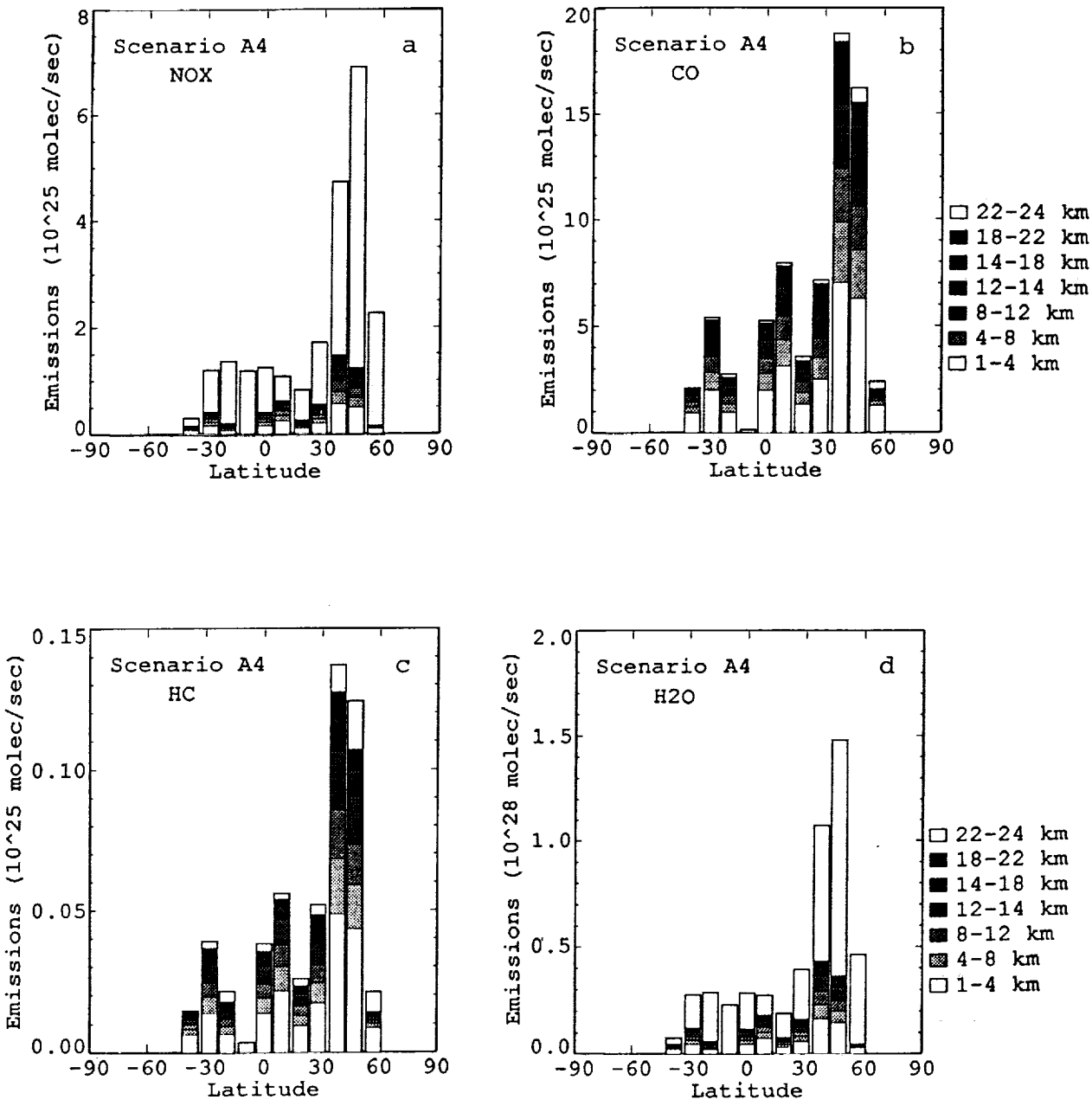

Figure 5. Emissions of (a) NOY, (b) CO, (c) hydrocarbon as CH_4, and (d) water vapor for Scenario A4 as a function of latitude. The height of the bar represents total emissions for the 9.5 degree latitude band in molecules per second. Shadings within bars represent the contribution to emissions from difference model altitude levels.

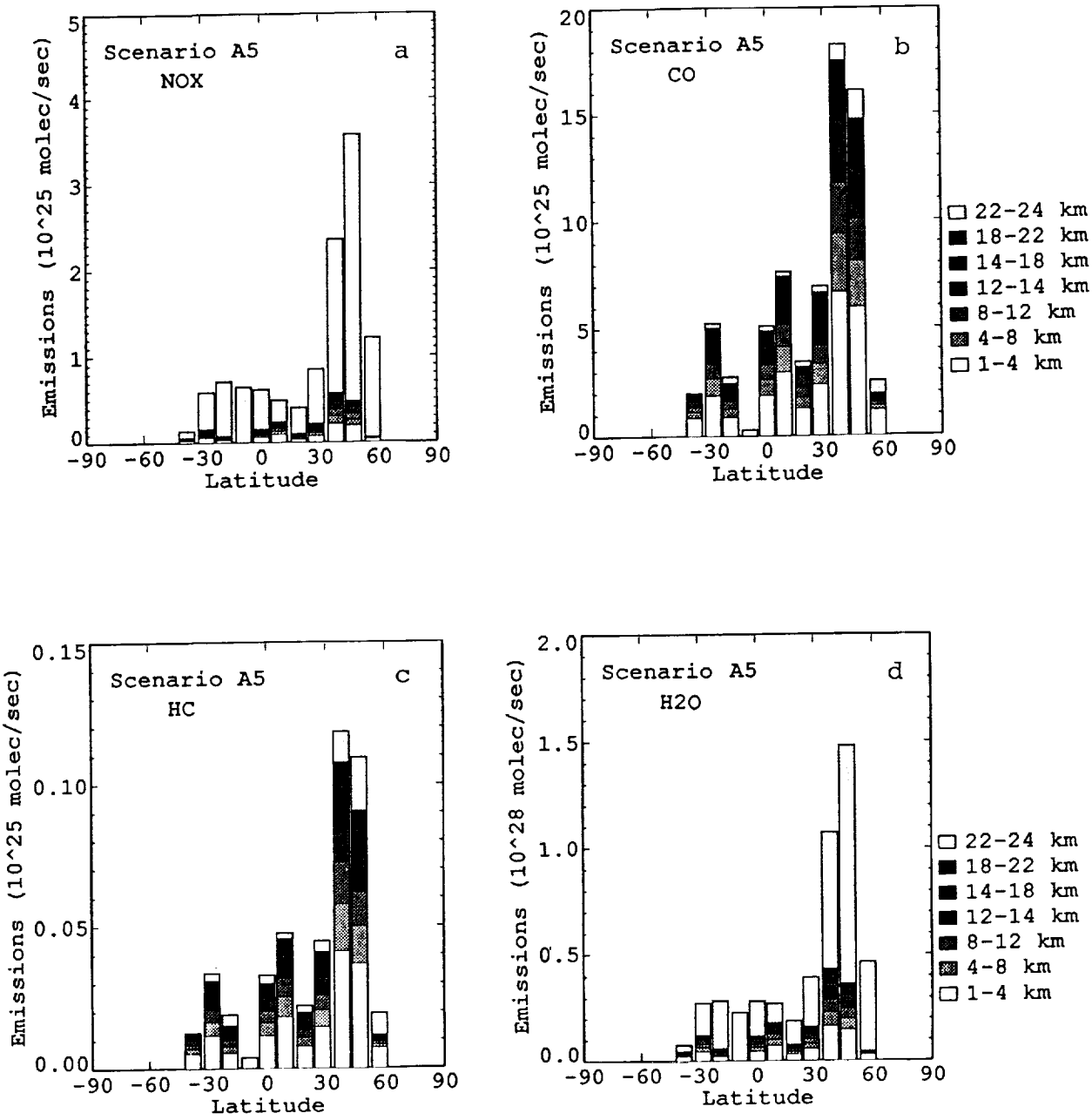

Figure 6. Emissions of (a) NOY, (b) CO, (c) hydrocarbon as CH_4, and (d) water vapor for Scenario A5 as a function of latitude. The height of the bar represents total emissions for the 9.5 degree latitude band in molecules per second. Shadings within bars represent the contribution to emissions from difference model altitude levels.

Scenario B7 : NOY

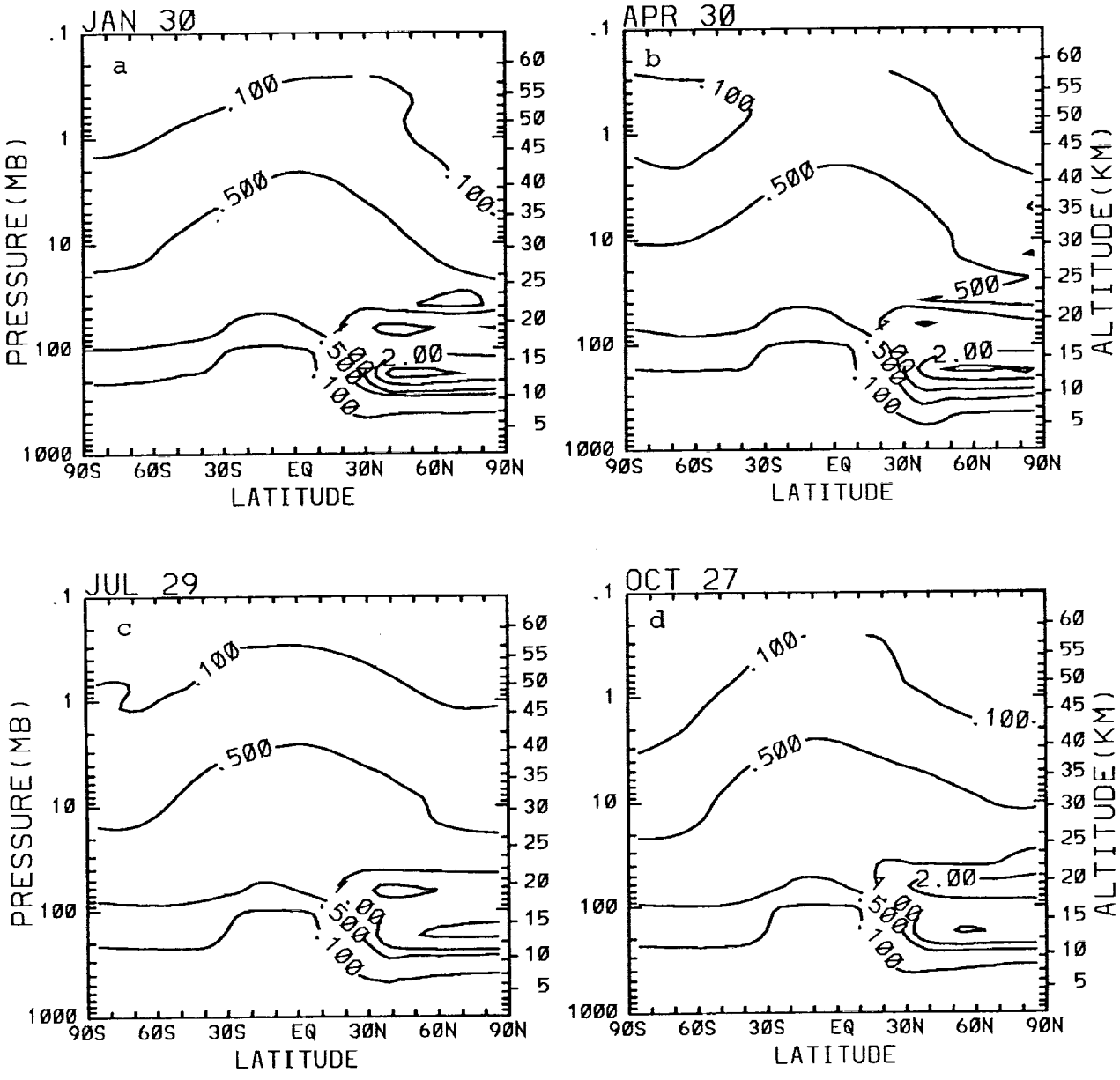

Figure 7. The calculated change in NOY in ppbv from the baseline case (shown in Figure A4) for Scenario B7, as a function of latitude and altitude for (a) January, (b) April, (c) July, and (d) October. Contour levels are 0.1, 0.5, 1.0, 2.0, 3.0 ppbv.

Scenario B7 : CO

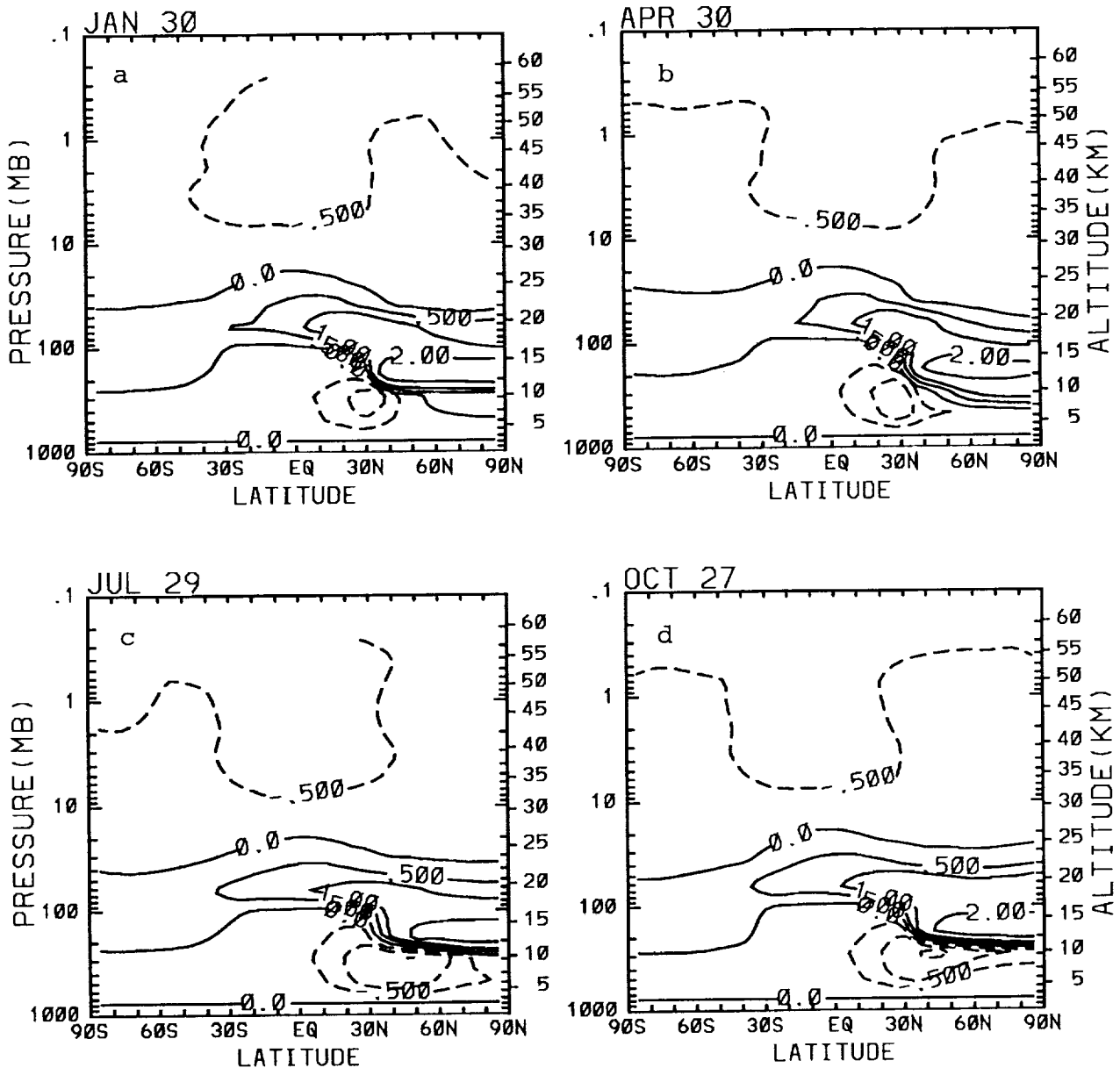

Figure 8. The calculated change in CO in ppbv from the baseline case (shown in Figure A5) for Scenario B7, as a function of latitude and altitude for (a) January, (b) April, (c) July, and (d) October. Contour levels are 0, ±0.5, ±1.0, and ±2.0 ppbv.

Scenario B7 : CH_4

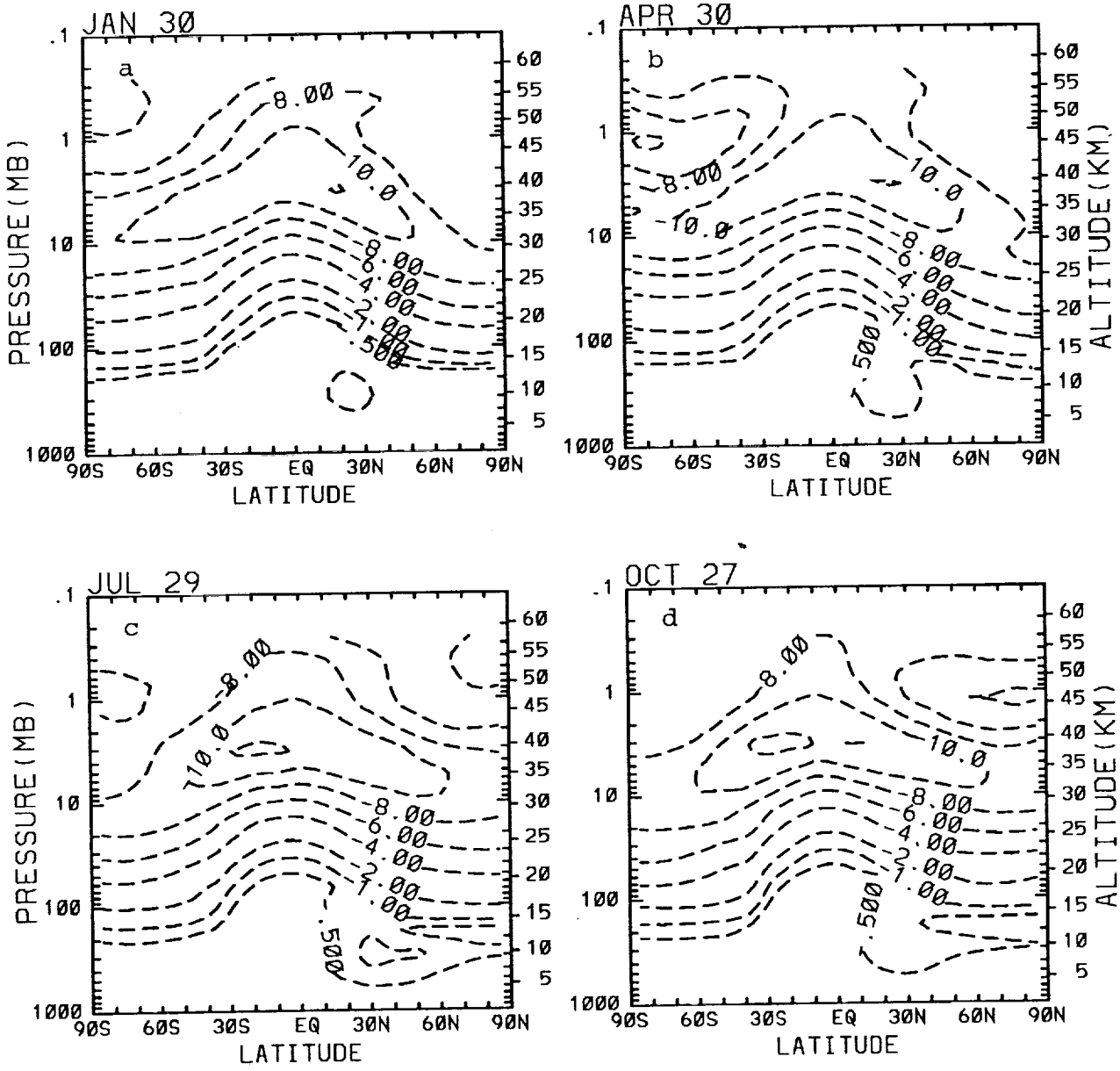

Figure 9. The calculated change in CH_4 in ppbv from the baseline case (shown in Figure A6) for Scenario B7, as a function of latitude and altitude for (a) January, (b) April, (c) July, and (d) October. Contour levels are -0.5, -1, -2, -4, -6, -8, -10, -12 ppbv.

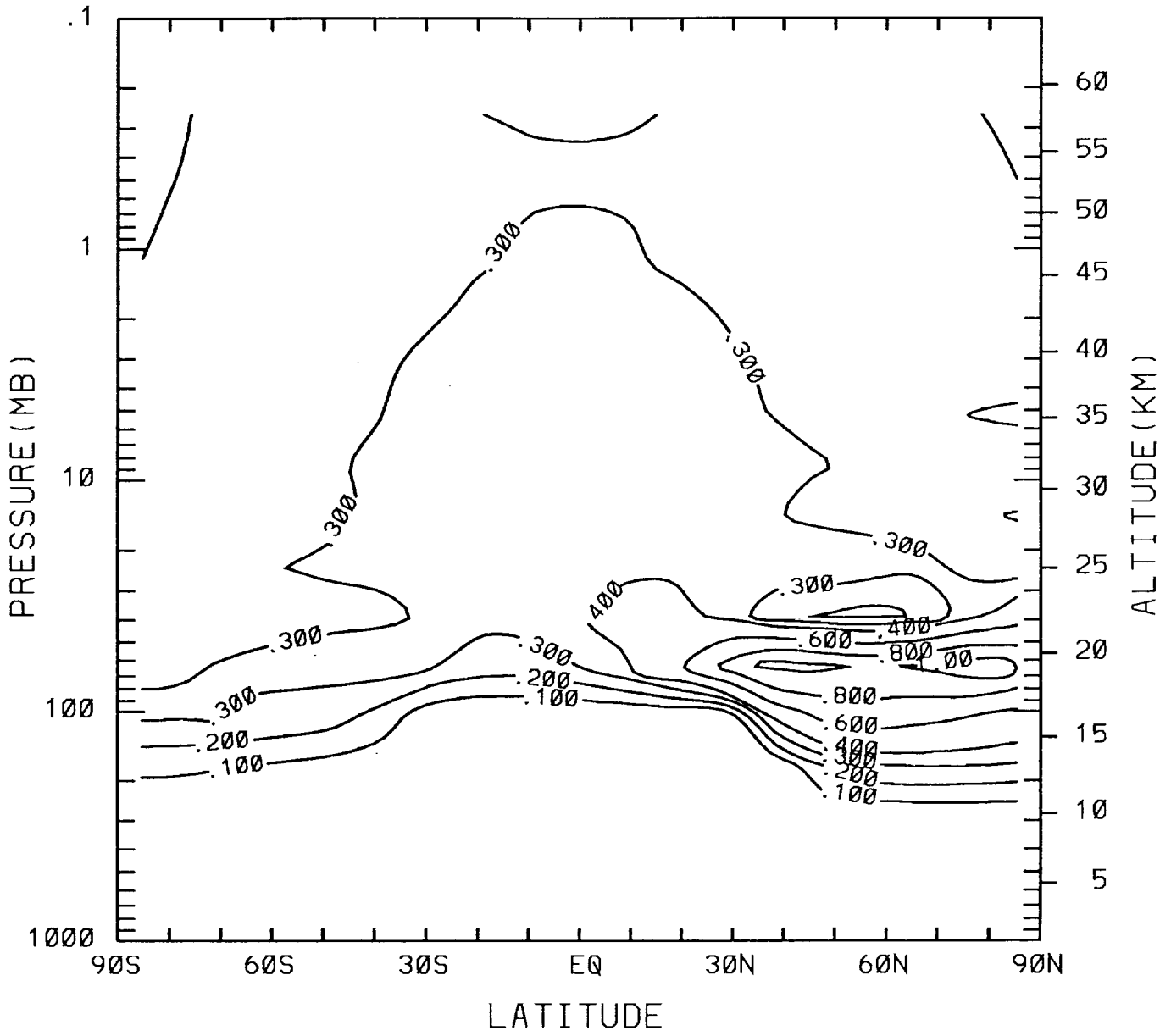

Figure 10. The calculated change in water vapor in ppmv from the baseline case (shown in Figure A7) for Scenario B7, as a function of latitude and altitude. Stratospheric water vapor concentration is held fixed for all seasons within the model. Contour levels are 0.1, 0.2, 0.3, 0.4, 0.6, 0.8, 1.0 ppmv.

Scenario B7 : O_3

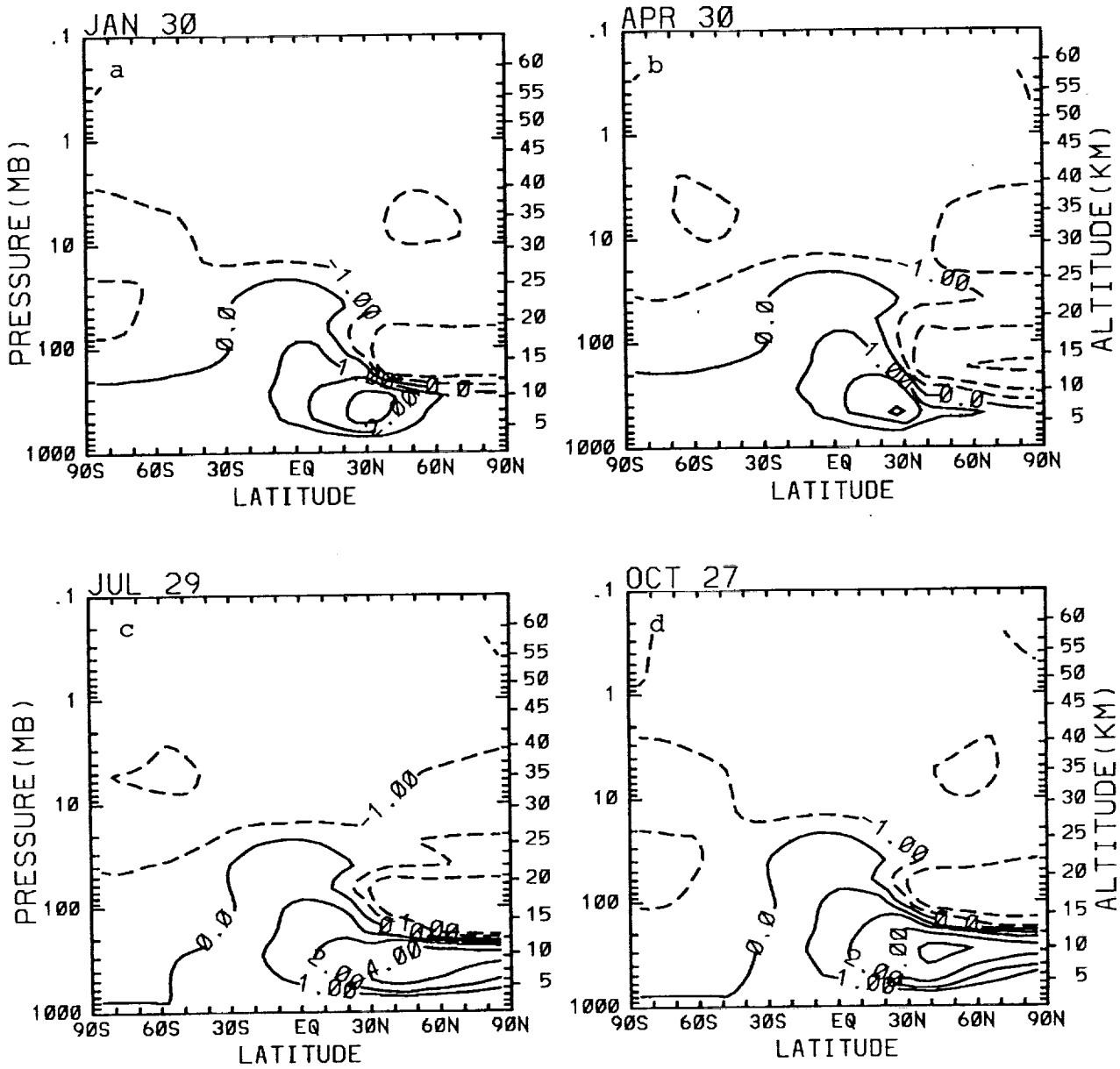

Figure 11. The calculated percent change in ozone mixing ratio from the baseline case (shown in Figure A2) for Scenario B7, as a function of latitude and altitude for (a) January, (b) April, (c) July, and (d) October. Contour levels are 0, ±1, ±2, ±4%.

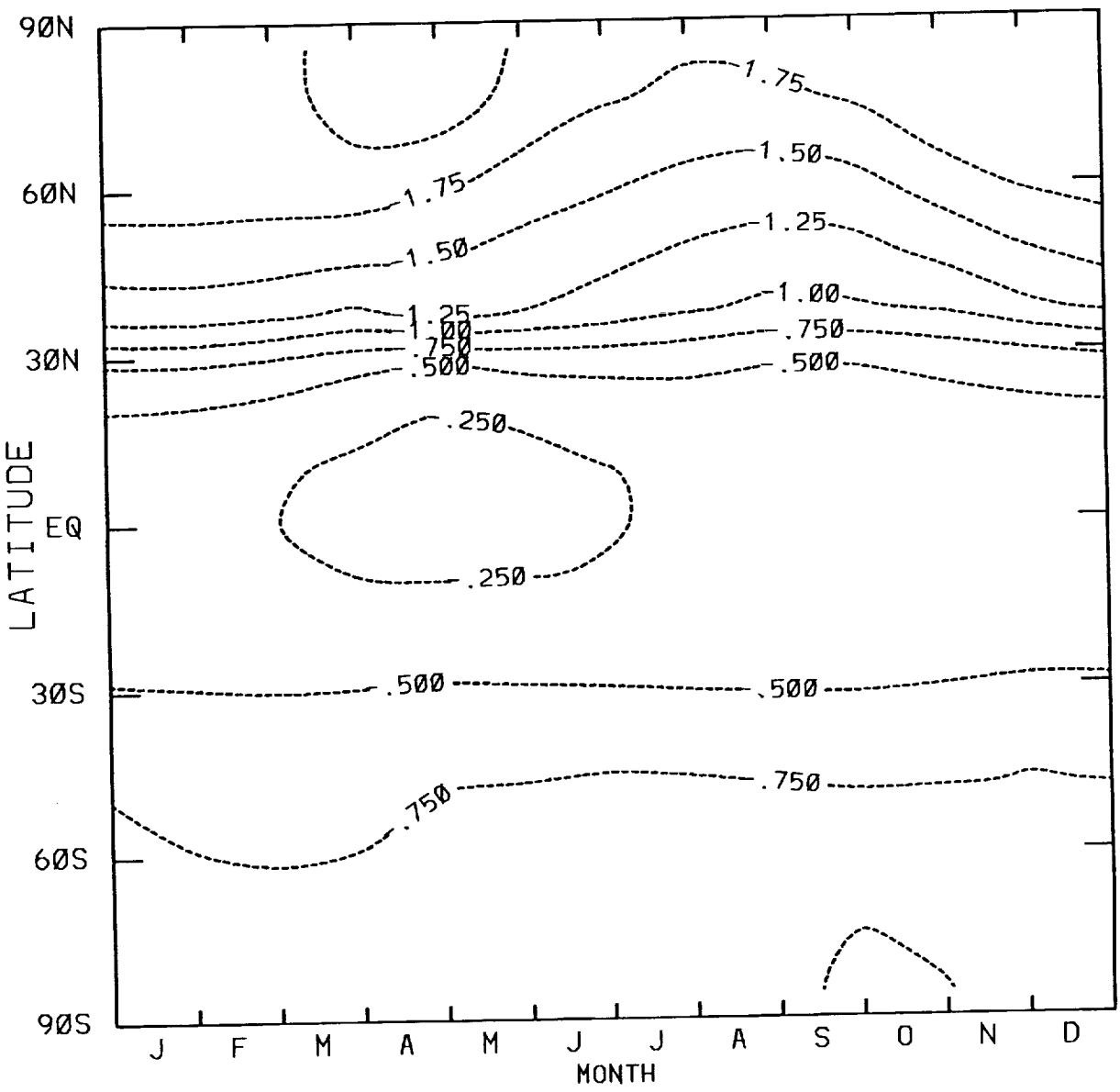

Figure 12. The calculated percent change in total ozone column from the baseline case [shown in Figure A1 (a)] for Scenario B7, as a function of latitude and time of year.

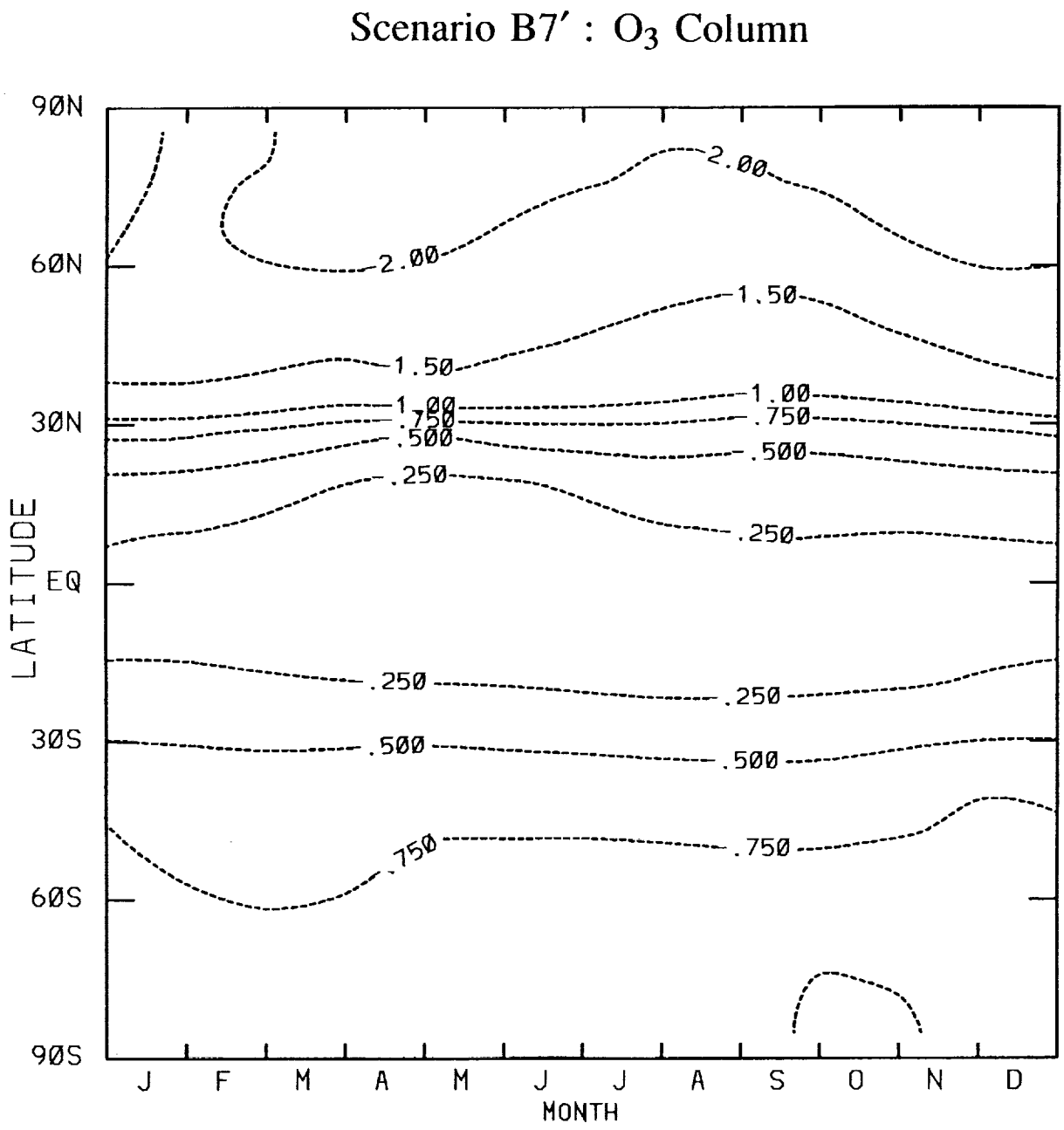

Figure 13. The calculated percent change in total ozone column from the baseline case for Scenario B7′, as a function of latitude and time of year. Emissions were the same as B7 except that the emissions of CO, H_2O, and CH_4 were not included in the calculation.

Scenario B8 : NOY

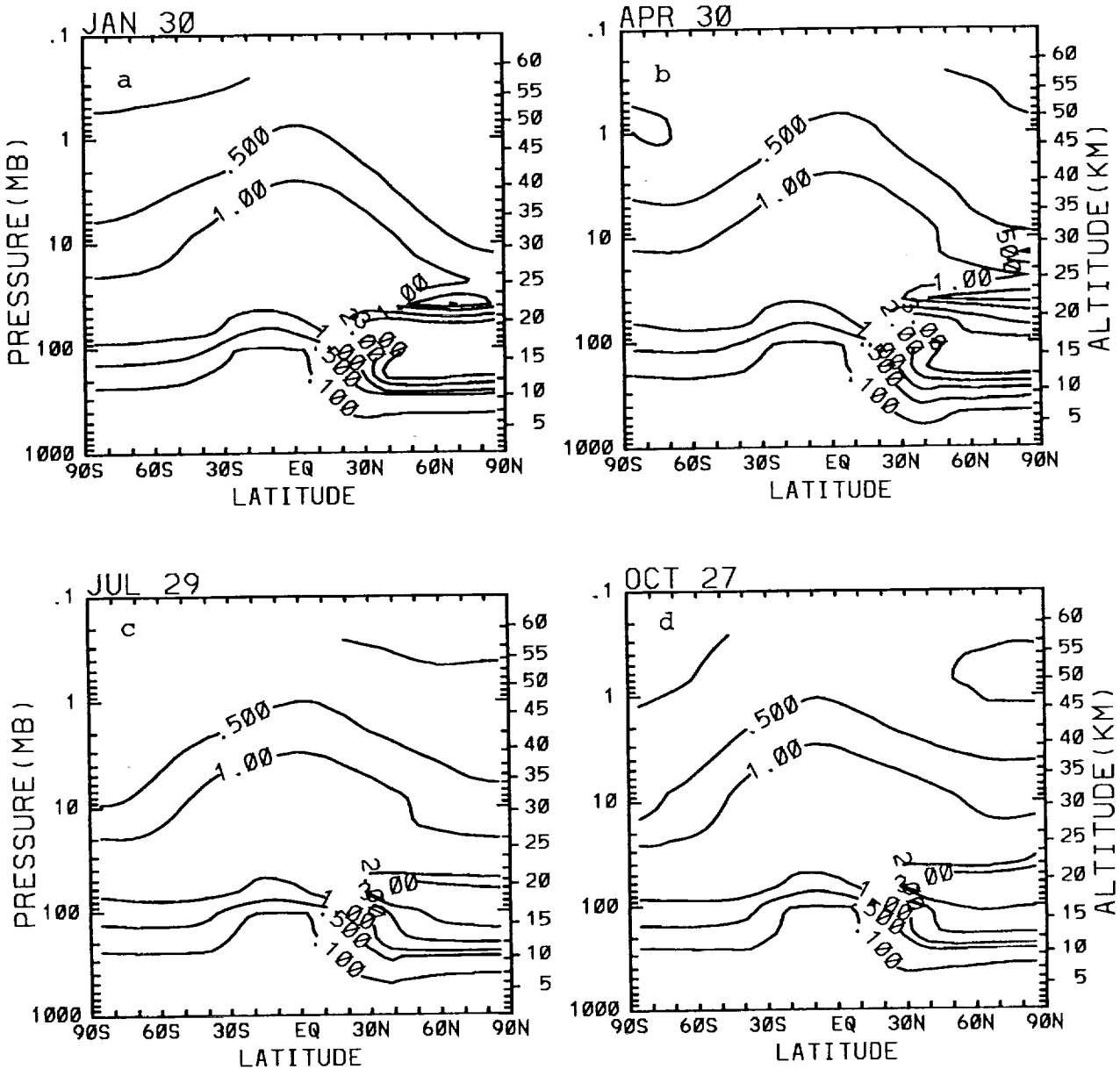

Figure 14. The calculated change in NOY in ppbv from the baseline case for Scenario B8, as a function of latitude and altitude for (a) January, (b) April, (c) July, and (d) October. Contour levels are 0.1, 0.5, 1.0, 2.0, 3.0 ppbv.

Scenario B8 : O_3

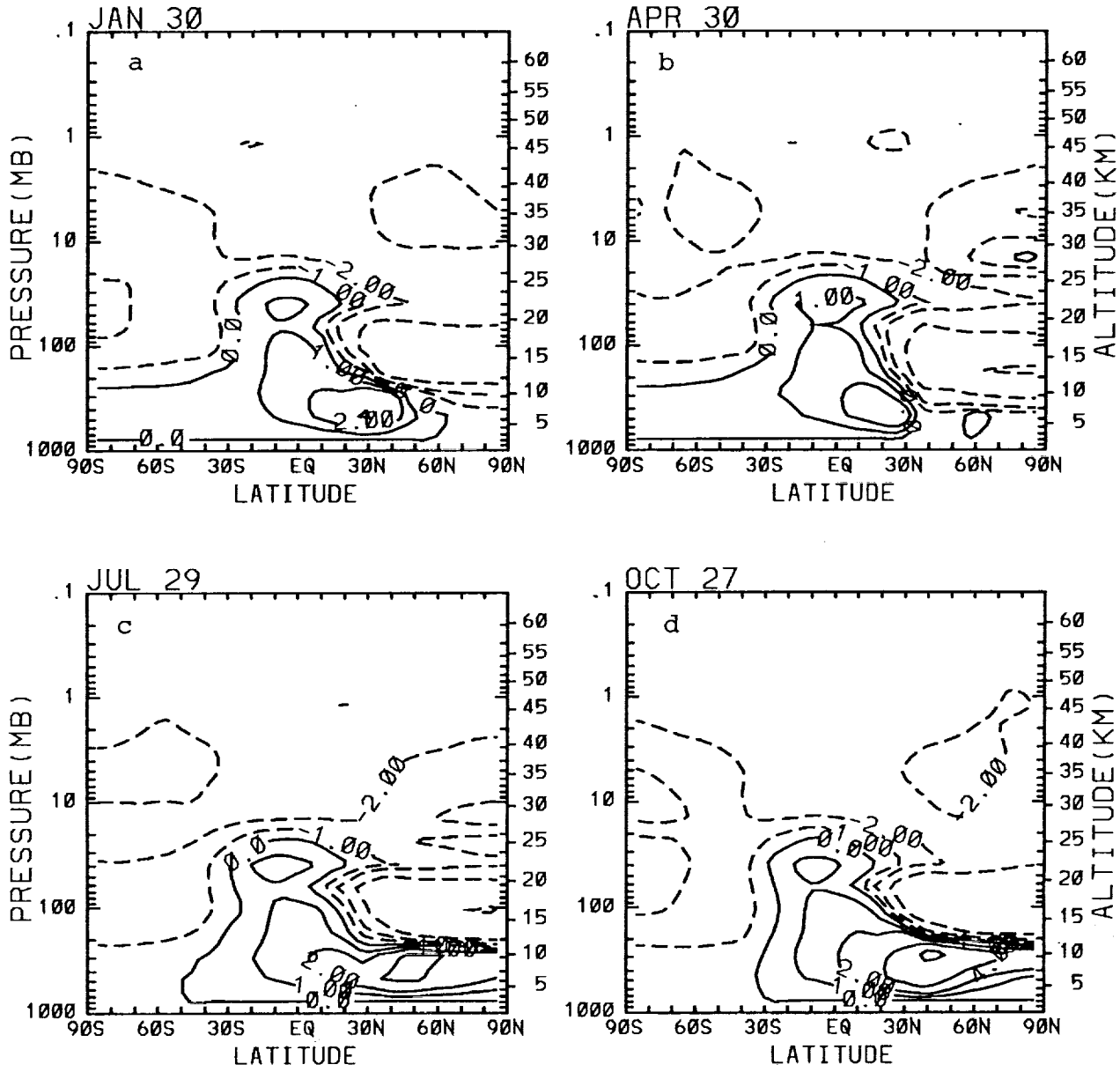

Figure 15. The calculated percent change in ozone mixing ratio from the baseline case for Scenario B8, as a function of latitude and altitude for (a) January, (b) April, (c) July, and (d) October. Contour levels are 0, ±1, ±2, ±4, ±8%.

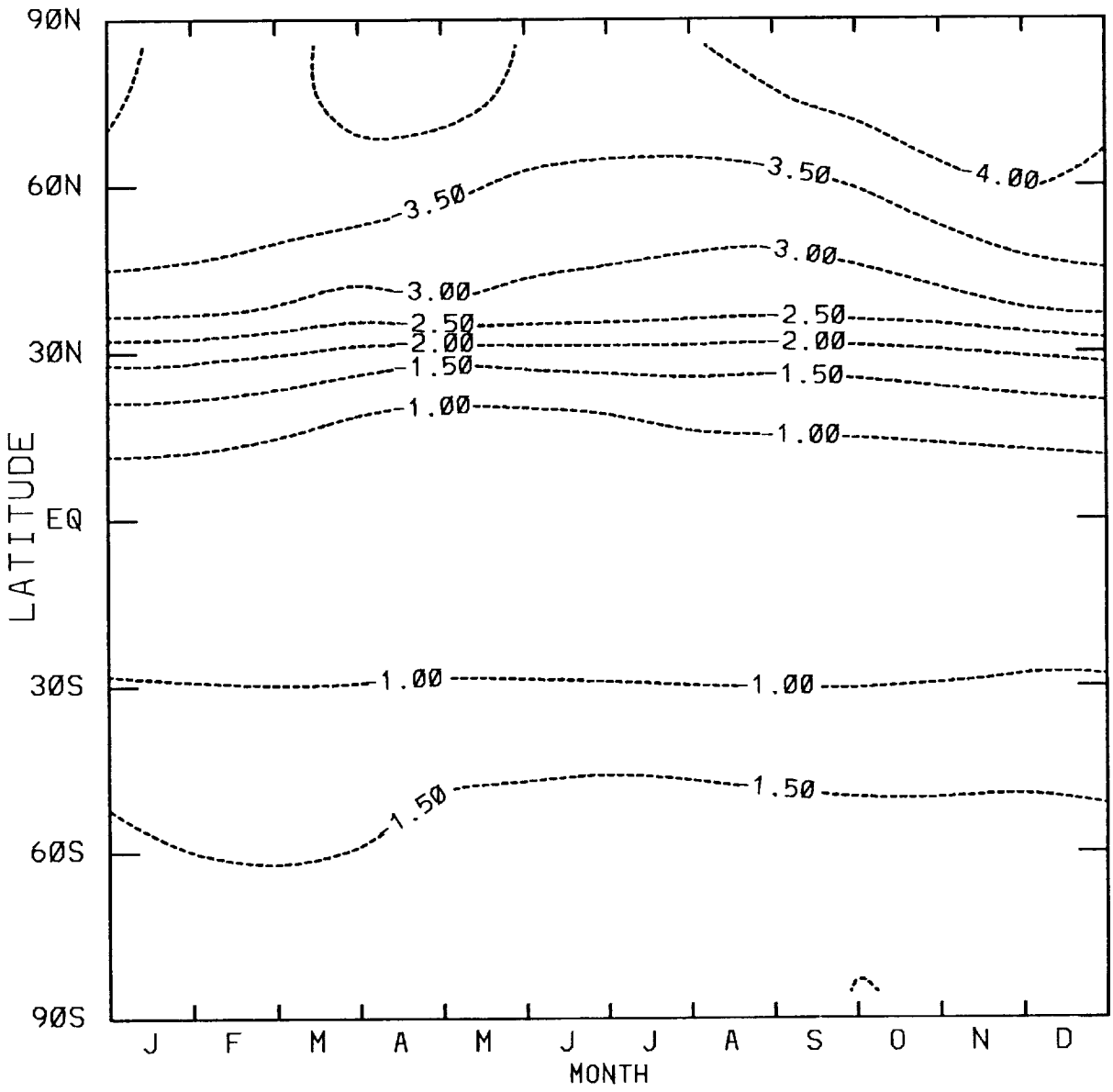

Figure 16. The calculated percent change in total ozone column from the baseline case for Scenario B8, as a function of latitude and time of year.

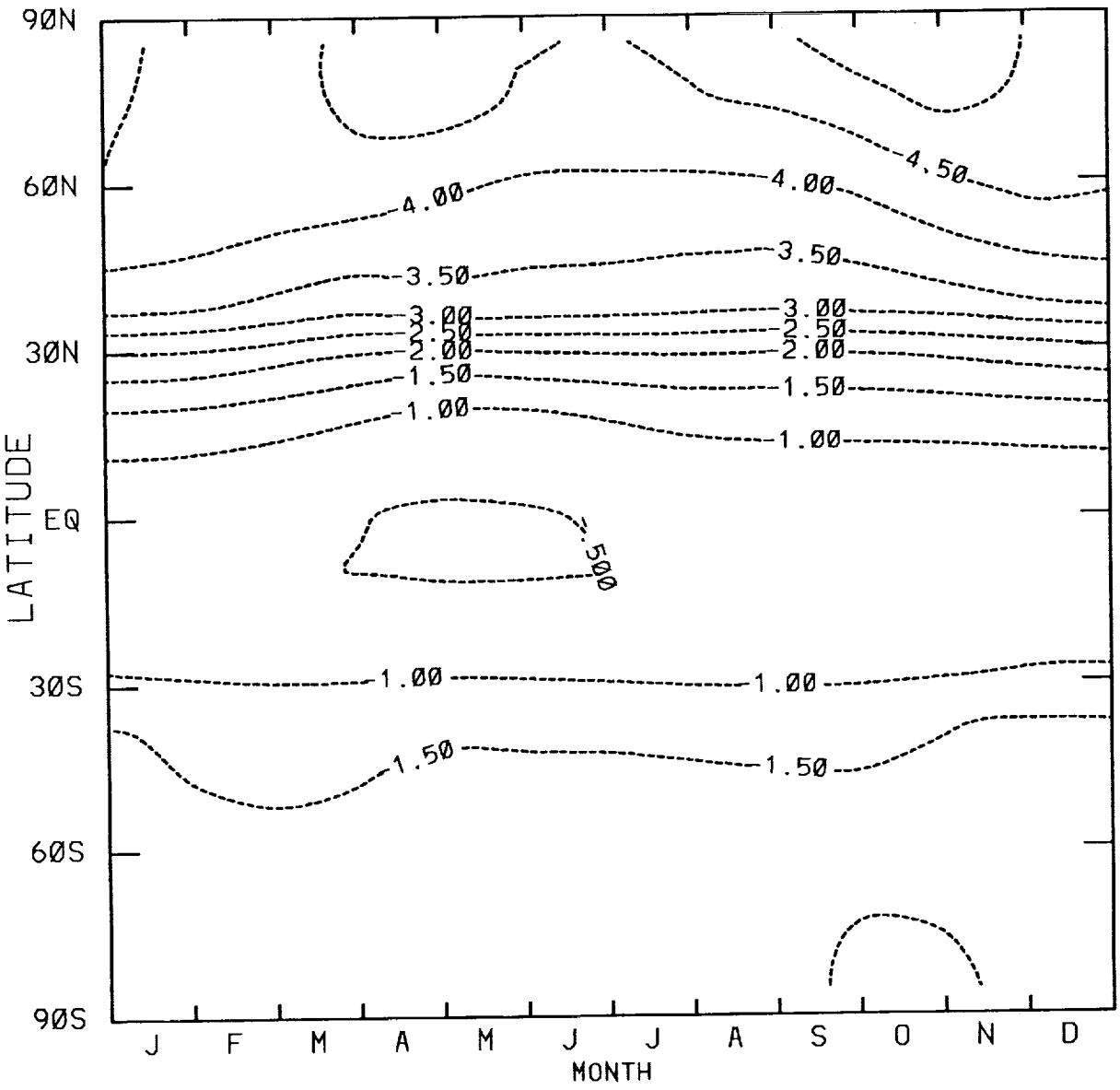

Figure 17. The calculated percent change in total ozone column from the baseline case for Scenario B8′, as a function of latitude and time of year. Emissions were the same as B8, except that emissions of CO, H_2O, and CH_4 were not included in the calculation.

Scenario B10 : NOY

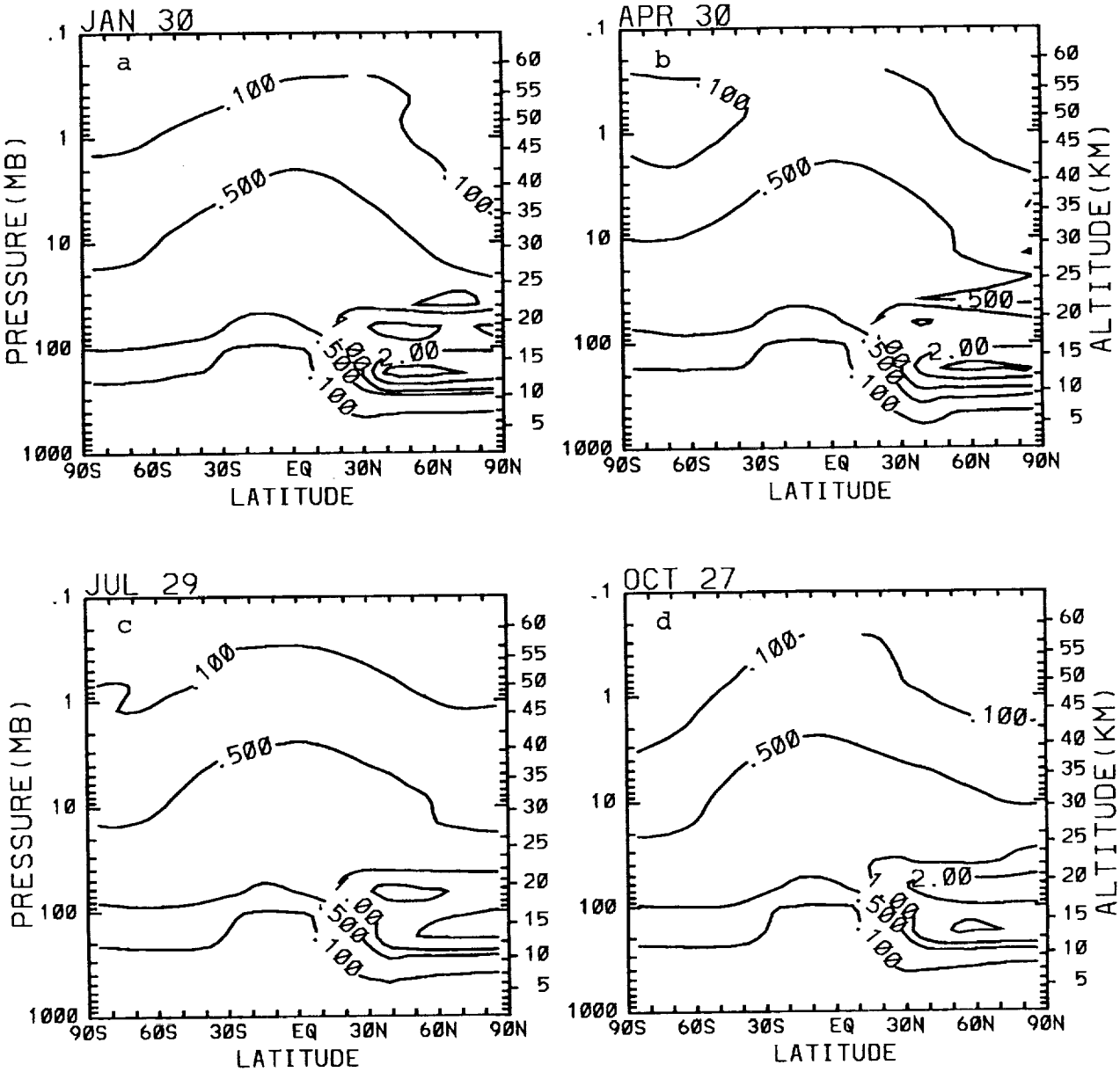

Figure 18. The calculated change in NOY in ppbv from the baseline case for Scenario B10, as a function of latitude and altitude for (a) January, (b) April, (c) July, and (d) October. Contour levels are 0.1, 0.5, 1.0, 2.0, 3.0 ppbv.

Scenario B10 : O_3

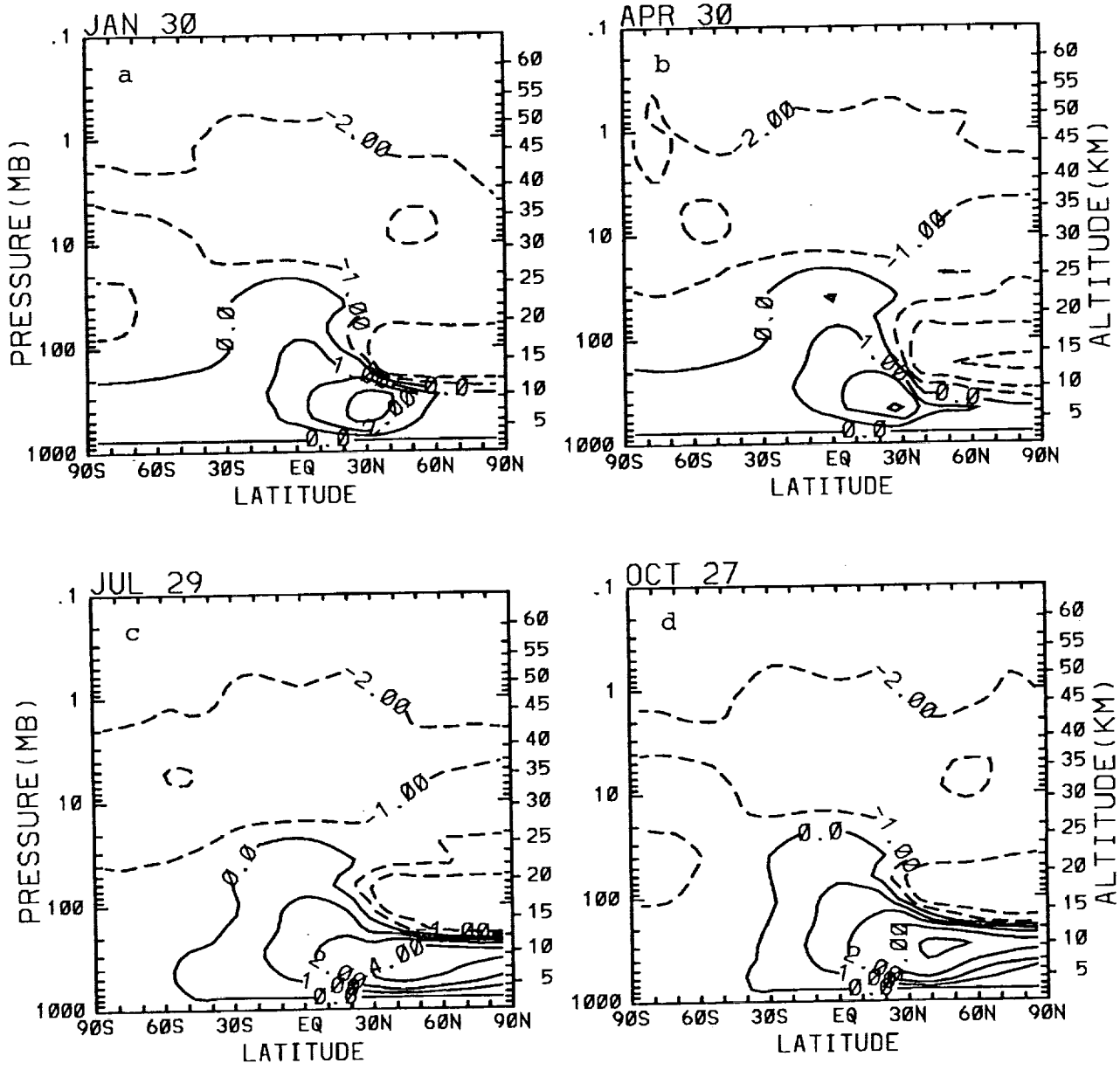

Figure 19. The calculated percent change in ozone mixing ratio from the baseline case for Scenario B10, as a function of latitude and altitude for (a) January, (b) April, (c) July, and (d) October. Contour levels are 0, ±1, ±2, ±4, ±8%.

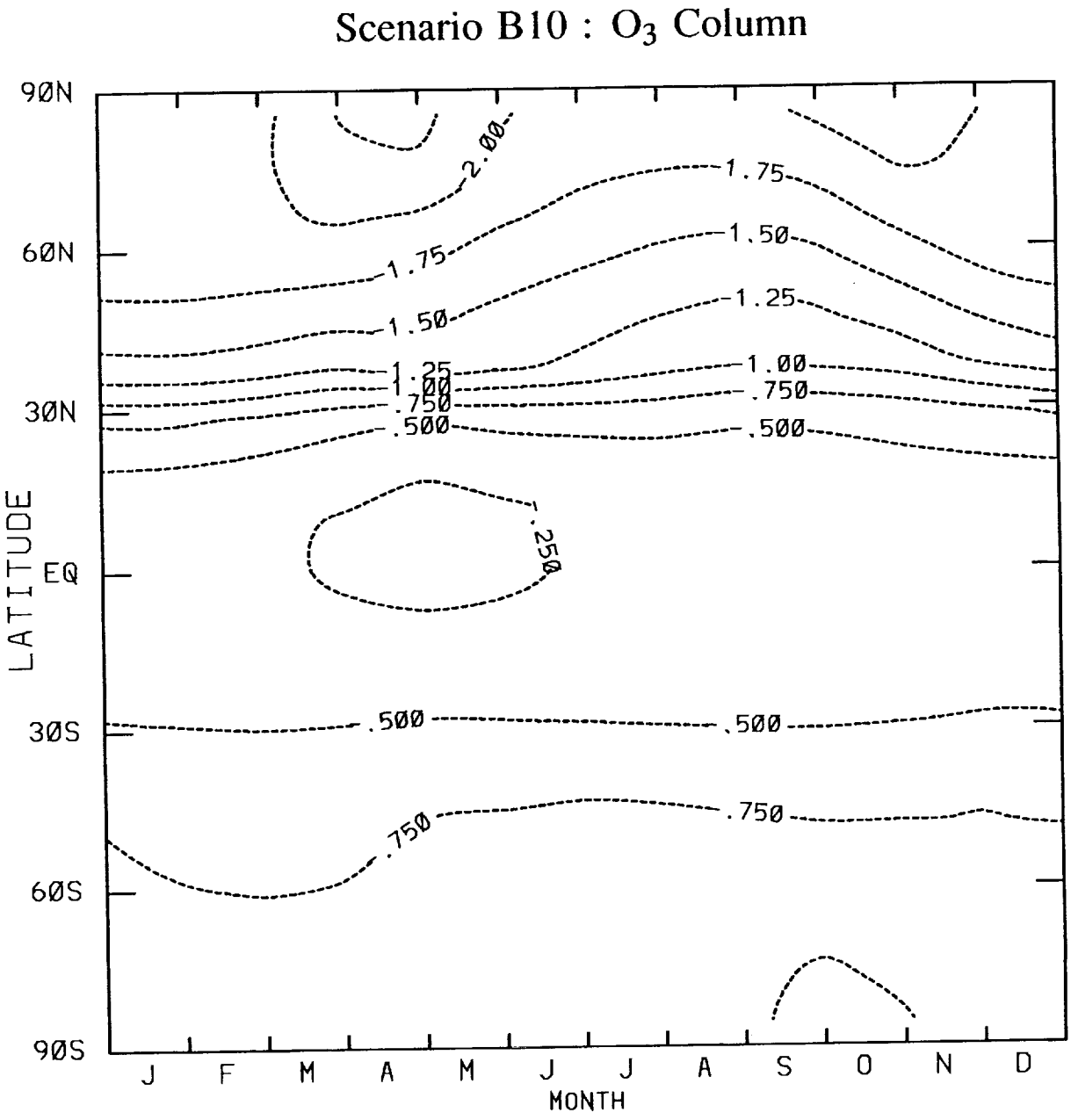

Figure 20. The calculated percent change in total ozone column from the baseline case for Scenario B10, as a function of latitude and time of year.

Scenario A3 : NOY

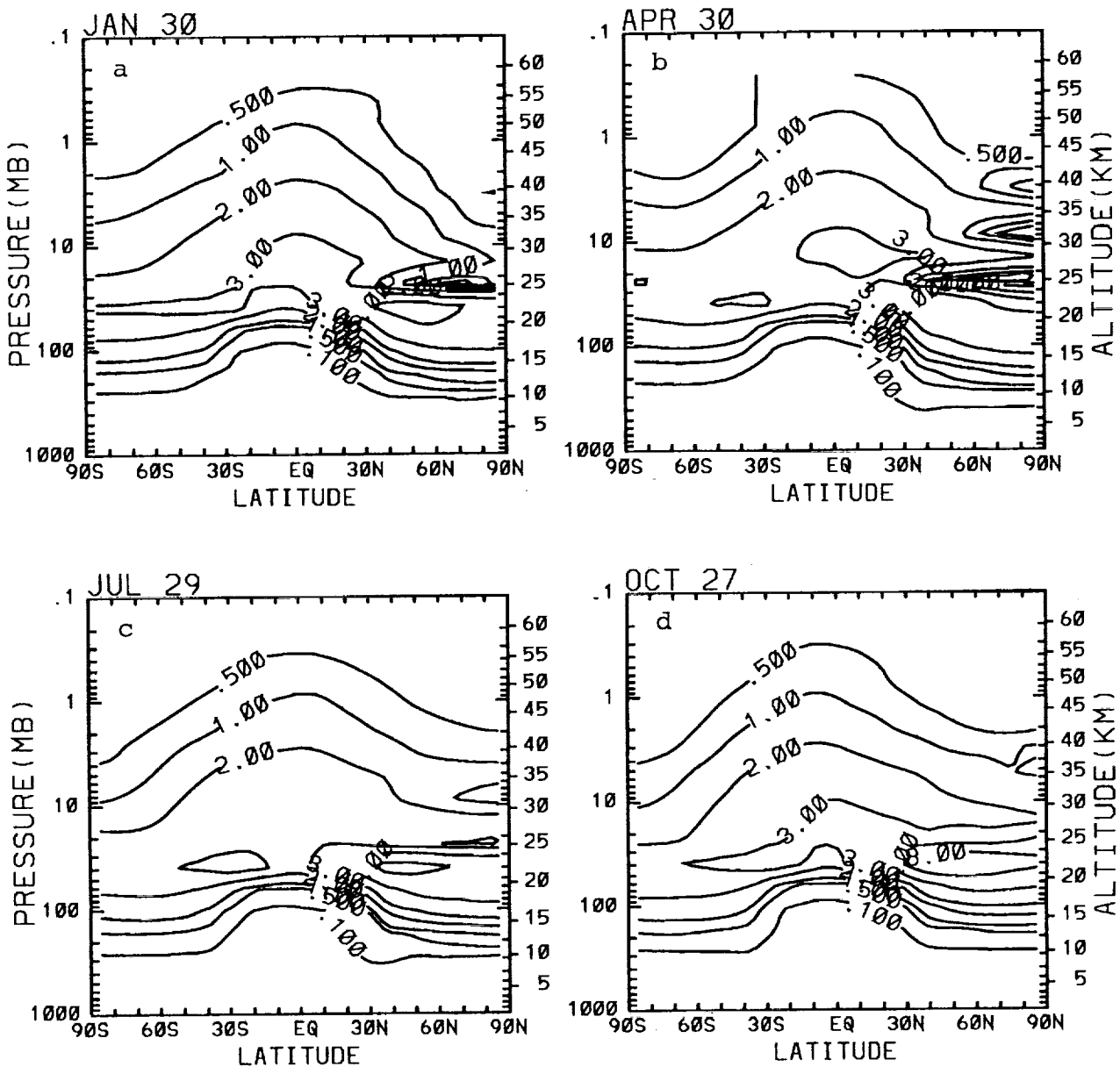

Figure 21. The calculated change in NOY in ppbv from the baseline case for Scenario A3, as a function of latitude and altitude for (a) January, (b) April, (c) July, and (d) October. Contour levels are 0.5, 1.0, 2.0, 3.0, 5.0, 8.0 ppbv.

Scenario A3 : O_3

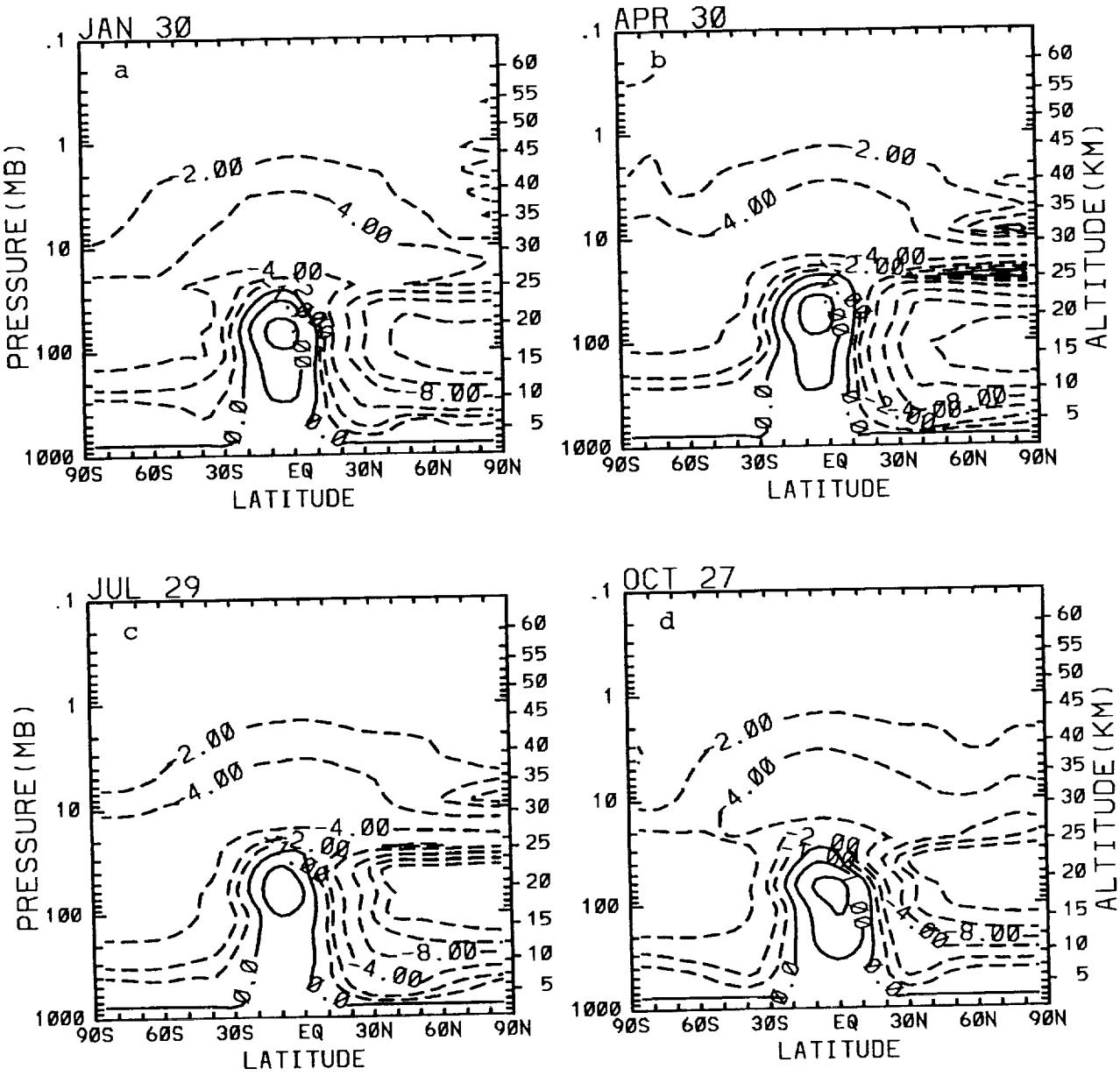

Figure 22. The calculated percent change in ozone mixing ratio from the baseline case for Scenario A3, as a function of latitude and altitude for (a) January, (b) April, (c) July, and (d) October. Contour levels are 0, ±1, ±2, ±4, ±8, ±12, ±16%.

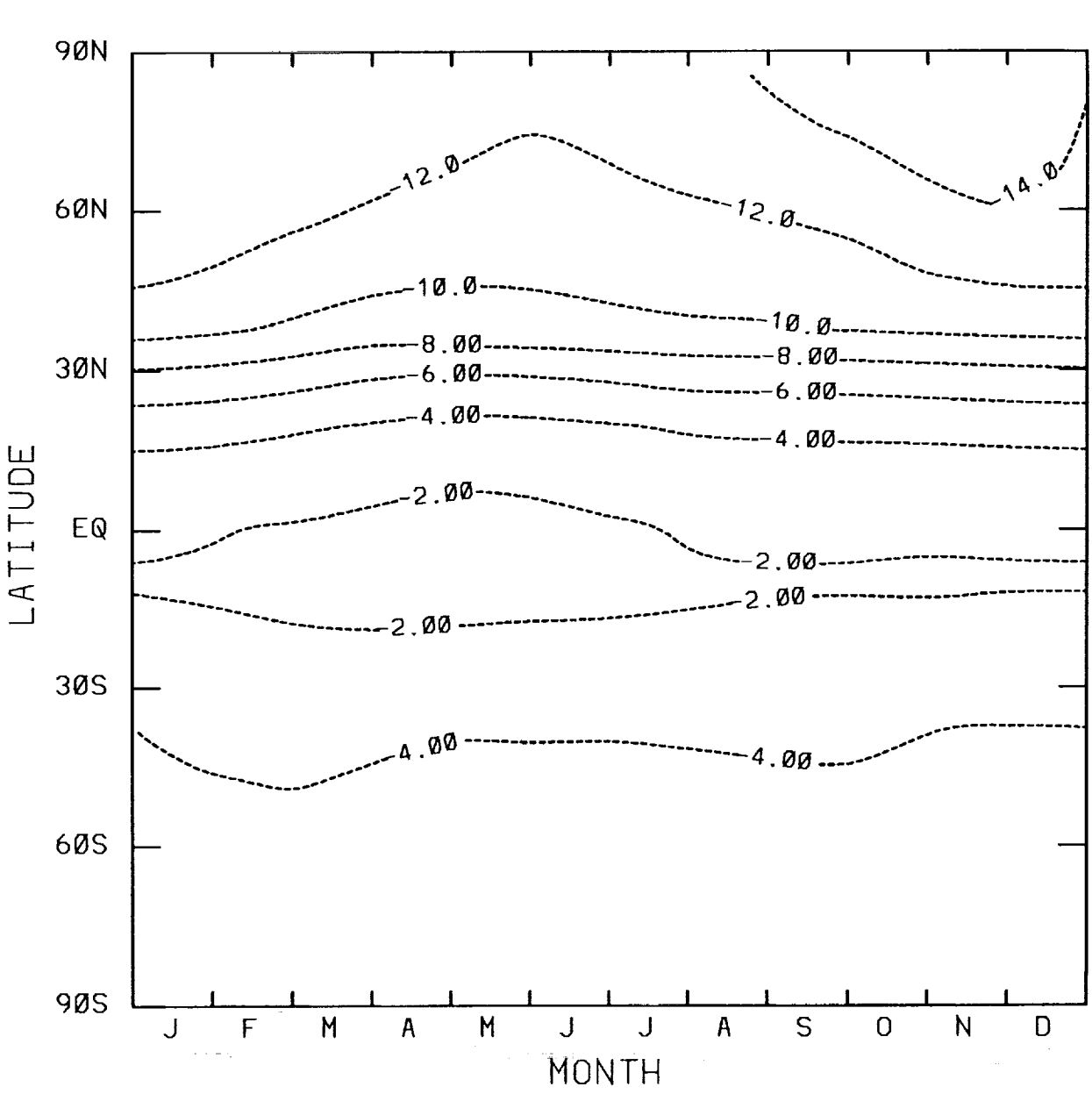

Figure 23. The calculated percent change in total ozone column from the baseline case for Scenario A3, as a function of latitude and time of year.

Scenario A4 : NOY

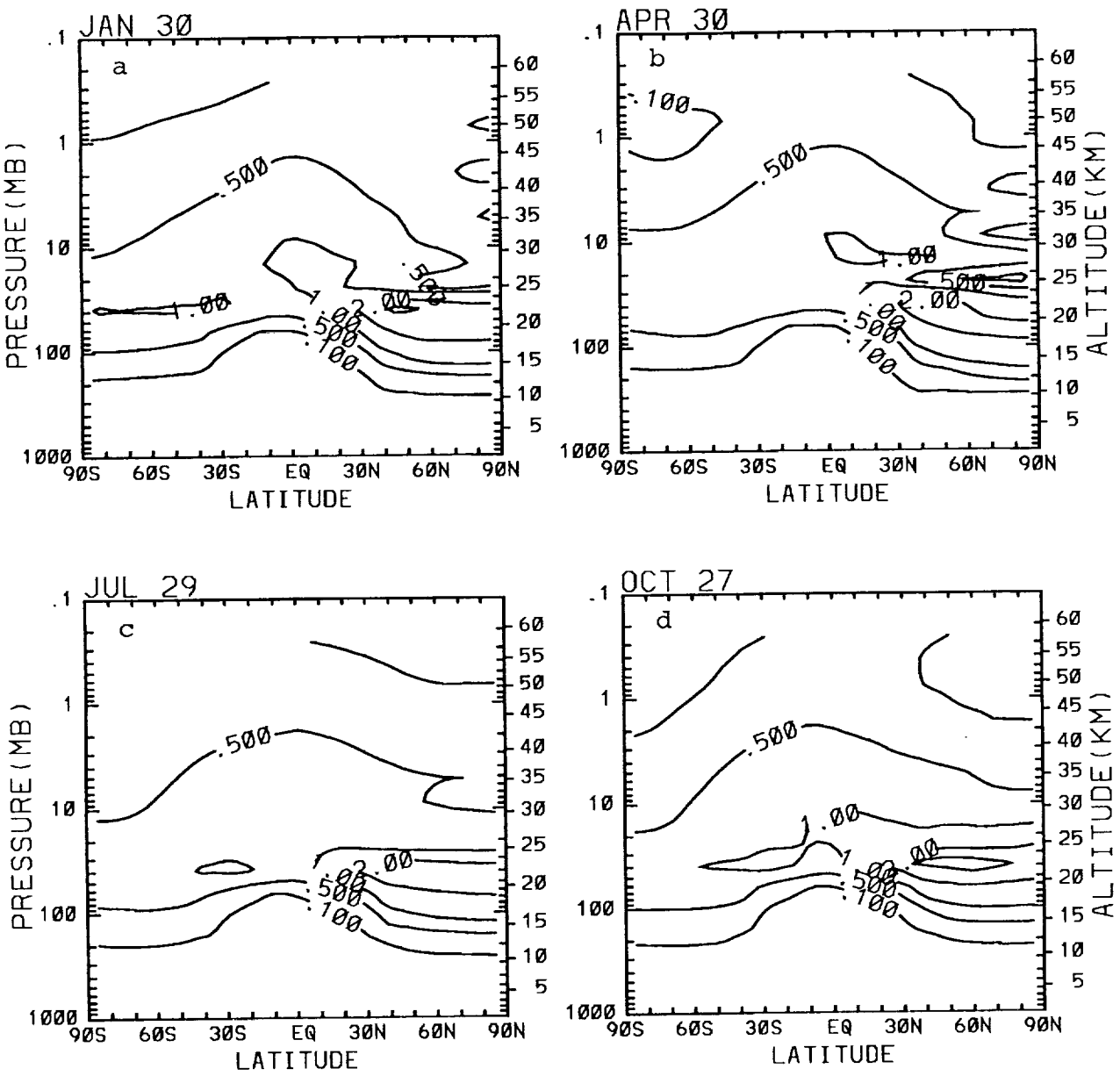

Figure 24. The calculated change in NOY in ppbv from the baseline case for Scenario A4, as a function of latitude and altitude for (a) January, (b) April, (c) July, and (d) October. Contour levels are 0.1, 0.5, 1.0, 2.0, 3.0 ppbv.

Scenario A4 : O_3

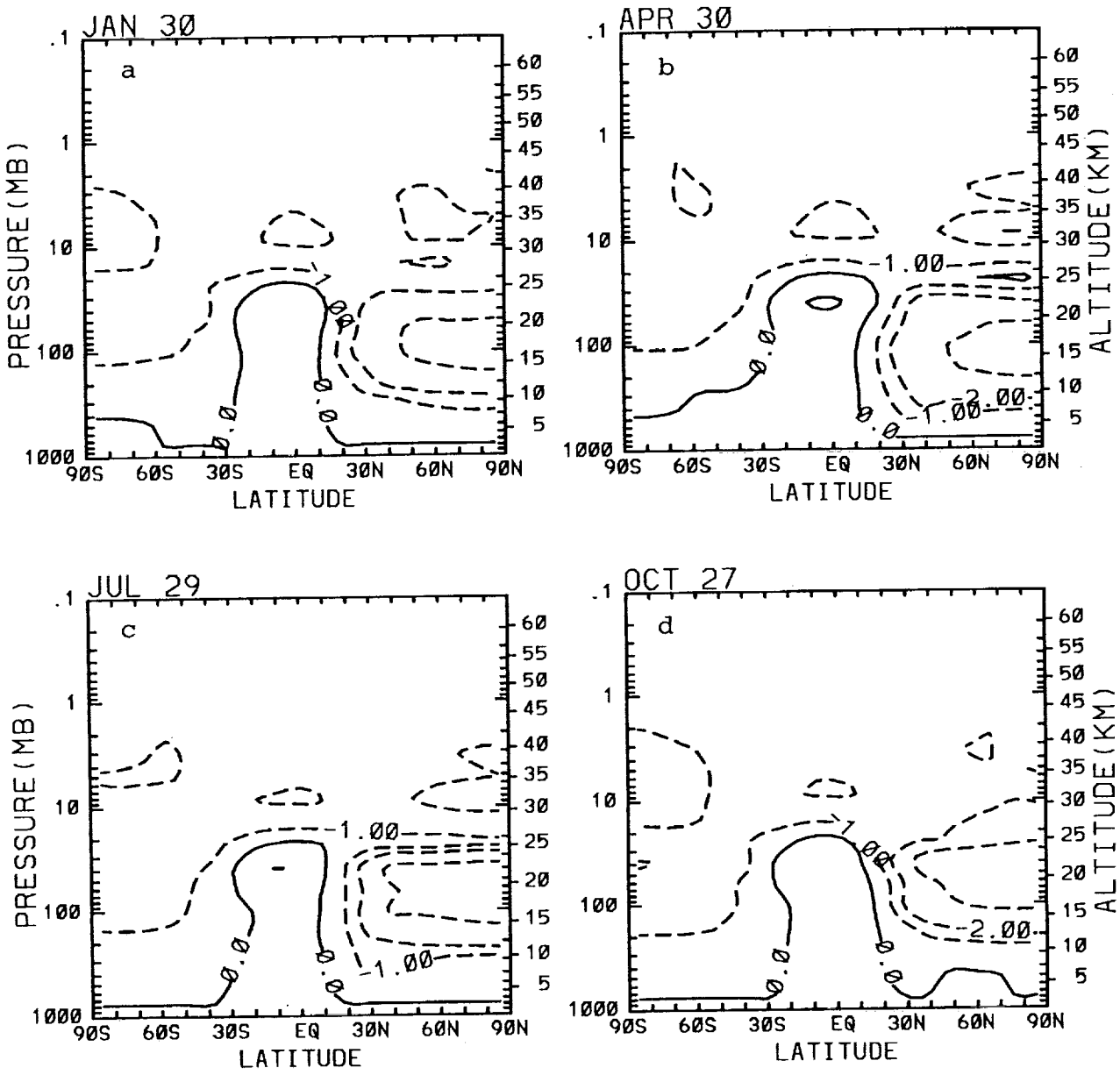

Figure 25. The calculated percent change in ozone mixing ratio from the baseline case for Scenario A4, as a function of latitude and altitude for (a) January, (b) April, (c) July, and (d) October. Contour levels are 0, ±1, ±2, ±4%.

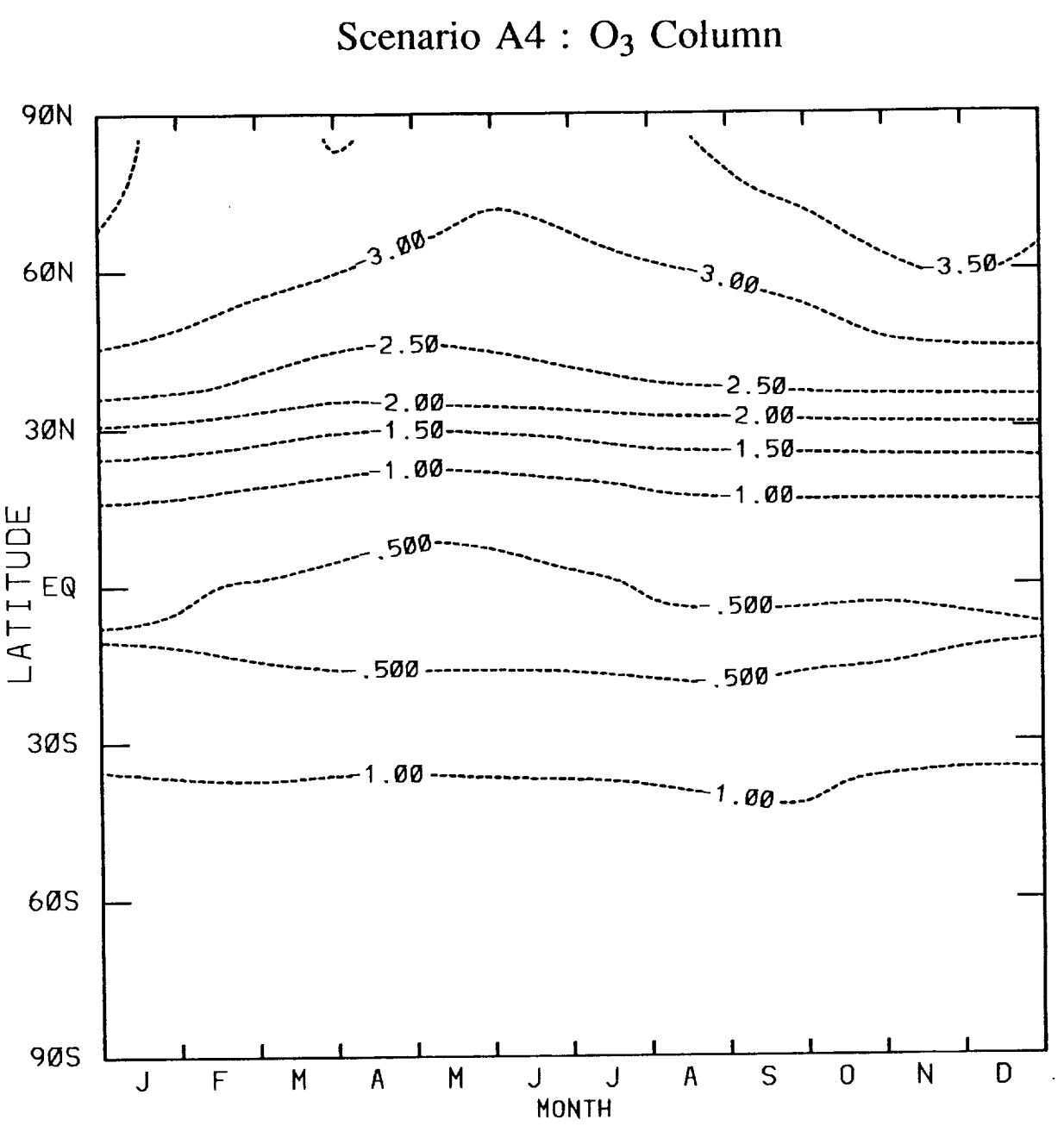

Figure 26. The calculated percent change in total ozone column from the baseline case for Scenario A4, as a function of latitude and time of year.

Scenario A5 : NOY

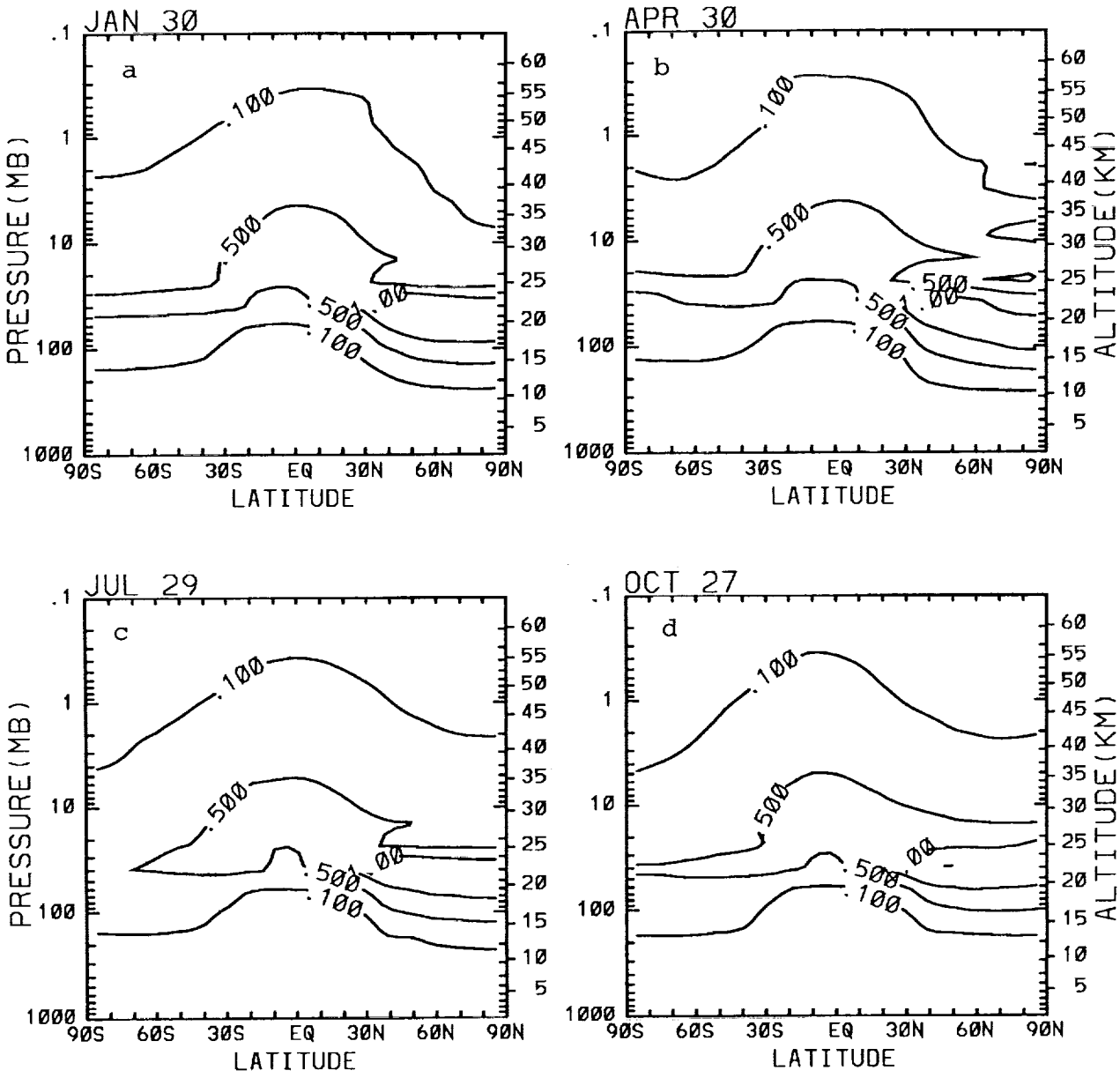

Figure 27. The calculated change in NOY in ppbv from the baseline case for Scenario A5, as a function of latitude and altitude for (a) January, (b) April, (c) July, and (d) October. Contour levels are 0.1, 0.5, 1.0 ppbv.

Scenario A5 : O_3

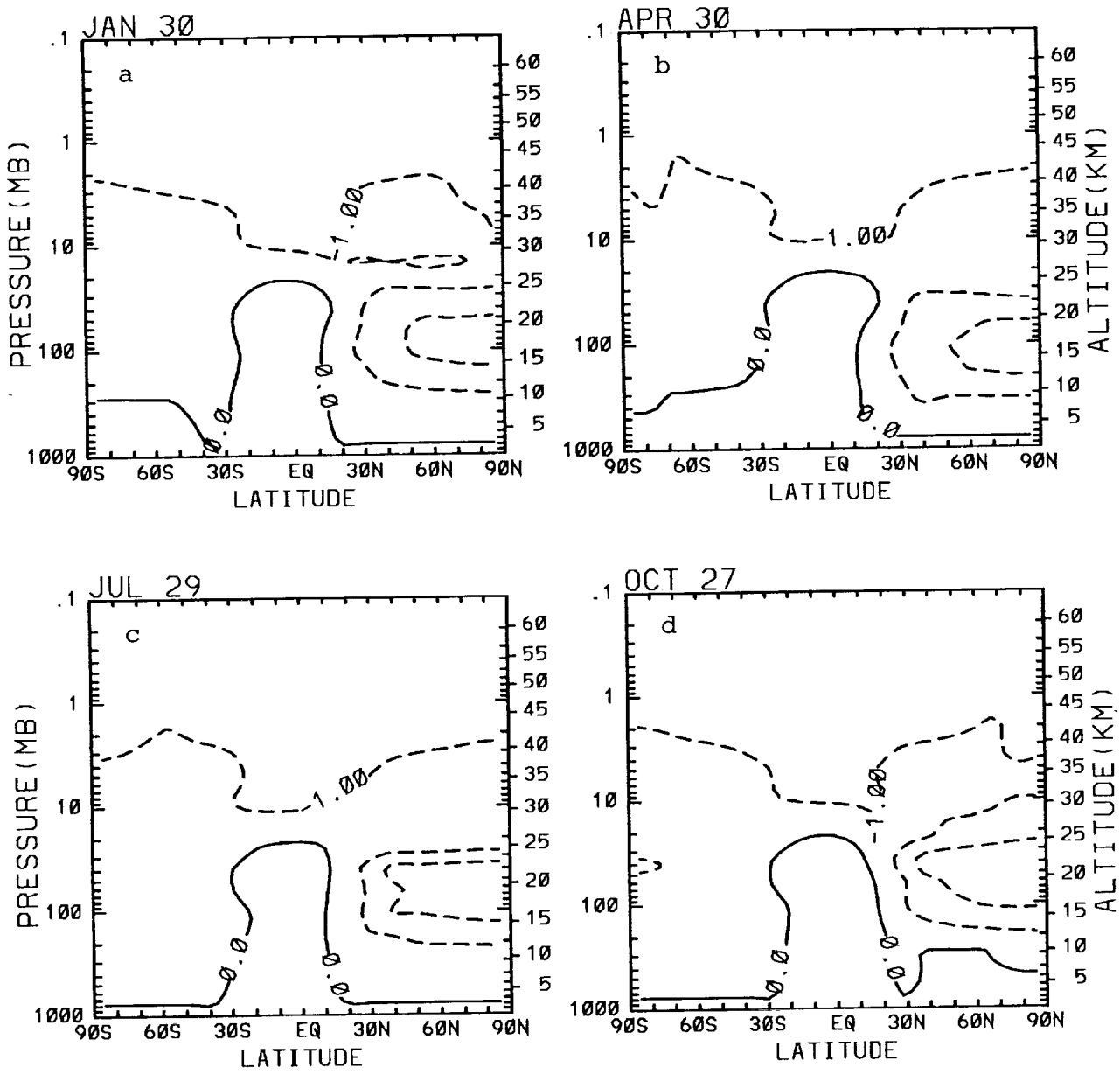

Figure 28. The calculated percent change in ozone mixing ratio from the baseline case for Scenario A5, as a function of latitude and altitude for (a) January, (b) April, (c) July, and (d) October. Contour levels are 0, ±1, ±2%.

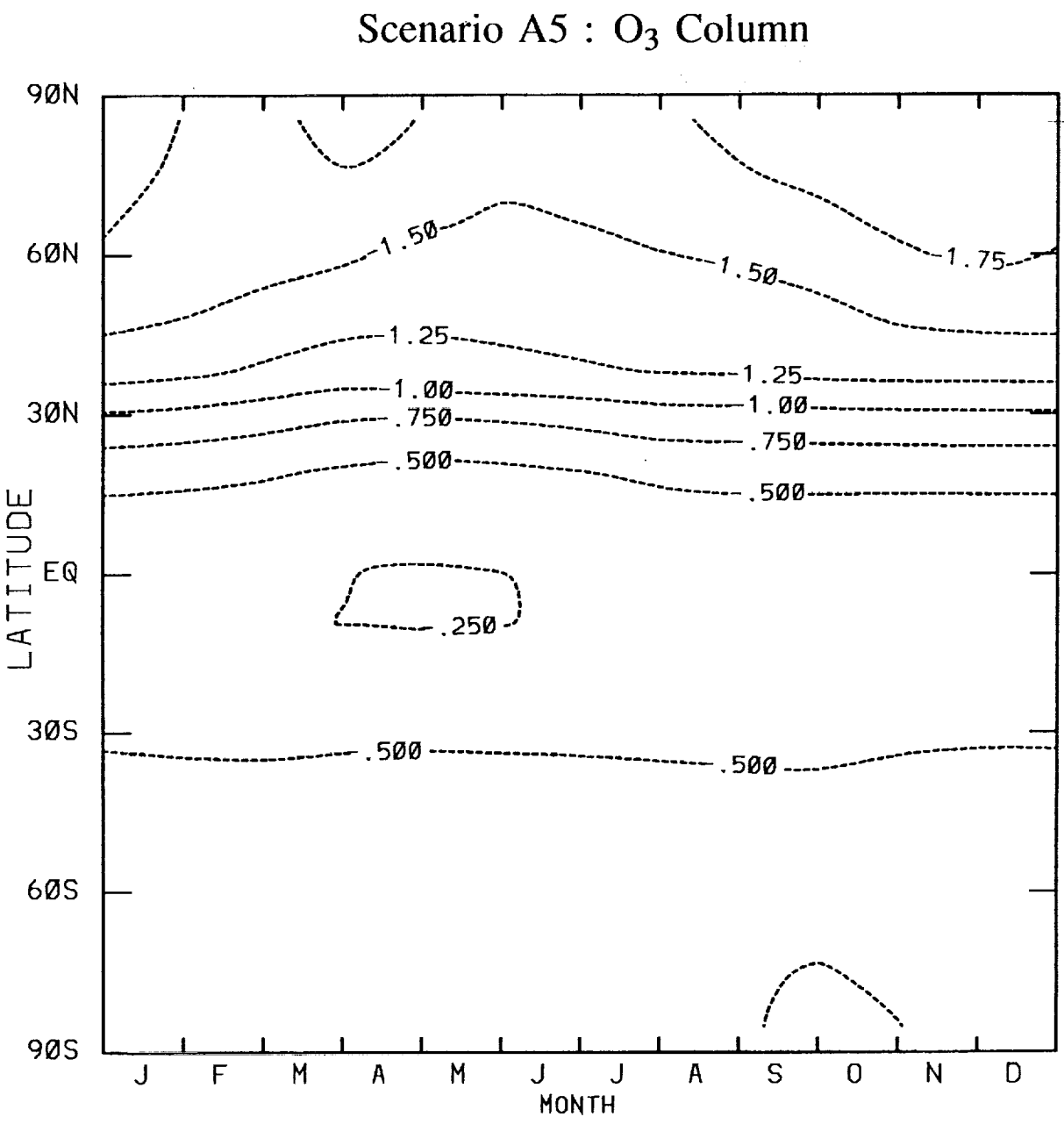

Figure 29. The calculated percent change in total ozone column from the baseline case for Scenario A5, as a function of latitude and time of year.

Case 1 : NOY

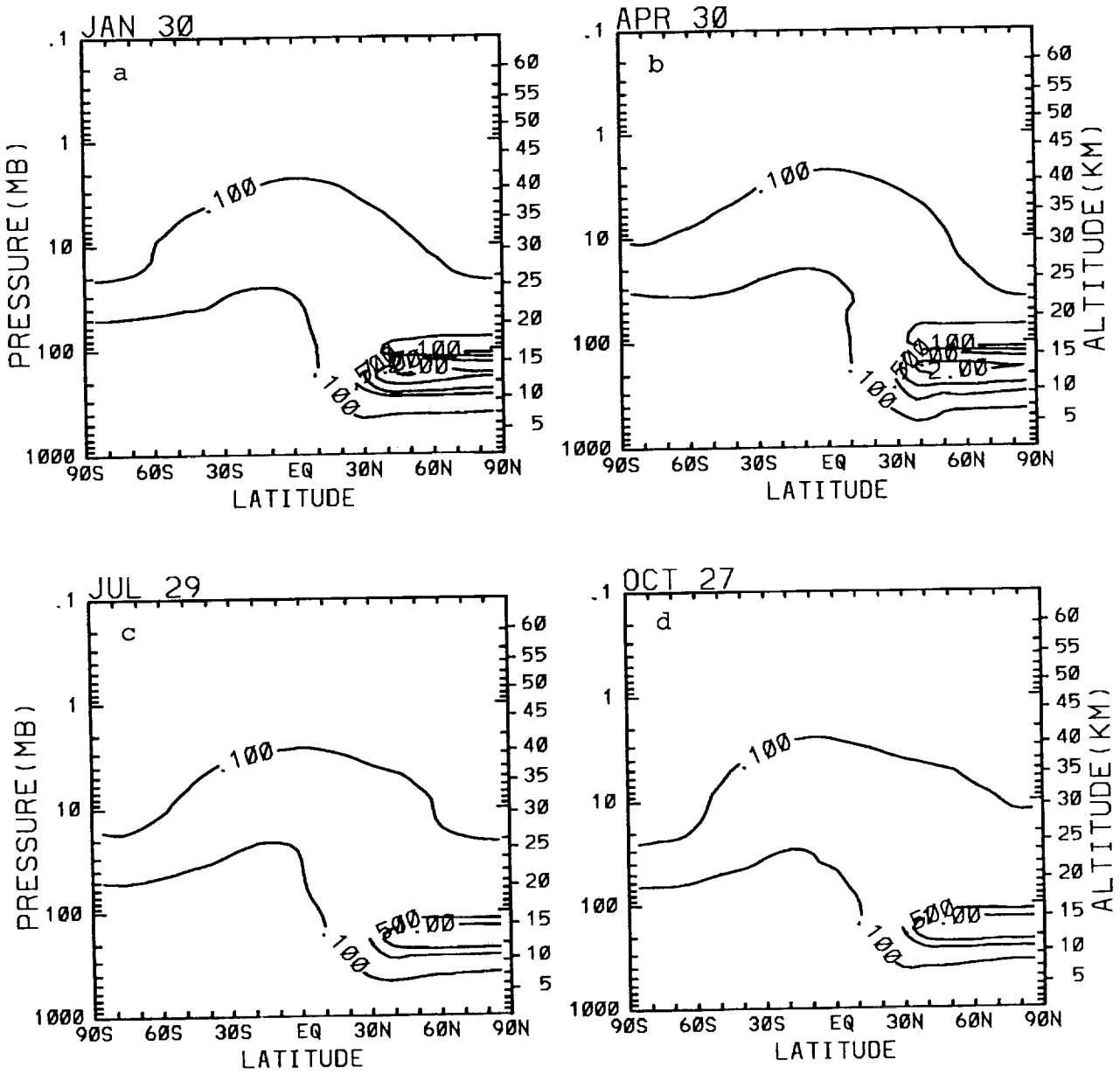

Figure 30. The calculated change in NOY in ppbv from the baseline case for Case 1, as a function of latitude and altitude for (a) January, (b) April, (c) July, and (d) October. Emissions were the same as the Scenario B8 emissions, but at altitude levels 8-12 km and 12-14 km only. Contour levels are 0.1, 0.5, 1.0, 2.0, 3.0 ppbv.

Case 1 : O_3

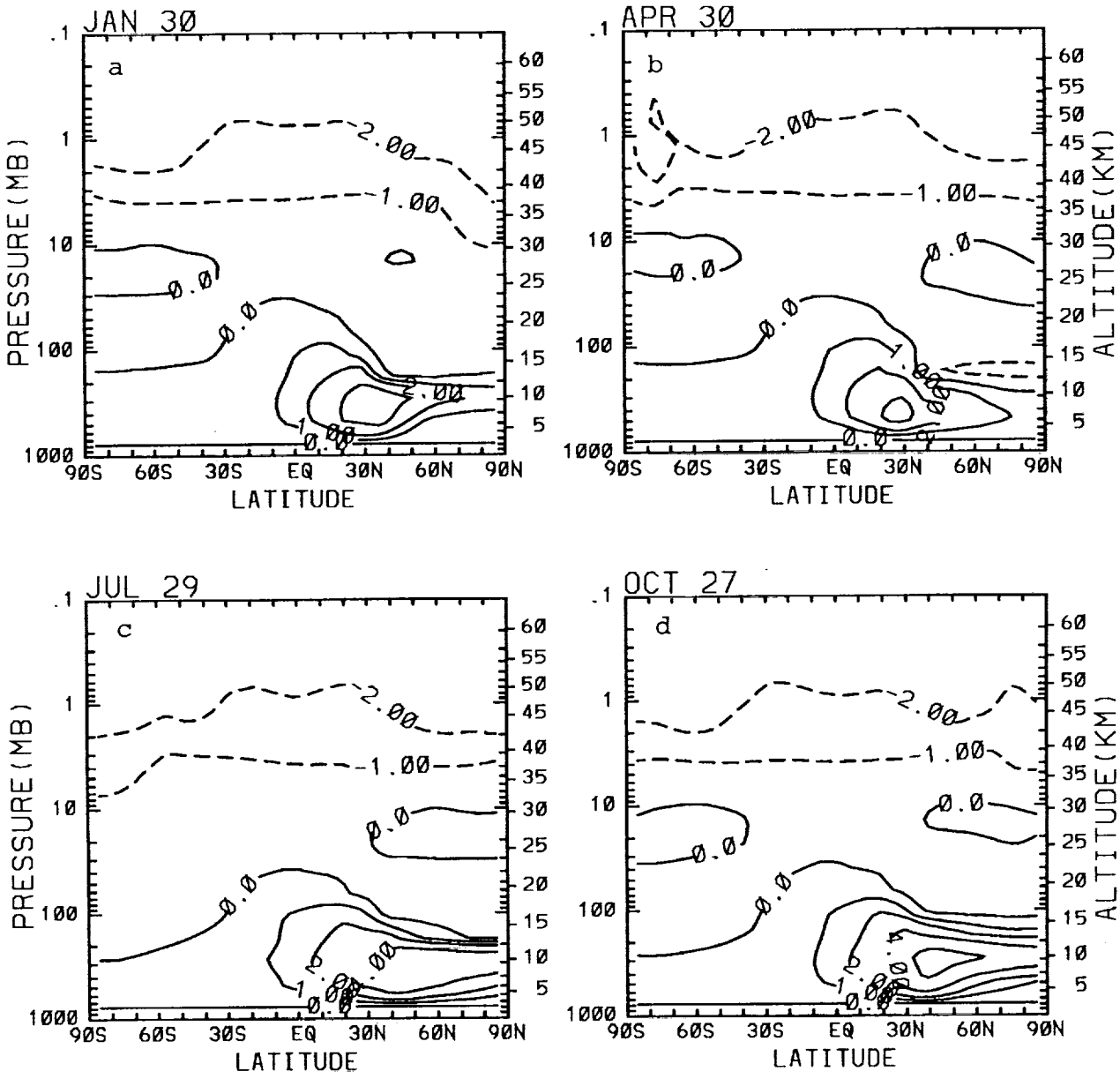

Figure 31. The calculated percent change in ozone mixing ratio from the baseline case for Case 1, as a function of latitude and altitude for (a) January, (b) April, (c) July, and (d) October. Contour levels are 0, ±1, ±2, ±4, ±8%.

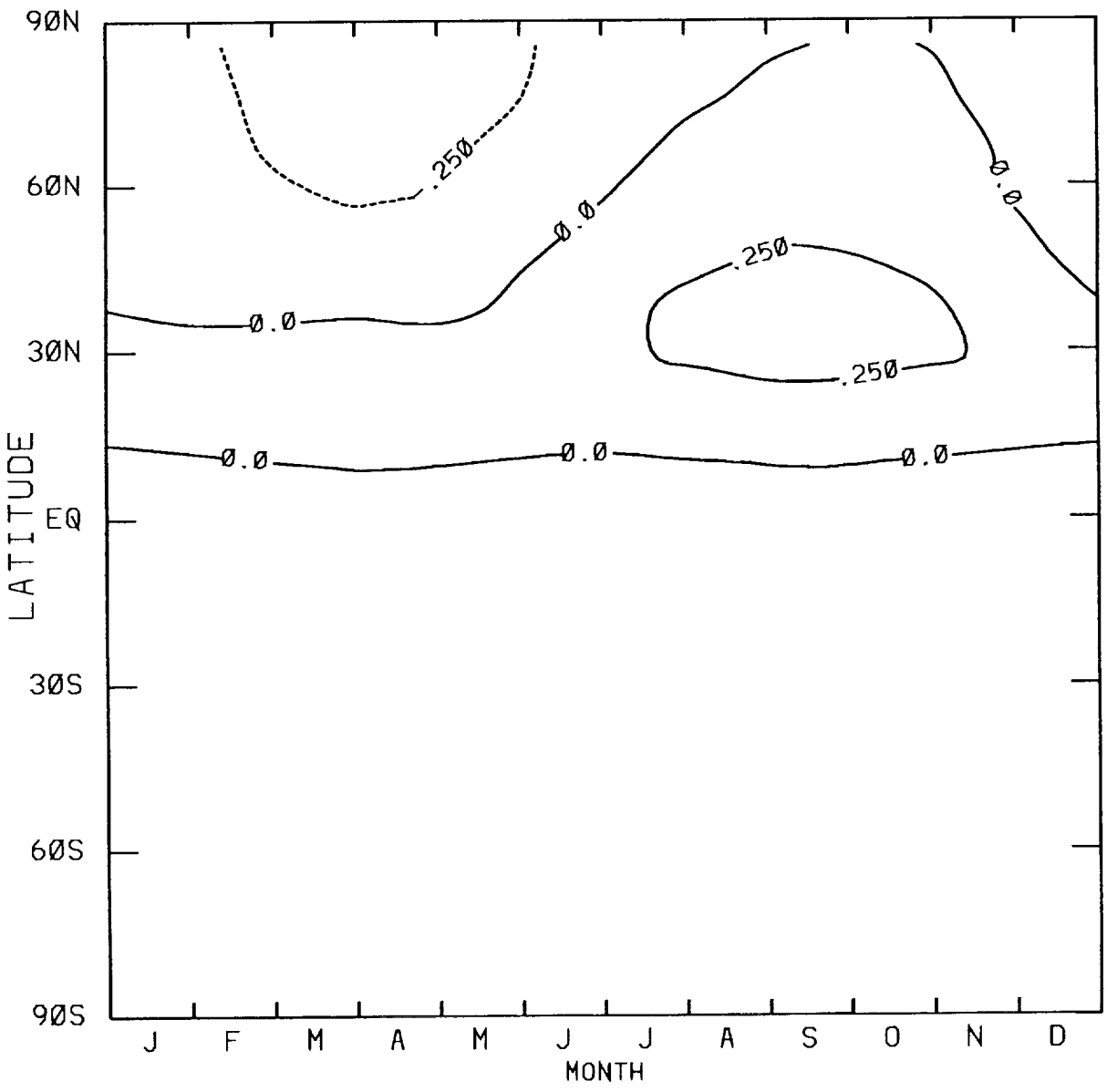

Figure 32. The calculated percent change in total ozone column from the baseline case for Case 1, as a function of latitude and time of year.

Case 2 : NOY

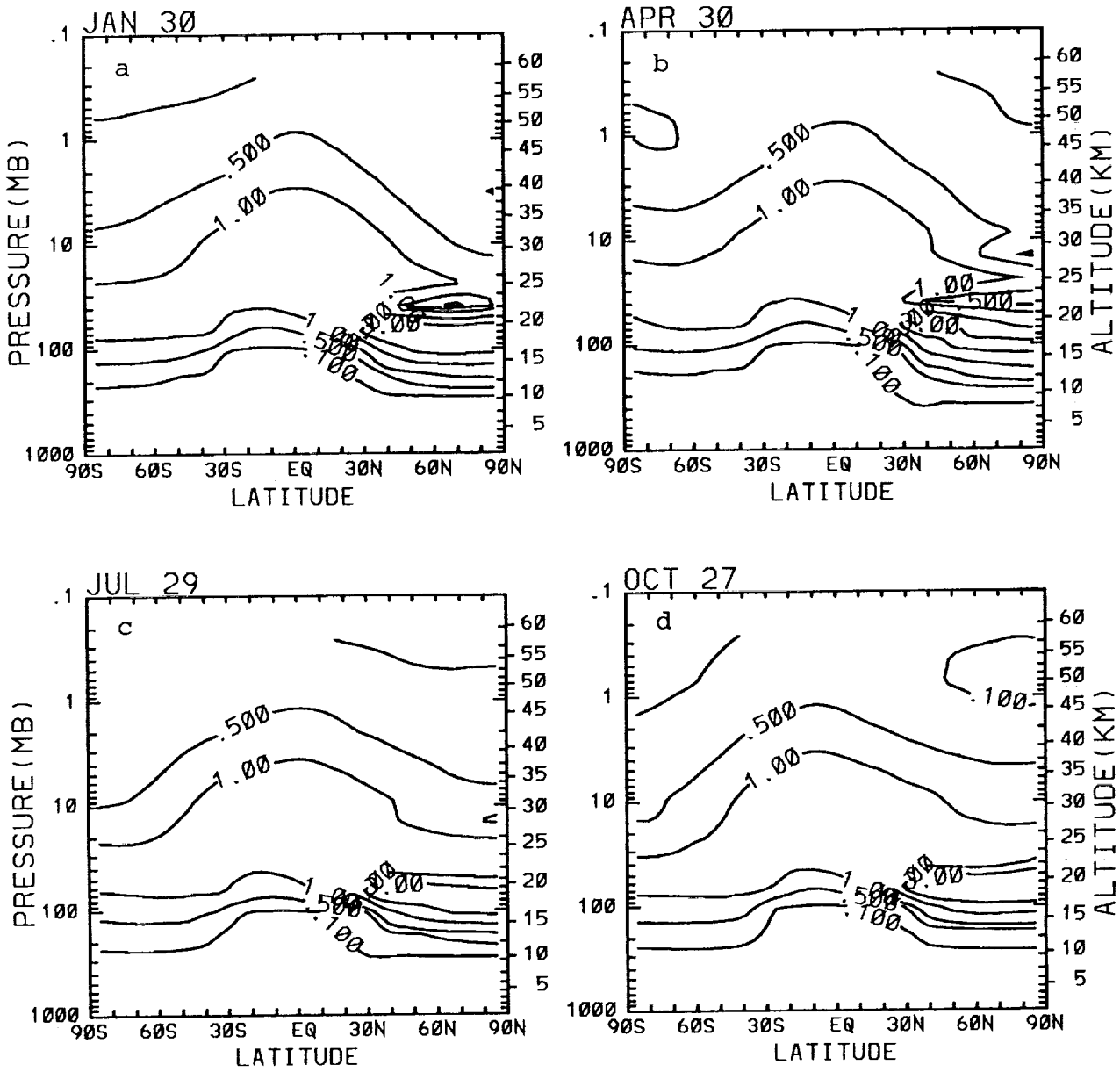

Figure 33. The calculated change in NOY in ppbv from the baseline case for Case 2, as a function of latitude and altitude for (a) January, (b) April, (c) July, and (d) October. Emissions were the same as the Scenario B8 emissions at altitude level 18-22 km only. Contour levels are 0.1, 0.5, 1.0, 2.0, 3.0 ppbv.

Case 2 : O_3

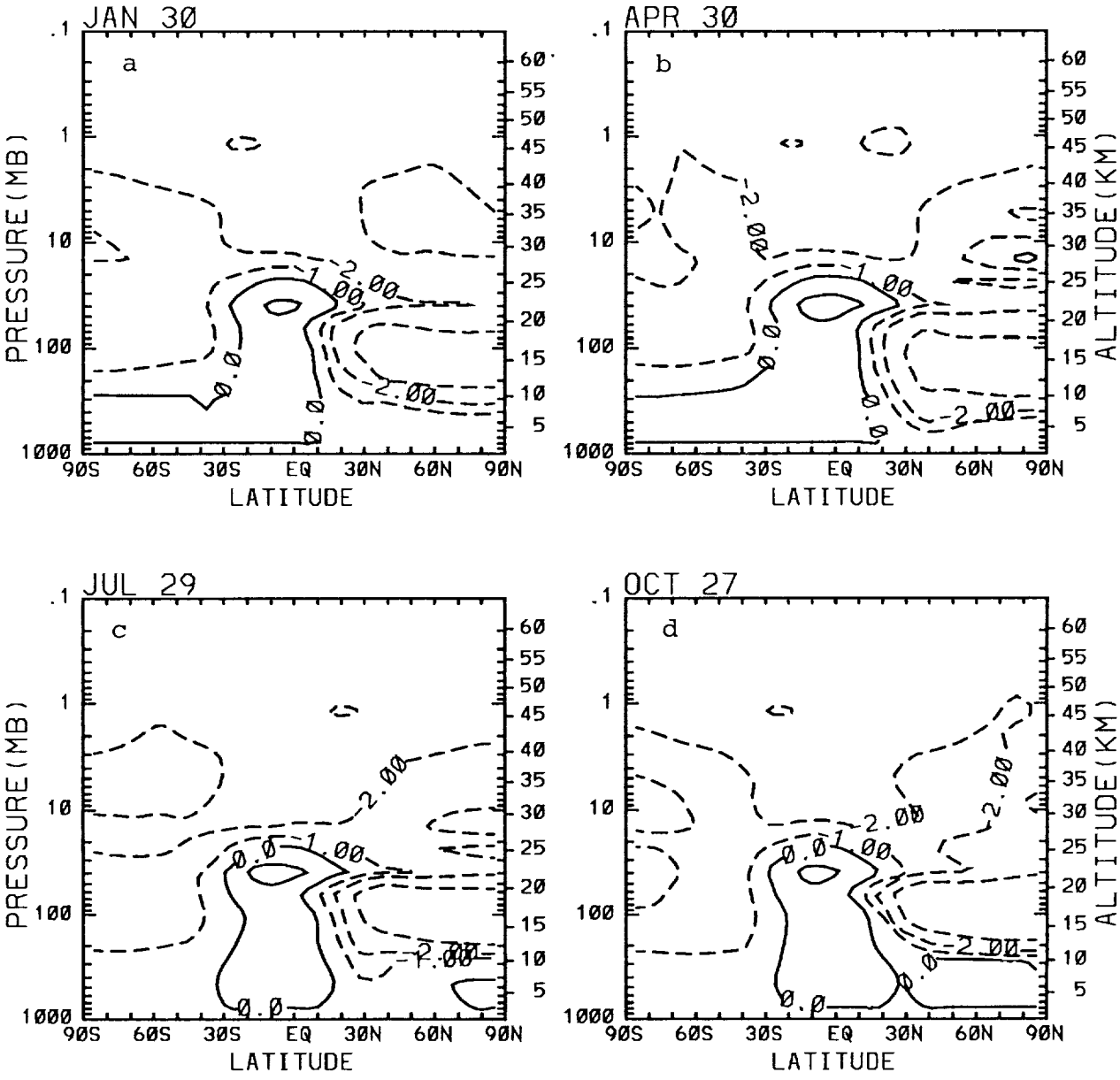

Figure 34. The calculated percent change in ozone mixing ratio from the baseline case for Case 2, as a function of latitude and altitude for (a) January, (b) April, (c) July, and (d) October. Contour levels are 0, ±1, ±2, ±4%.

Case 2 : O_3 Column

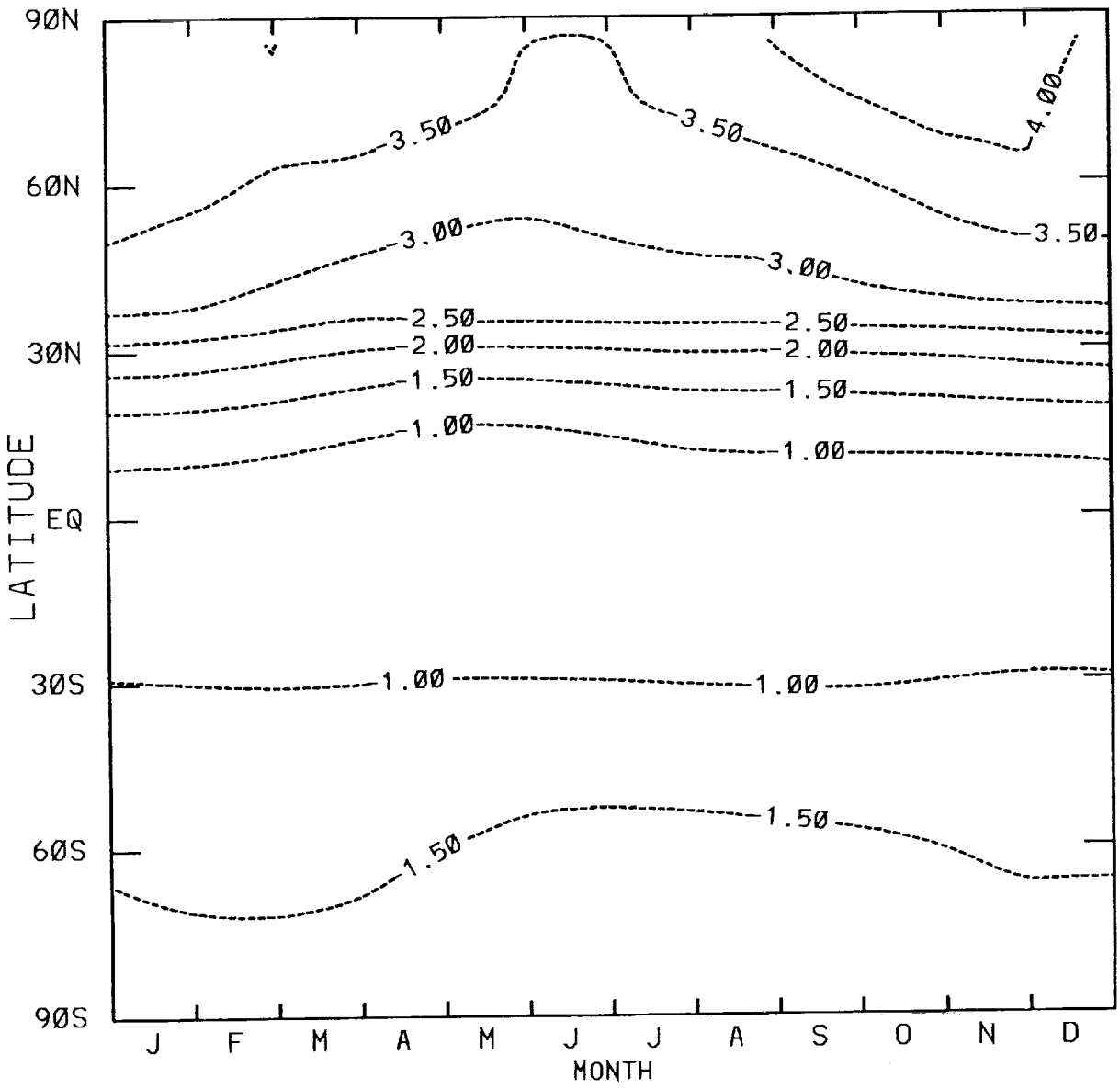

Figure 35. The calculated percent change in total ozone column from the baseline case for Case 2, as a function of latitude and time of year.

Case 3 : NOY

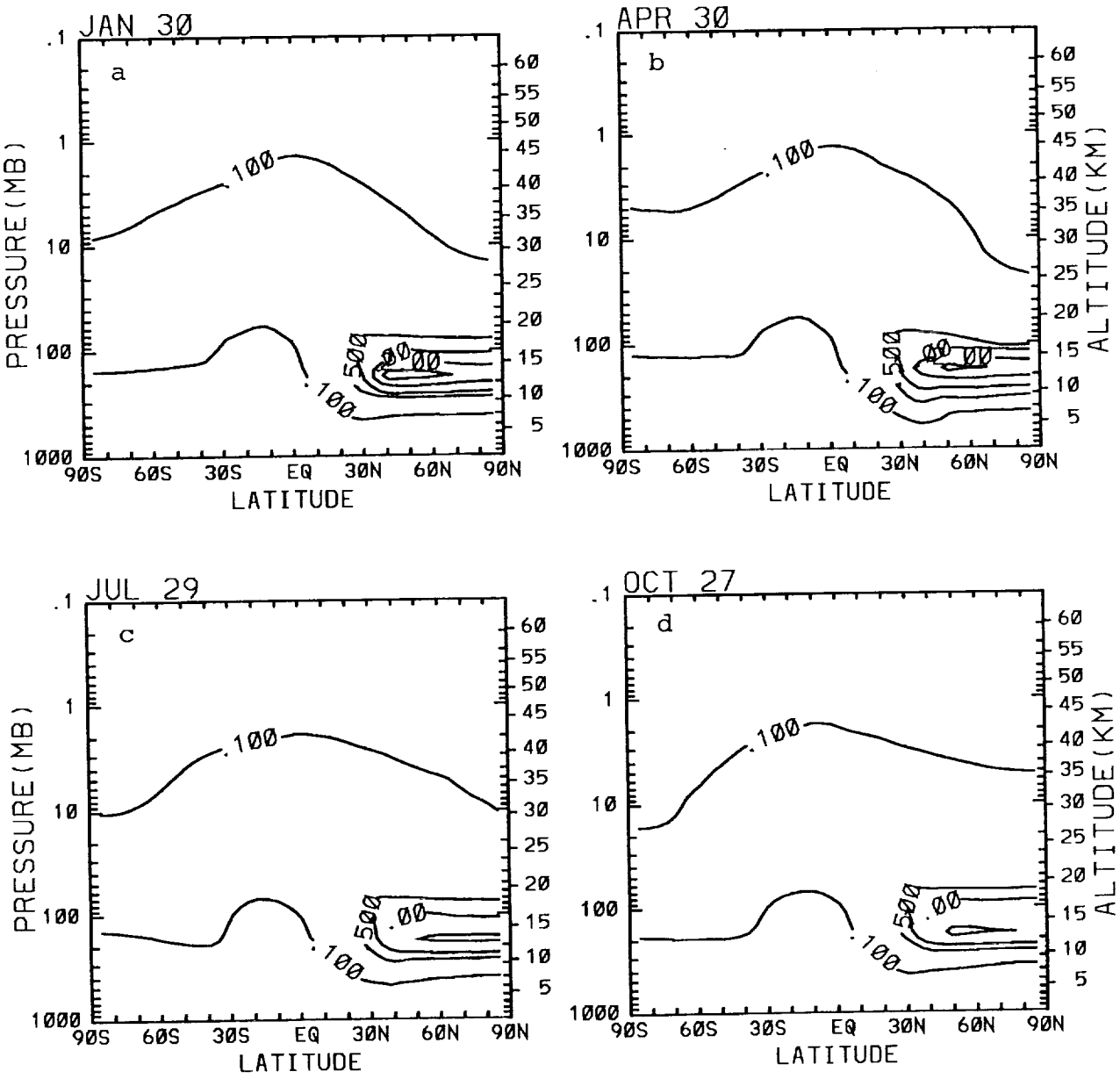

Figure 36. The calculated change in NOY in ppbv from the baseline case for Case 3, as a function of latitude and altitude for (a) January, (b) April, (c) July, and (d) October. Emissions were the same as the Scenario B10 emissions below 14 km, but emissions from the two altitude levels above 14 km were injected into the 14-18 km level. Contour levels are 0.1, 0.5, 1.0, 2.0, 3.0 ppbv.

Case 3 : O_3

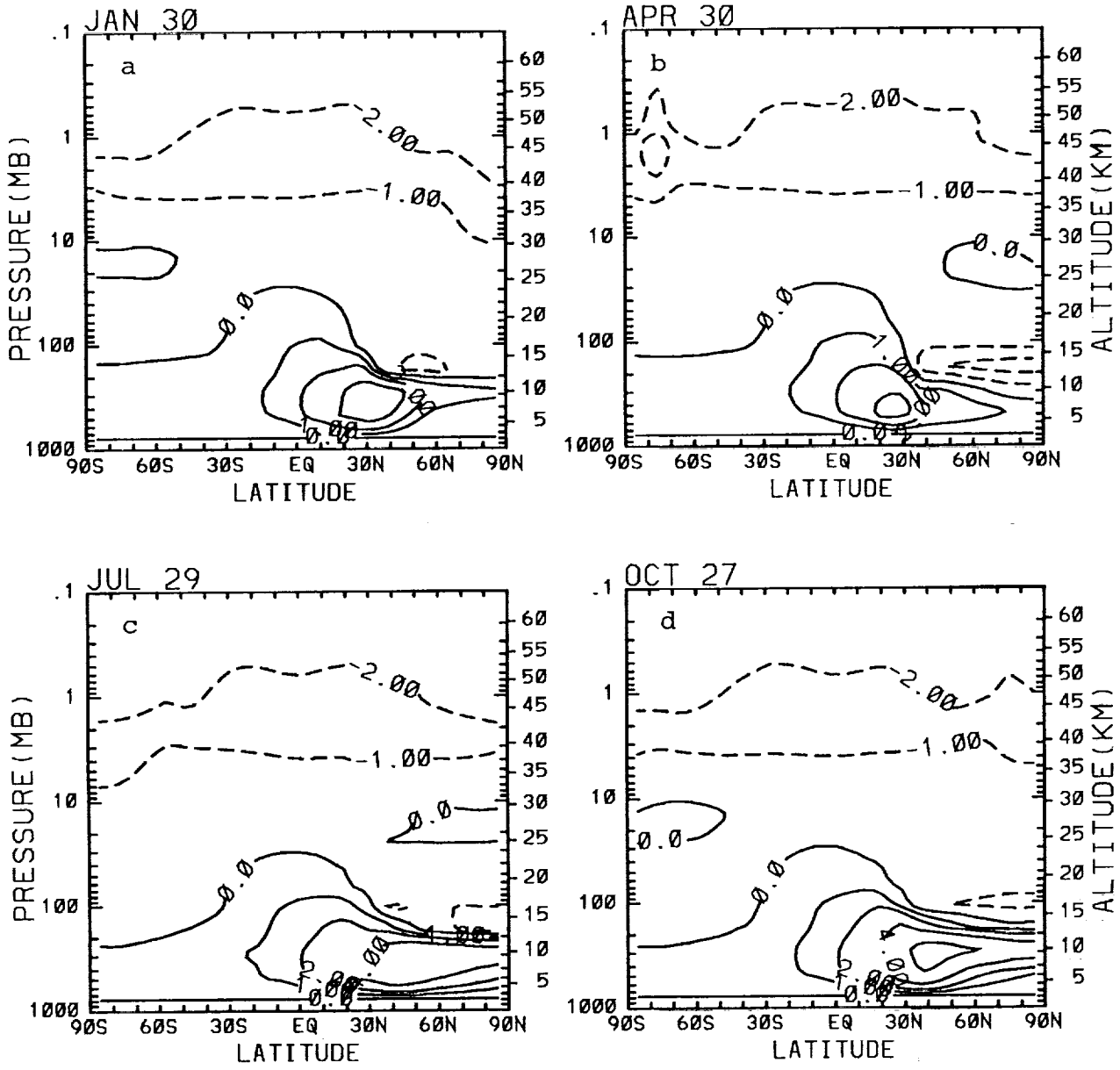

Figure 37. The calculated percent change in ozone mixing ratio from the baseline case for Case 3, as a function of latitude and altitude for (a) January, (b) April, (c) July, and (d) October. Contour levels are 0, ±1, ±2, ±4, ±8%.

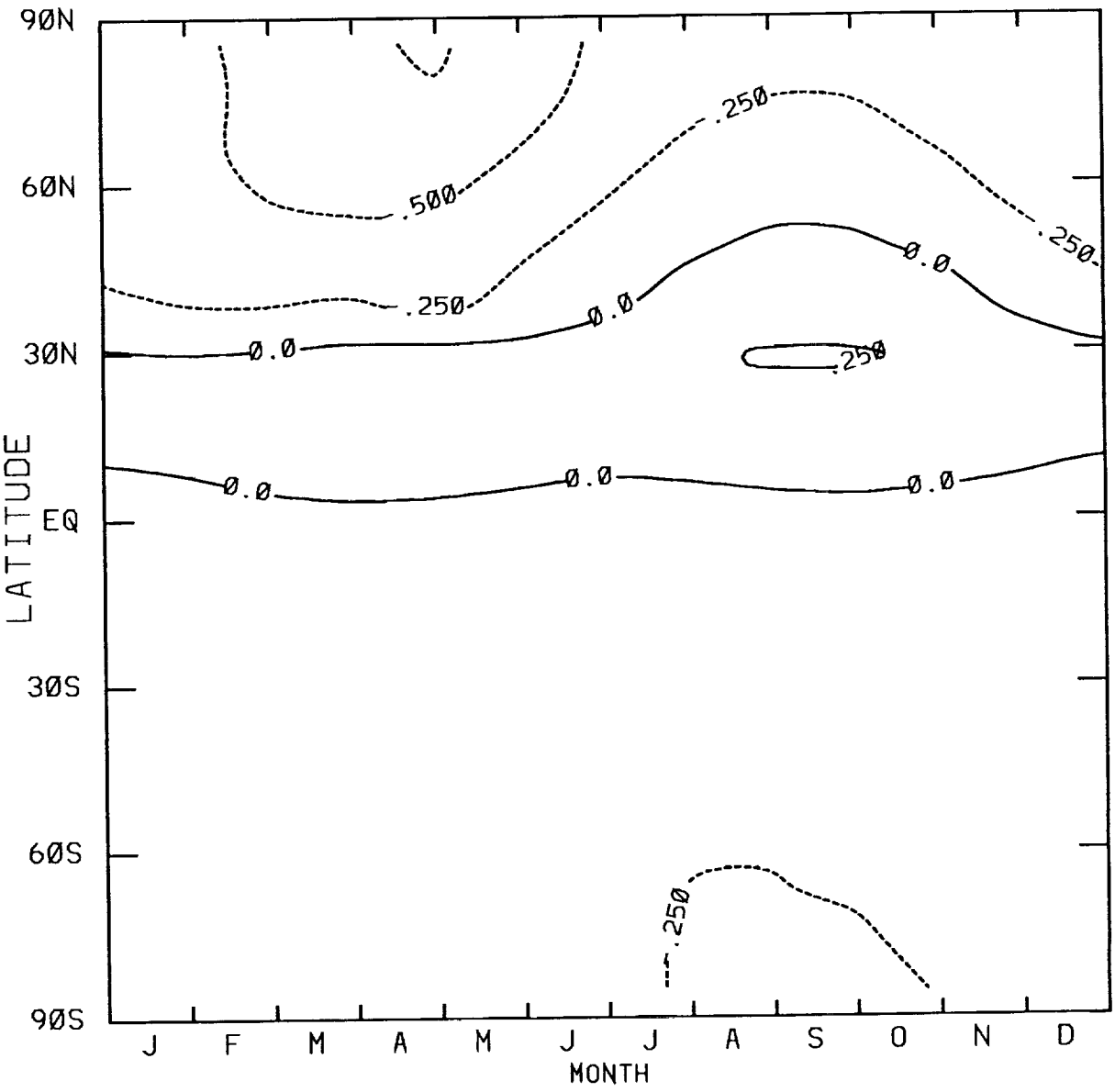

Figure 38. The calculated percent change in total ozone column from the baseline case for Case 3, as a function of latitude and time of year.

Case 4 : NOY

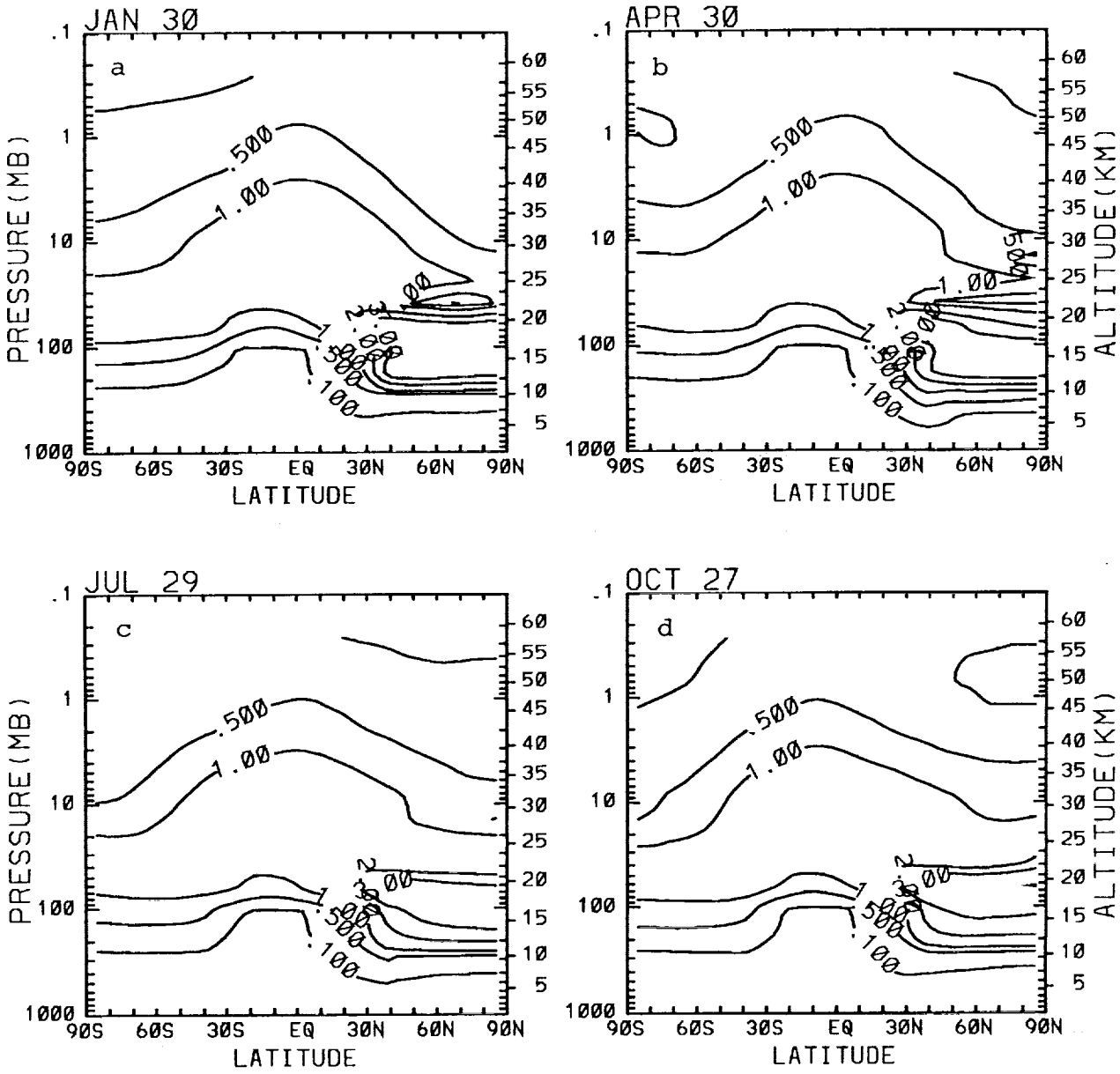

Figure 39. The calculated change in NOY in ppbv from the baseline case (shown in Figure A4) for Case 4, as a function of latitude and altitude for (a) January, (b) April, (c) July, and (d) October. Emissions were the same as the Scenario B10 emissions, but emissions at the upper two altitude levels (14-18 km and 18-22 km) were doubled. Contour levels are 0.1, 0.5, 1.0, 2.0, 3.0 ppbv.

Case 4 : O_3

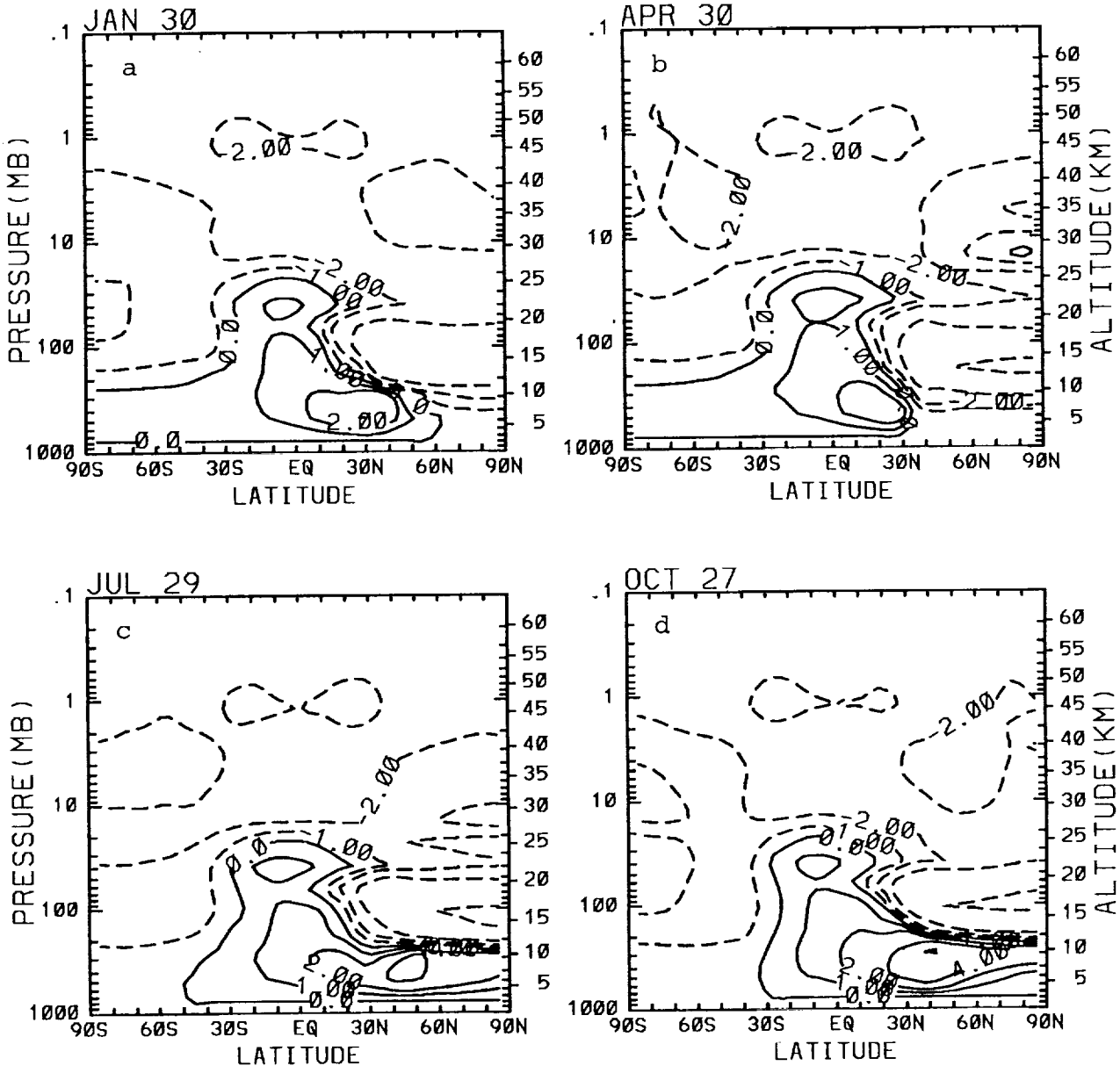

Figure 40. The calculated percent change in ozone mixing ratio from the baseline case for Case 4, as a function of latitude and altitude for (a) January, (b) April, (c) July, and (d) October. Contour levels are 0, ±1, ±2, ±4, ±8%.

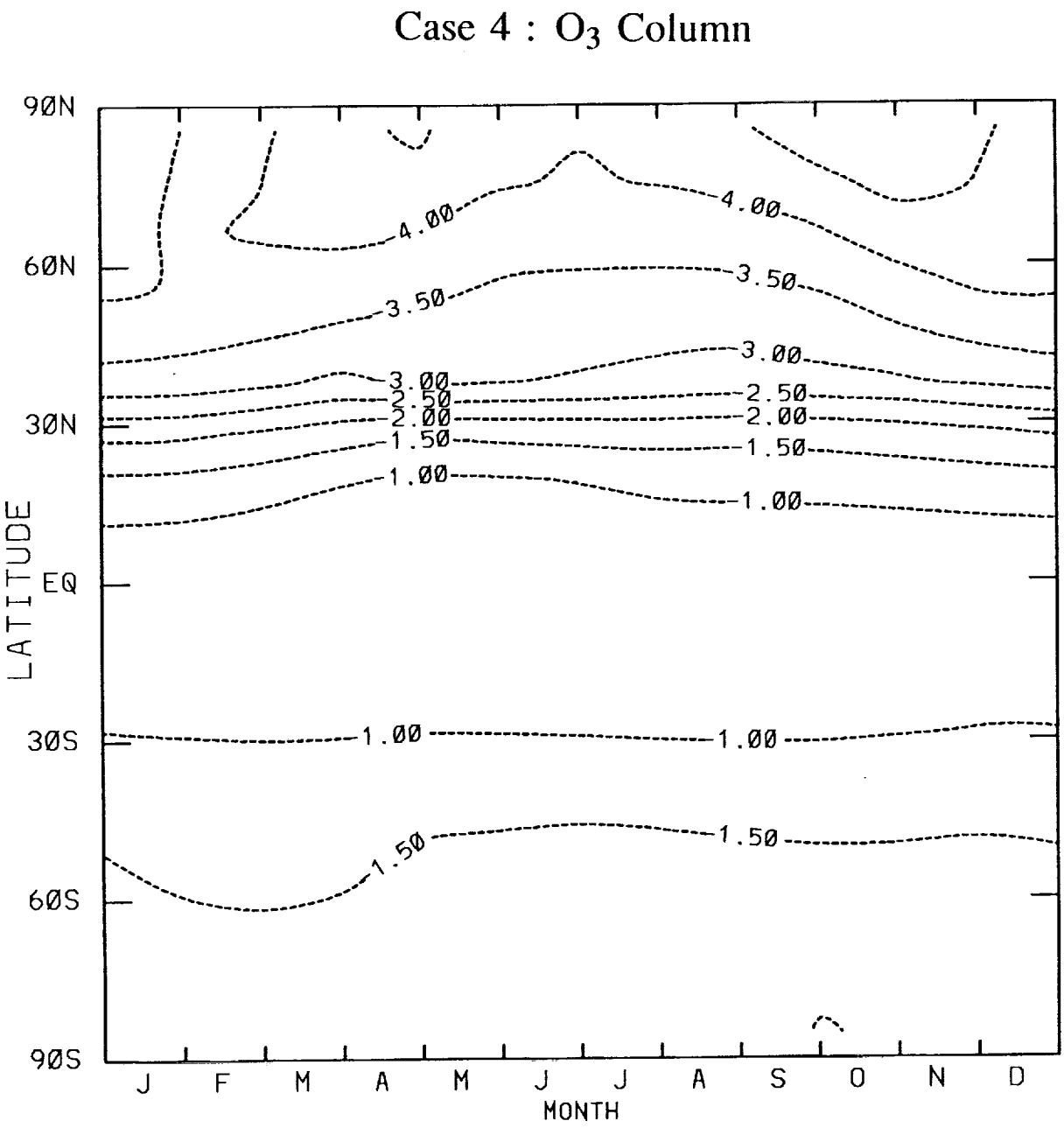

Figure 41. The calculated percent change in total ozone column from the baseline case for Case 4, as a function of latitude and time of year.

Experiment I : O_3 Column

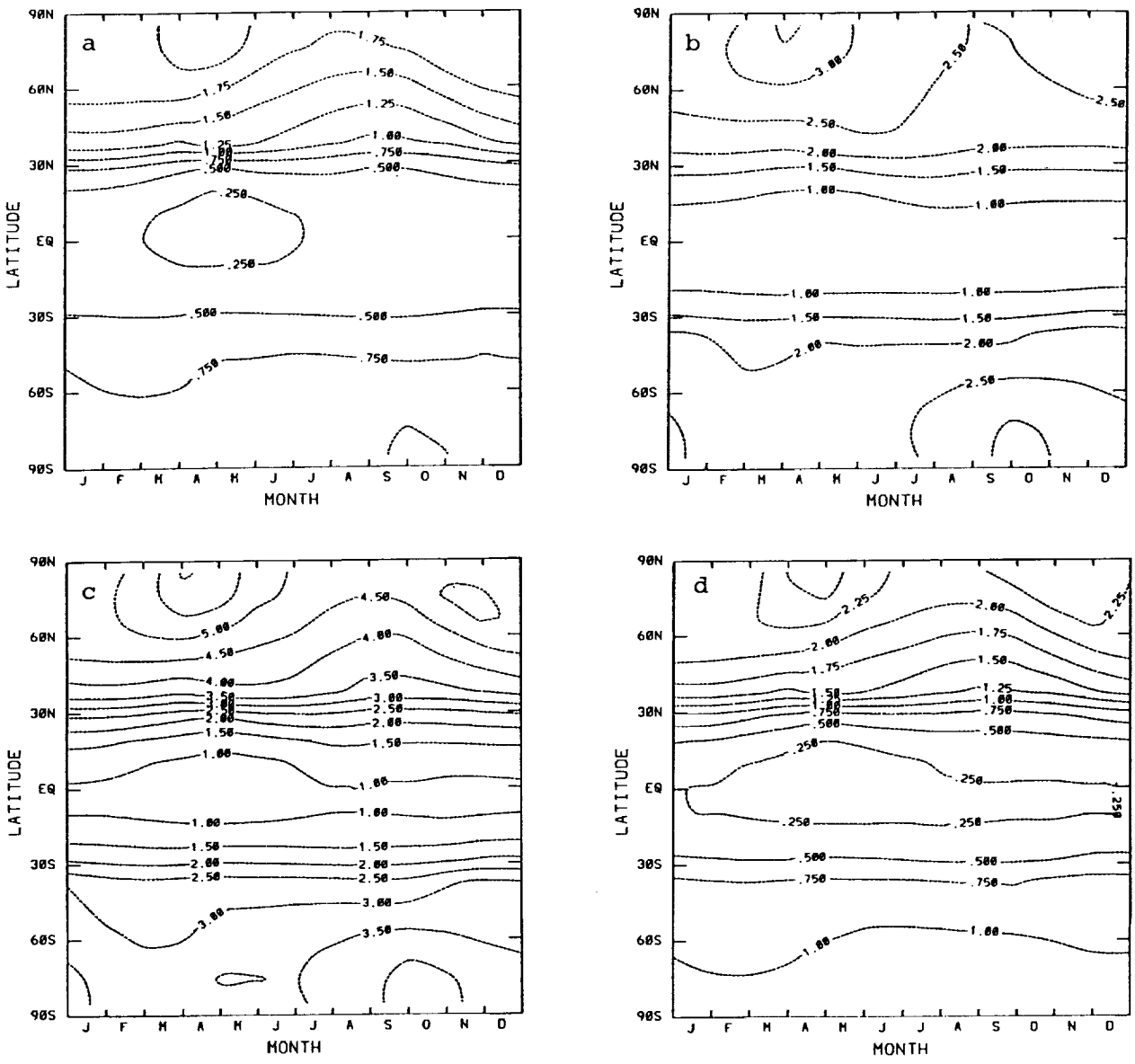

Figure 42. Four figures representing the response of total ozone column to the emissions of Scenario B7 for Experiment I, a future atmosphere containing 20% more N_2O than the present-day atmosphere. Panel (a) shows the response of O3 column to B7 emissions in the present day atmosphere. Panel (b) shows the change in the background ozone column of the future atmosphere as a percent of the background ozone of the present day atmosphere. Panel (c) shows the change in ozone column with Scenario B7 emissions in the future atmosphere as a percent of the present day ozone background. Panel (d) is the same as Panel (c) but as a percentage of the background ozone of the future atmosphere.

Experiment II : O_3 Column

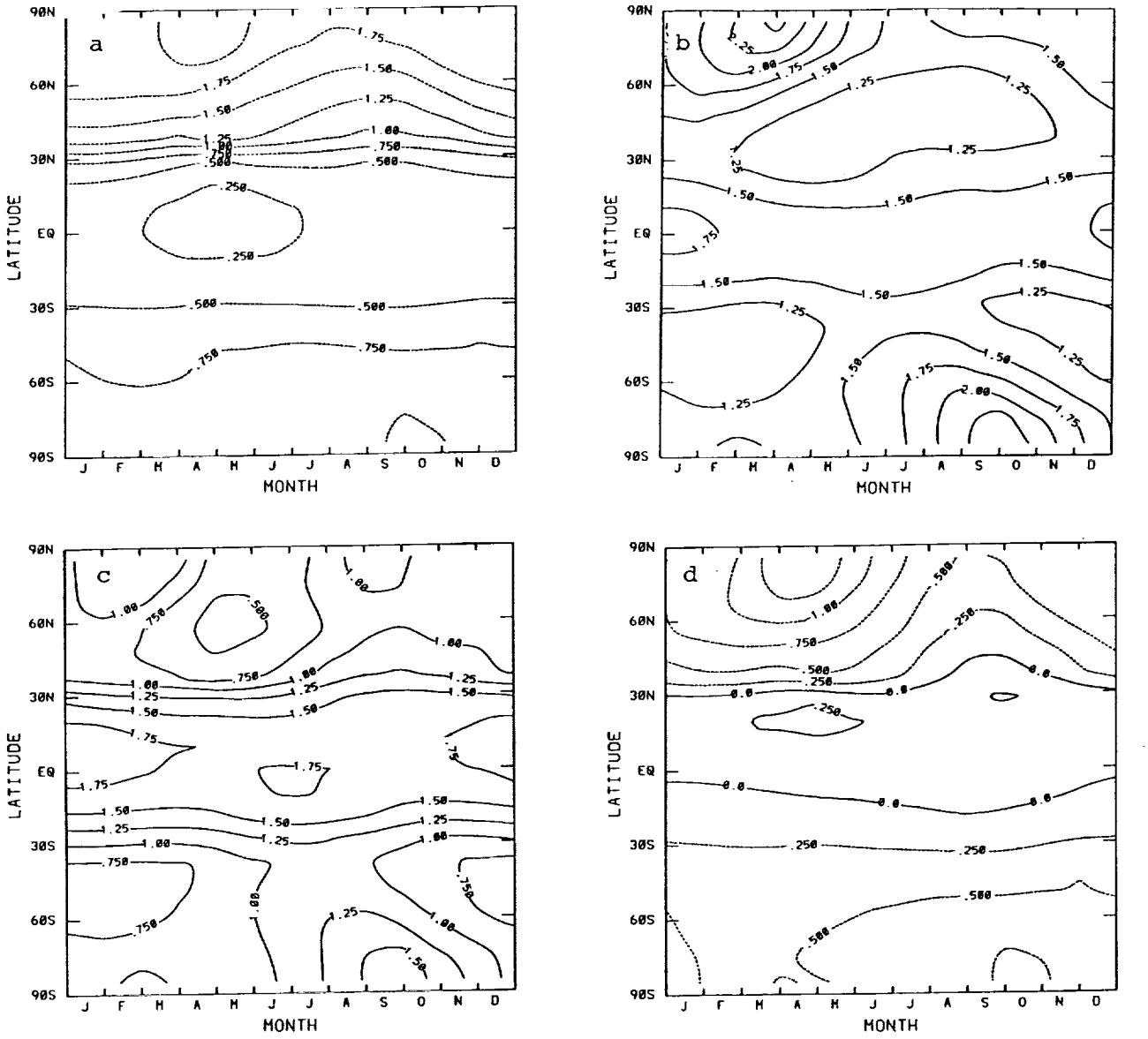

Figure 43. Four figures representing the response of total ozone column to the emissions of Scenario B7 for Experiment II, a future atmosphere with double the CH_4 of the present-day atmosphere. Panel (a) shows the response of O3 column to B7 emissions in the present day atmosphere. Panel (b) shows the change in the background ozone column of the future atmosphere as a percent of the background ozone of the present day atmosphere. Panel (c) shows the change in ozone column with Scenario B7 emissions in the future atmosphere as a percent of the present day ozone background. Panel (d) is the same as Panel (c) but as a percentage of the background ozone of the future atmosphere.

Experiment III : O_3 Column

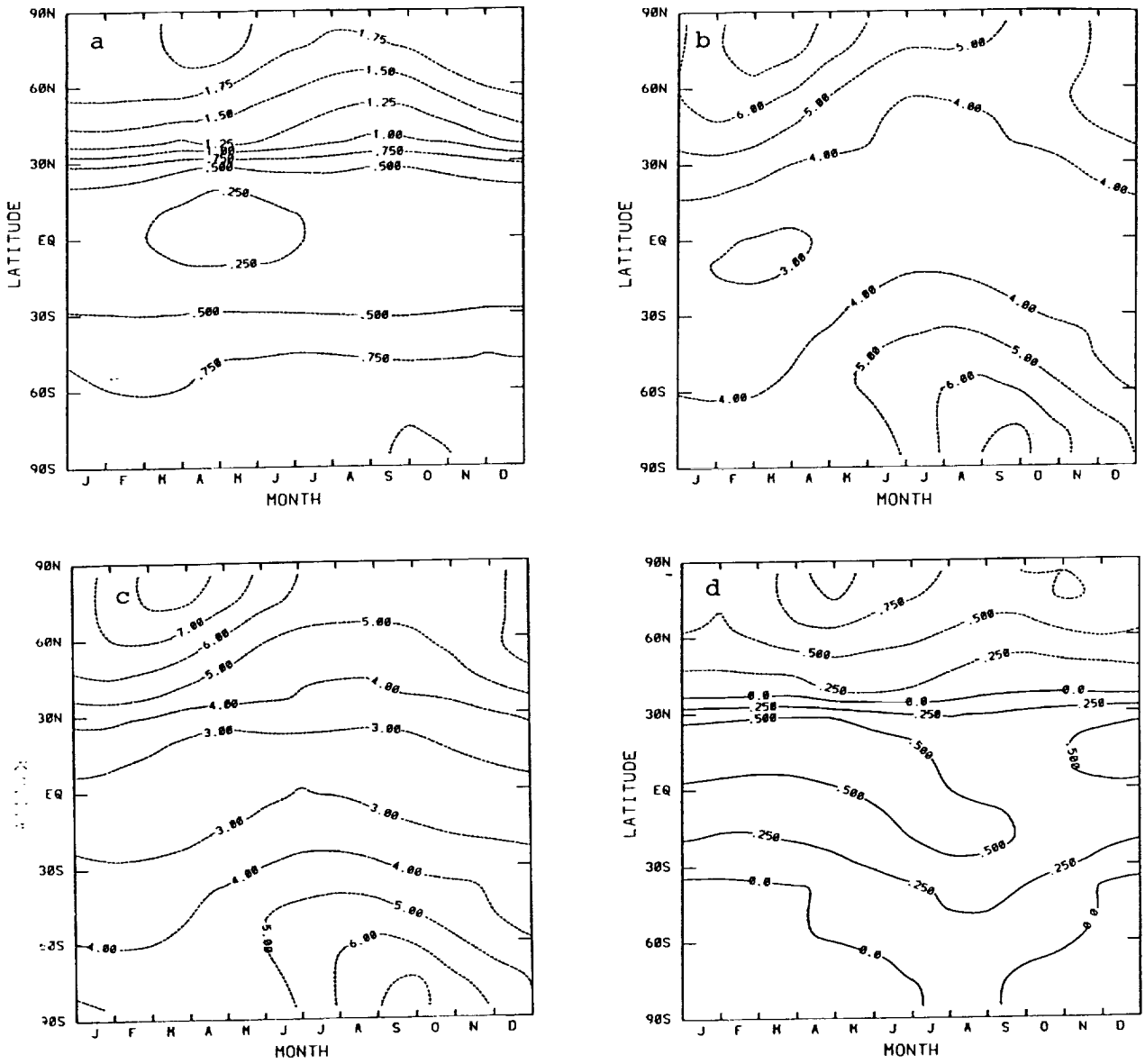

Figure 44. Four figures representing the response of total ozone column to the emissions of Scenario B7 for Experiment III, a future atmosphere with increased CFC concentrations, yeilding a total odd chlorine content of 6 ppb. Panel (a) shows the response of 03 column to B7 emissions in the present day atmosphere. Panel (b) shows the change in the background ozone column of the future atmosphere as a percent of the background ozone of the present day atmosphere. Panel (c) shows the change in ozone column with Scenario B7 emissions in the future atmosphere as a percent of the present day ozone background. Panel (d) is the same as Panel (c) but as a percentage of the background ozone of the future atmosphere.

Experiment IV : Temperature

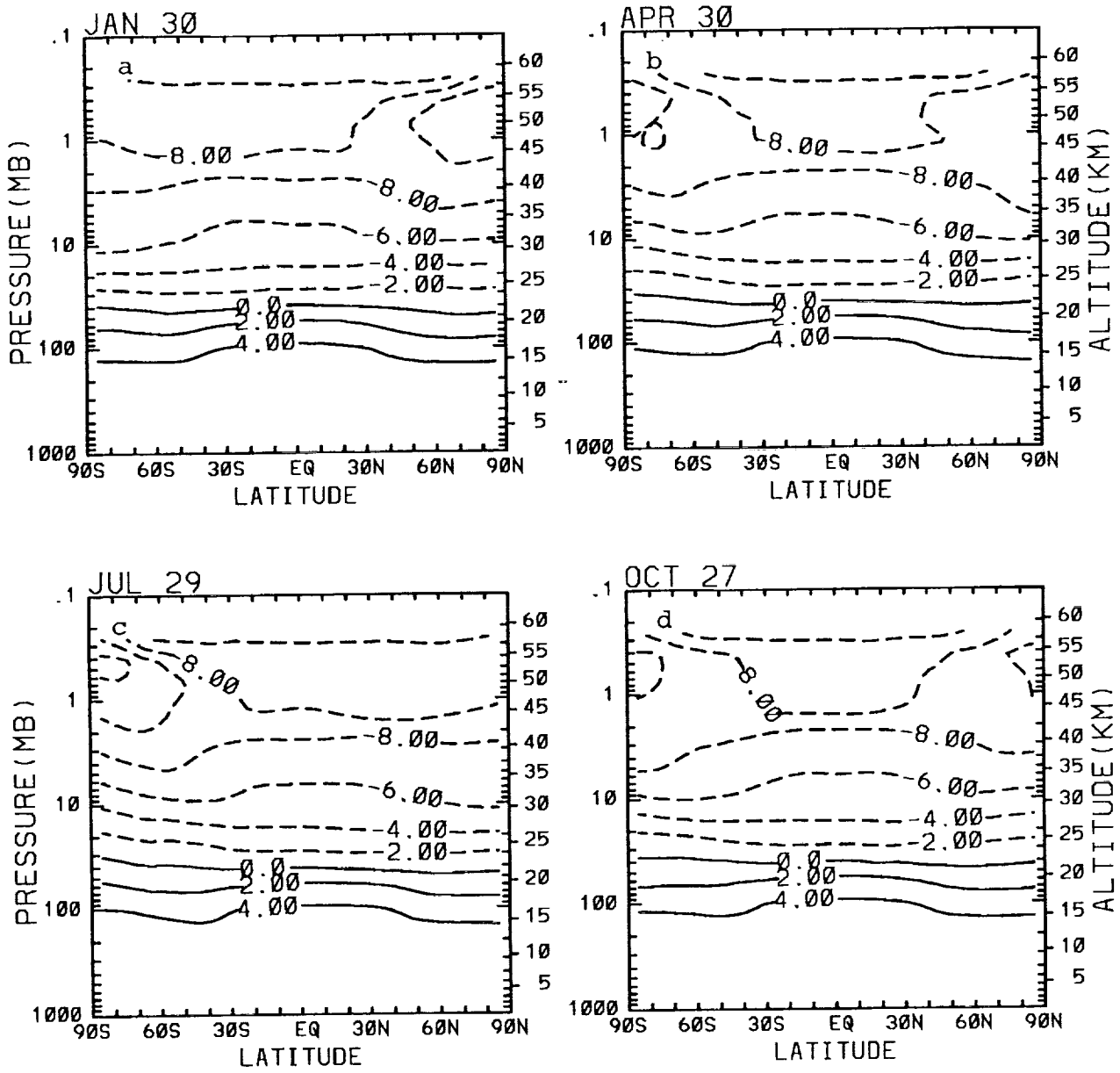

Figure 45. The change in temperature (°K) as a function of latitude and altitude used to simulate the response of the model to CO_2 doubling. Shown are differences between the double-CO_2 temperature and the baseline temperature for (a) January, (b) April, (c) July, and (d) October. Contours are from -12°K to 4°K by 2°.

Experiment IV : O_3 Column

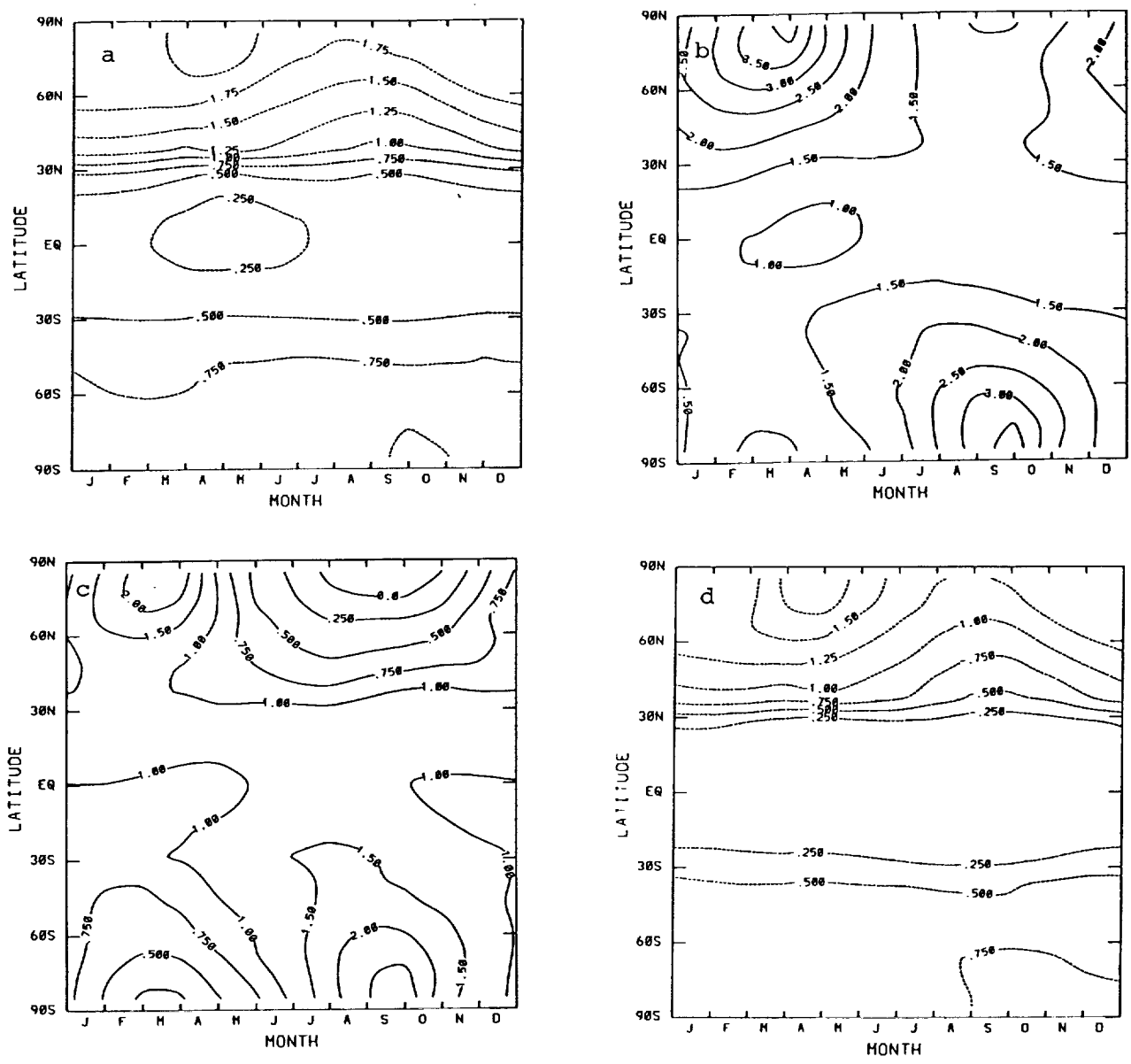

Figure 46. Four figures representing the response of total ozone column to the emissions of Scenario B7 for Experiment IV, a future atmosphere with double the CO_2 of the present day atmosphere. This experiment represents the response to CO_2-induced temperature change only. Panel (a) shows the response of O3 column to B7 emissions in the present day atmosphere. Panel (b) shows the change in the background ozone column of the future atmosphere as a percent of the background ozone of the present day atmosphere. Panel (c) shows the change in ozone column with Scenario B7 emissions in the future atmosphere as a percent of the present day ozone background. Panel (d) is the same as Panel (c) but as a percentage of the background ozone of the future atmosphere.

Experiment V : O_3 Column

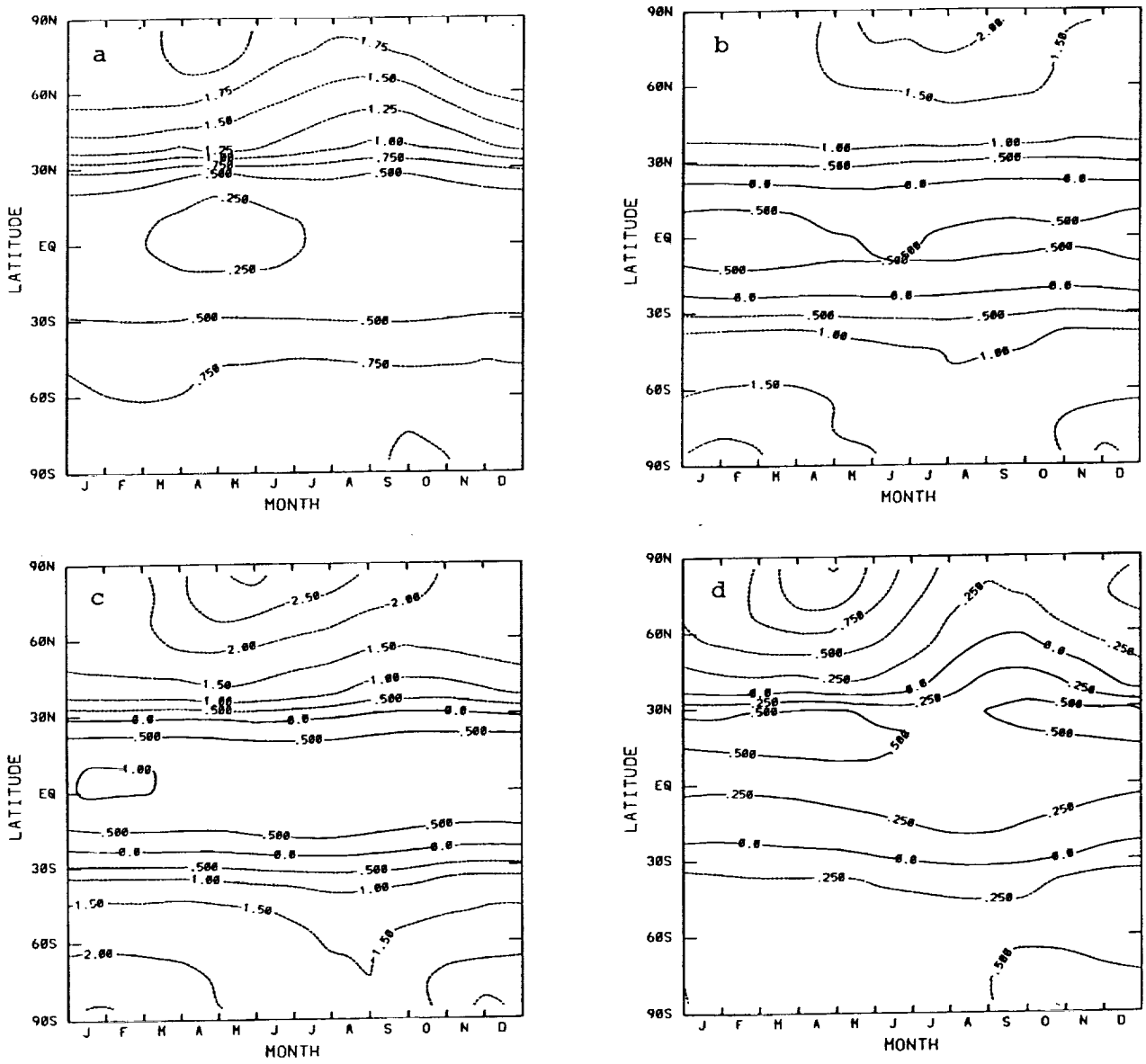

Figure 47. Four figures representing the response of total ozone column to the emissions of Scenario B7 for Experiment V, a future atmosphere with 20% more N_2O, double CH_4, increased CFCs, and double CO_2. Panel (a) shows the response of O3 column to B7 emissions in the present day atmosphere. Panel (b) shows the change in the background ozone column of the future atmosphere as a percent of the background ozone of the present day atmosphere. Panel (c) shows the change in ozone column with Scenario B7 emissions in the future atmosphere as a percent of the present day ozone background. Panel (d) is the same as Panel (c) but as a percentage of the background ozone of the future atmosphere.

Appendix

AER 2-D Chemistry-Transport Model

Model Description

The AER two-dimensional (2D) model simulates the seasonal, latitudinal, and vertical distribution of atmospheric trace gases by accounting for chemical interactions among the gases and dynamical transport. The model covers the globe from pole to pole with a latitudinal resolution of 9.5 degrees. Vertical coverage is from the ground to approximately 60 km in a log-pressure grid. The vertical resolution is approximately 3.5 km.

The model includes approximately 40 chemical species which interact through over 100 chemical reactions. The kinetic reaction rates are those given by NASA/JPL (1988). The solar flux and absorption cross sections are from WMO/NASA (1986). The chemical scheme employs the grouping technique to deal with chemicals having vastly different atmospheric lifetimes. Table A1 show the species in the model classified according to their lifetimes. Short-lived species are calculated assuming photochemical equilibrium. Their concentrations are allowed to vary diurnally. Long-lived species are calculated using the mass-continuity equation.

The temperature in the atmosphere is specified as a function of latitude, height and season with values determined from climatology. Dynamical transport within the model is effected by the zonal-mean circulation, by quasi-horizontal diffusion along isentropic surfaces, and by vertical diffusion in the troposphere and upper stratosphere. The model circulation was derived from diabatic heating rates based on those calculated by Murgatroyd and Singleton (1961) for the upper stratosphere and Dopplick (1979) for the lower stratosphere.

The horizontal eddy diffusion coefficient, K_{yy}, for the troposphere and lower stratosphere varies from 3×10^{9} cm^2/sec at low latitudes to 6×10^{9} cm^2/sec at mid-latitudes in fall and winter or 2×10^{10} cm^2/sec at mid-latitudes in spring and summer. These values yield a good fit to observed ozone profiles in the lower stratosphere and are close to the magnitudes derived by Newman and Schoeberl (1986). The value of K_{yy} in the stratosphere above 25 km is 3×10^{9} cm^2/sec for all latitudes and seasons. This is based on the work of Kida (1983) and Tung (1984) in estimating an average horizontal diffusion coefficient for the stratosphere.

The vertical diffusion coefficient, K_{zz}, is 1×10^{5} cm^2/sec in the

troposphere, 1×10^3 cm^2/sec in the stratosphere below 40 km, and 1×10^4 cm^2/sec above 40 km. Stratospheric vertical diffusion was estimated by Kida (1983) to be 1×10^3 cm^2/sec. Enhanced vertical mixing above 40 km is based on the work of Garcia and Solomon (1985) regarding gravity wave breaking.

Concentrations of long-lived atmospheric species are integrated forward in time, with the change in mixing ratio per unit time in the latitude (ϕ) - log-pressure (ζ) coordinate system given by:

$$\frac{\partial f}{\partial t} = -\frac{1}{a\cos\phi}\frac{\partial}{\partial\phi}(fv\cos\phi) - e^{\zeta}\frac{\partial}{\partial\zeta}(fwe^{-\zeta}) + \frac{1}{a^2\cos\phi}\frac{\partial}{\partial\phi}\left(K_{yy}\cos\phi\frac{\partial f}{\partial\phi}\right) + e^{\zeta}\frac{\partial}{\partial\zeta}\left(K_{zz}e^{-\zeta}\frac{\partial f}{\partial\zeta}\right) + P - Lf \quad (4)$$

where f represents the zonal-mean volume mixing ratio of a trace atmospheric specie, a is the radius of the earth, v is the horizontal transport velocity, w the vertical transport velocity, and K_{yy} and K_{zz} are the horizontal and vertical eddy mixing coefficients. Chemical production and loss are represented by the terms P and Lf, respectively.

The finite differencing scheme used is that developed by Smolarkiewicz (1984). It is an iterative upstream scheme which removes much of the implicit diffusion of upwind differencing by adding a corrective step to each time step. Negative mixing ratios are not generated provided the time step is small enough. The scheme computes fluxes at grid box boundaries and transports mass only in the direction of fluid flow. The time step used in the AER model is 12 hours, or 2 steps per day.

Present Day Atmosphere

The total column ozone generated by our model for the present-day atmosphere is shown in Figure A1(a) as a function of latitude and time of the year. Figure A1(b) shows the corresponding observed ozone column abundance. The model successfully simulates both the magnitude of the observed ozone column and its seasonal and latitudinal variation. The ozone column shows a minimum near the equator and maximums at high latitudes in the springtime. Since ozone is generated primarily near the equator by photolysis of molecular oxygen, this indicates the importance of transport to the global ozone distribution. The calculated ozone mixing ratios as functions of latitude and height for January, April, July, and October are shown in Figure A2. Ozone

profiles derived from satellite observations are shown in Figure A3 for comparison.

The mixing ratios of total odd nitrogen (NOY) generated by the model for the present-day atmosphere are shown in Figure A4. The model-generated NOY is 20% smaller than that inferred from LIMS satellite observations by Callis, el al. (1986). Underprediction of NOY mixing ratios is common to most models and may indicate that not all sources have been accounted for. Calculated mixing rations of carbon monoxide (CO) and methane (CH_4) are shown in Figures A5 and A6, respectively. The model-calculated CH_4 is similar to that observed by the SAMS satellite in 1979 (Jones and Pyle, 1984; Callis, et al., 1986).

Water is not calculated by the model. Instead, a fixed concentration, varying with latitude and height but constant with season, is used. Figure A7 shows the stratospheric water vapor concentration, which was derived from Remsberg, et. al. (1984). Tropospheric water vapor is derived from relative humidity profiles.

Tracer Study

Figure A8 shows the results of an inert tracer experiment performed with the AER chemistry-transport model. This numerical experiment is discussed in Plumb and Mahlman (1987) and can be used to compare the transport characteristics of one model with that of another. The initial tracer distribution, show in panel (a), as defined by the formula:

$$q(\phi,z) = 1000 * \exp\left\{ - (z-z_0)^2/2\Delta z^2 \right\} * \exp\left\{ - (\phi - \phi_0)^2/2\Delta\phi^2 \right\}$$

where $z_0 = 19.68$ km $\quad \Delta z = 5$ km $\quad \phi_0 = 45^0$ N $\quad \Delta\phi = 10^0$

There is a tropospheric sink for the tracer, defined by

$$S = -\Lambda q$$

where $\Lambda = (10 \text{ days})^{-1} (p-300 \text{ mb})/700 \text{ mb} \quad p > 300 \text{ mb}$

$\Lambda = 0 \quad p < 300 \text{ mb}$

The model experiment was begun on January 1 and run for 3 years. The

distribution of tracer on January 1 after 1, 2, and 3 years is shown in the figure. It can be seen the the tracer is distributed globally after one year, and that after three years the tracer distribution shows little hemispheric asymmetry.

References

Bowman, K. P., and A. J. Krueger (1985) A global climatology of total ozone from the Nimbus 7 total ozone mapping spectrometer. J. Geophys. Res., 90, 7967-7976.

Callis, L. B., M. Natarajan, R. E. Boughner, J. M. Russell III, and J. D. Lambeth (1986) Stratospheric photochemical studies using Nimbus 7 data: 2. Development of inferred trace specie distributions. J. Geophys. Res., 91, 1167-1197.

Dopplick, T. G. (1979) Radiative heating of the global atmosphere: Corrigendum. J. Atmos. Sci., 36, 1812-1817.

Garcia, R. R., and S. Solomon (1985) The effect of breaking gravity waves on the dynamics and chemical composition of the mesosphere and lower thermosphere. J. Geophys. Res., 90, 3850.

Gille, J. C., and J. M. Russell, III (1984) The limb infrared monitor of the stratosphere: Experiment description, performance, and results. J. Geophys. Res., 89, 5125-5140.

Jones, R. L., and J. A. Pyle (1984) Observations of CH_4 and N_2O by the NIMBUS 7 SAMS: A comparison with in situ data and two-dimensional numerical model calculation. J. Geophys. Res., 89, 5263-5279.

Kida, H., (1983) General circulation of air parcels and transport characteristics derived from a hemispheric GCM, 2, Very long-term motions of air parcels in the troposphere and stratosphere, J. Meteorol. Soc. Jpn, 61, 510-523.

Ko, M. K. W., K. K. Tung, D. K. Weisenstein, and N. D. Sze (1985a) A zonal-mean model of stratospheric tracer transport in isentropic coordinates: Numerical simulations for nitrous oxide and nitric acid. J. Geophys. Res., 90, 2313-2329.

Ko, M.K.W., D. Weisenstein, N.D. Sze, and K.K.Tung (1985b) Simulation of O_3 distribution using a two-dimensional zonal-mean model in isentropic coordinate. In: Atmospheric Ozone, C.S. Zerefos and A. Ghazi, Eds. D. Reidel, Hingham, Mass, pp. 19-23.

Ko, M. K. W., M. B. McElroy, D. K. Weisenstein, and N. D. Sze (1986) Lightning: A possible source of stratospheric odd nitrogen. J. Geophys. Res., 91, 5395-5404.

McPeters, R. D., D. F. Heath, and P. K. Bhartia (1984) Average ozone profiles for 1979 from the Nimbus 7 SBUV instrument. J. Geophys. Res., 89, 5199-5214.

Mount, G. H., D. W. Rusch, J. M. Zawodny, J. F. Noxon, C. A. barth, G. J. Rottman, R. J. Thomas, G. E. Thomas, R. W. Sanders, and G. M. Lawrence (1983) Measurement of NO_2 in Earth's stratosphere using a limb scanning visible light spectrometer. Geophys. Res. Lett., 10, 265.

Murgatroyd, R. J., and F. Singleton, (1961) Possible meridional circulation in the stratosphere and mesosphere, Q. J. R. Meteorol. Soc., 87, 125-135.

NASA/JPL (1988) Chemical Kinetics and Photochemical Data for Use in Stratospheric Modeling, Evaluation Number 8. JPL Publication 87-41.

Newman, P. A. and M. R. Schoeberl (1986) Horizontal mixing coefficients for two-dimensional chemical models calculated from National Meteorological Center data. J. Geophys. Res., 91, 7919-7924.

Plumb, R.A., and J.D. Mahlman (1987) The zonally averaged temperature characteristics of the GFDL general circulation/transport model. J. Atmos. Sci., 44, 298-327.

Remsberg, E. E., J. M. Russell, III, L. L. Gordley, J. C. Gille, and P. L. Bailey (1984) Implications of the stratospheric water vapor distribution as determined by the Nimbus 7 LIMS experiment. J. Atmos. Sci., 41, 2934-2945.

Rusch, D. W., and C. A. Barth (1975) Satellite measurements of nitric oxide in the polar region. J. Geophys. Res., 80, 3719.

Smolarkiewcz, P. (1983) A simple positive definite advective scheme with small implicit diffusion, Mon. Wea. Rev., 3, 479-486.

Smolarkiewicz, P.K. (1984) A fully multidimensional positive definite advection transport algorithm with small implicit diffusion. J. Comput. Phys., 54, 325.

Tung, K. K., (1984) Modeling of tracer transport in the middle atmosphere, in Dynamics of the Middle Atmosphere, edited by J. R. Holton and T. Matsuno, pages 412-444, Terra Scientific Publishing, Tokyo, Japan.

WMO/NASA (1986) Atmospheric Ozone: Assessment of Our Understanding of the Processes Controlling Its Present Distribution and Changes. World Meteorological Organization Report #16, Geneva.

Table A1: Summary of Chemical Species included in AER 2-D Model

Fixed Species

M	Bulk air density calculated from ideal gas law
O_2	Set equal to 21% of M
H_2O	Stratospheric values parameterized from Remsberg, et al. (1984). Tropospheric values calculated from seasonally varying relative humidity determined from climatology

Long-lived Species

N_2O

CH_4, H_2, CO

$CH_3C\ell$, $CH_3CC\ell_3$, $CC\ell_4$

CFC-11, CFC-12

CF_2O, $CFC\ell O$

$NOY = N + NO + NO_2 + NO_3 + 2 \times N_2O_5 + HNO_3 + C\ell NO_3 + HNO_4$

$C\ell Y = C\ell + C\ell O + C\ell NO_3 + HC\ell + HOC\ell + OC\ell O + 2 \times C\ell_2O_2$

$O_x = O + O(^1D) + O_3$

Short-lived Species

Oxygen	O, $O(^1D)$
Hydrogen	H, OH, HO_2, H_2O_2
Methyl	CH_2O_2, CH_2O, CH_3OOH
Nitrogen	N, NO, NO_2, NO_3, N_2O_5, HNO_3, $C\ell NO_3$, HNO_4
Chlorine	$C\ell$, $C\ell O$, $C\ell NO_3$, $HC\ell$, $HOC\ell$, $OC\ell O$, $C\ell_2O_2$

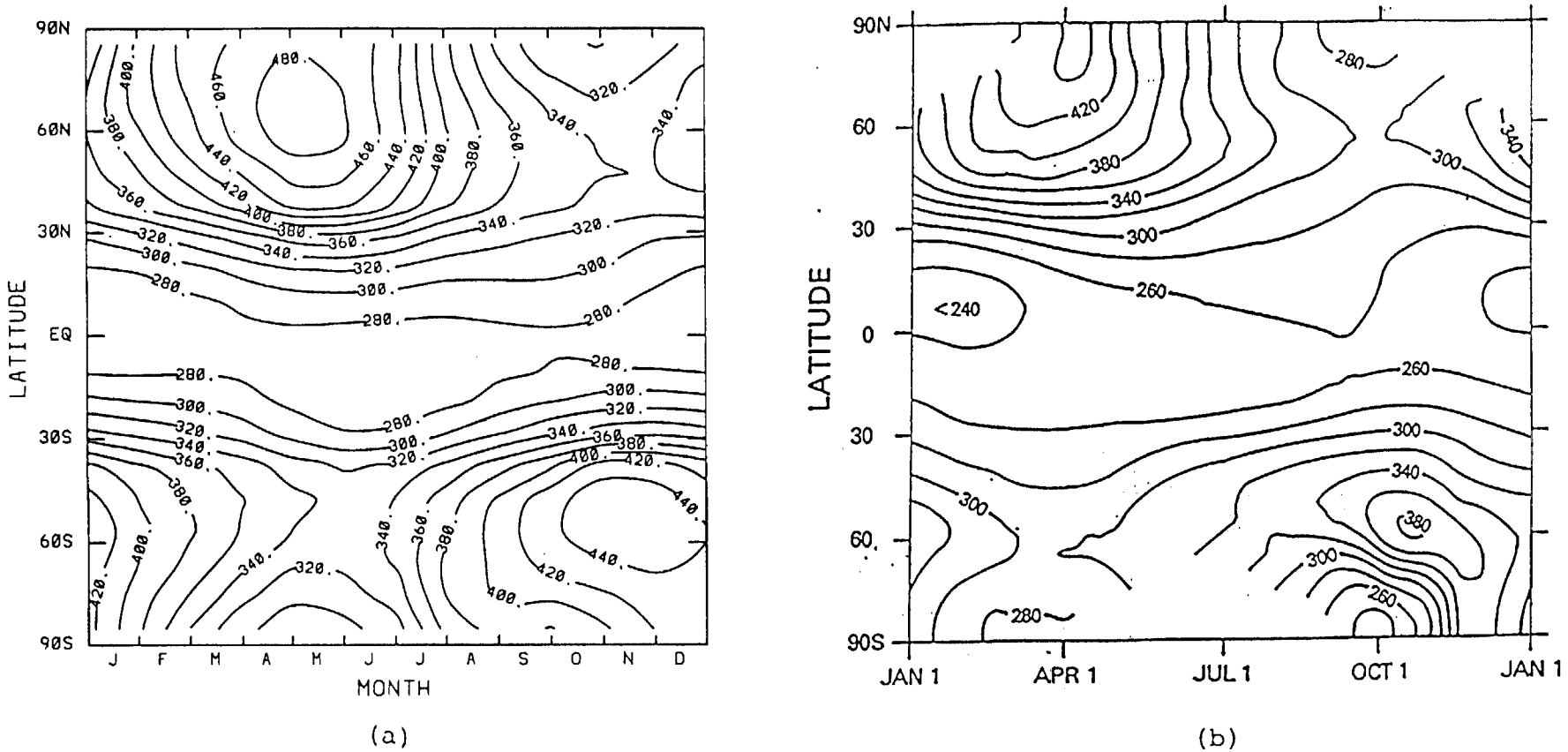

Figure A1. Total ozone column (Dobson units) as a function of latitude and time of the year (a) as calculated by the AER 2D chemical-transport model for present-day atmospheric conditions, and (b) derived from Nimbus 7 satellite observations (Bowman and Krueger, 1985) for the years 1978-1982. Observations have been averaged into zonal means and smoothed by computing 10-day averages.

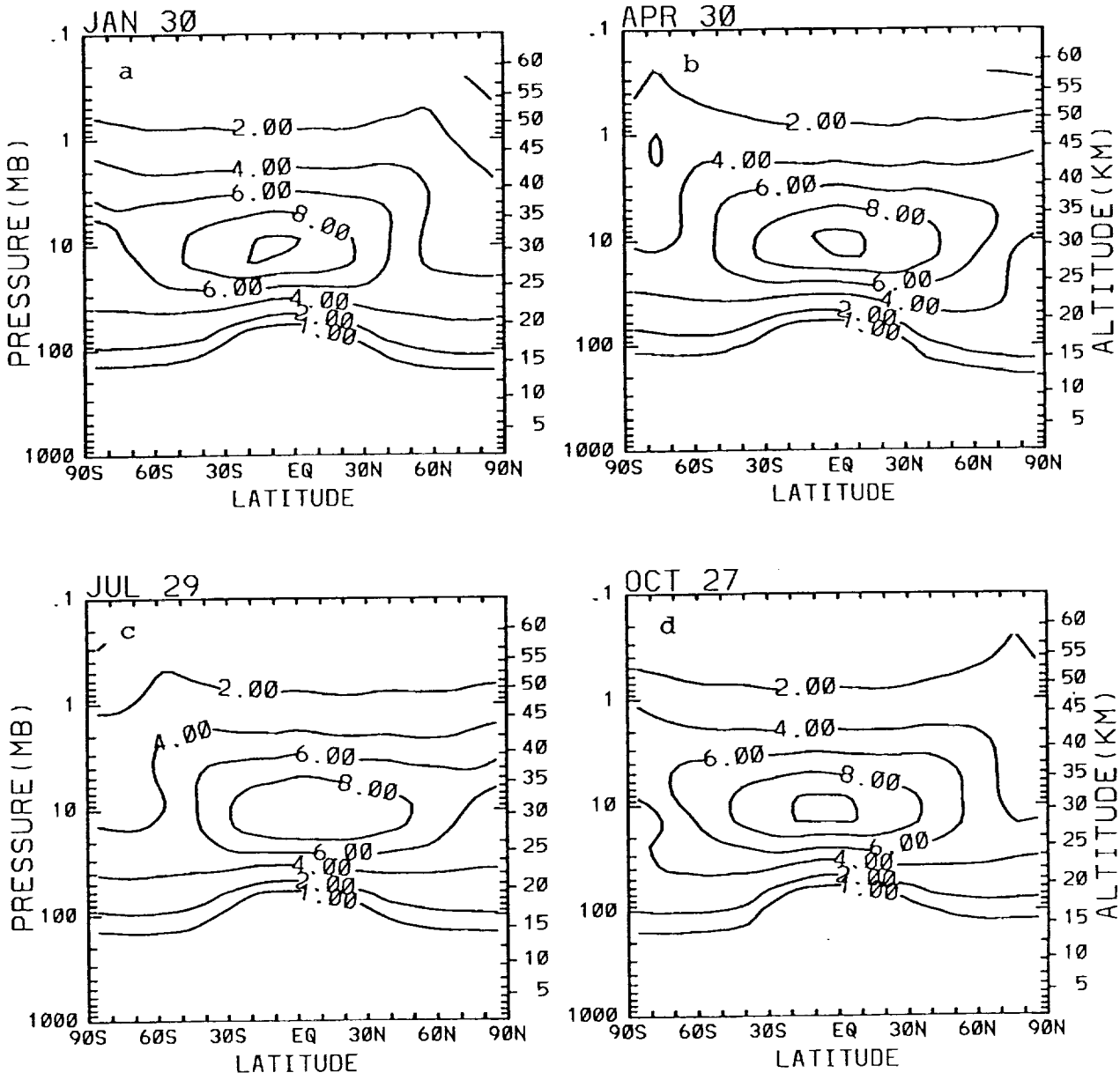

Figure A2. Model-calculated cross-sections of ozone mixing ratio (ppmv) as a function of latitude and height for (a) January, (b) April, (c) July, and (d) October for present-day conditions. Contours are 1, 2, 4, 6, 8, 10 ppmv.

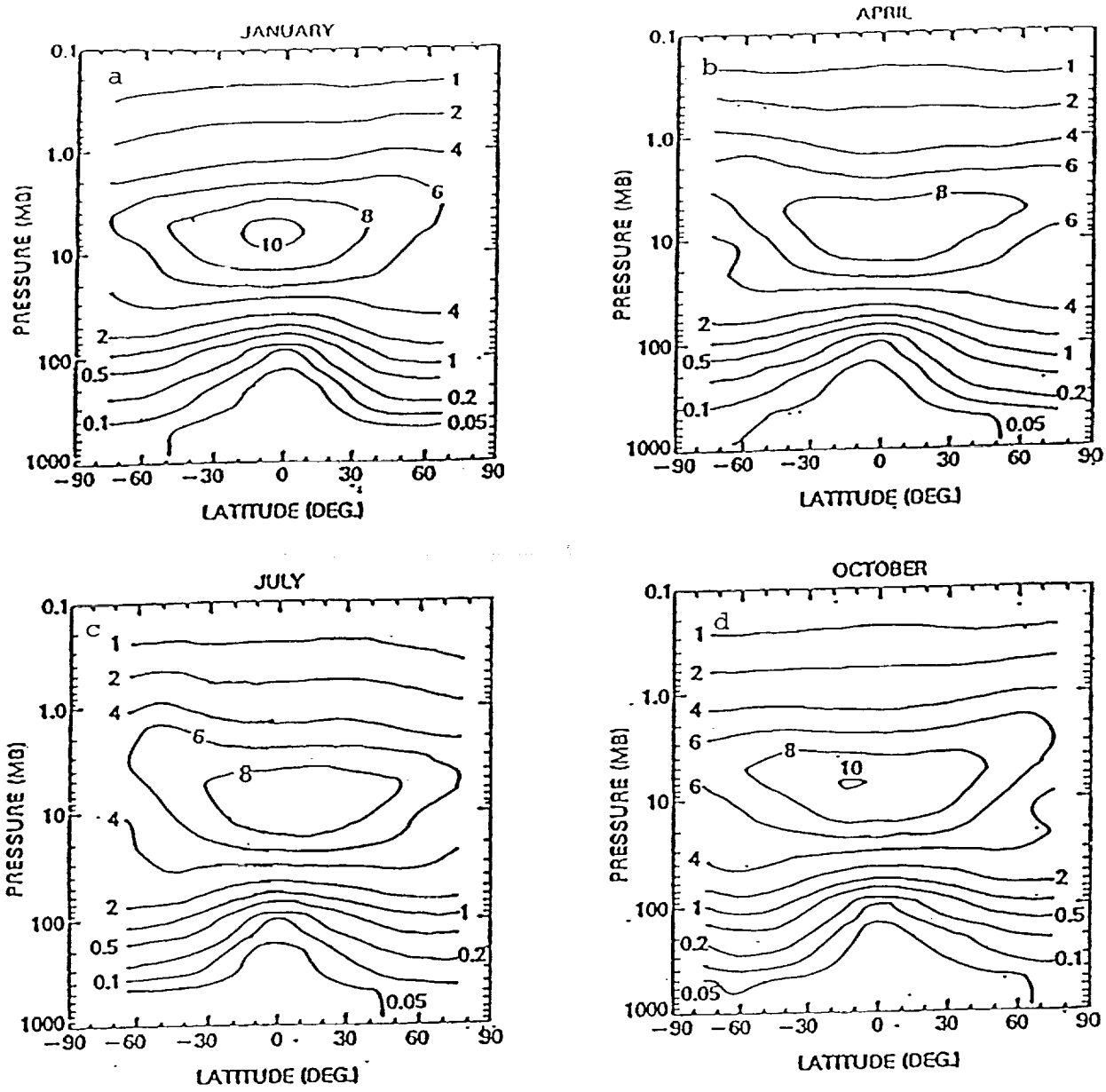

Figure A3. Observed cross-sections of ozone mixing ratio (ppmv) from the Nimbus 7 satellite as a function of latitude and height. Shown are monthly averages for (a) January, (b) April, (c) July, and (d) October 1979, averaged by 10 degree latitude bands, from McPeters, et. al. 1984. Contours are 0.05, 0.1, 0.2, 0.5, 1, 2, 4, 6, 8, 10 ppmv.

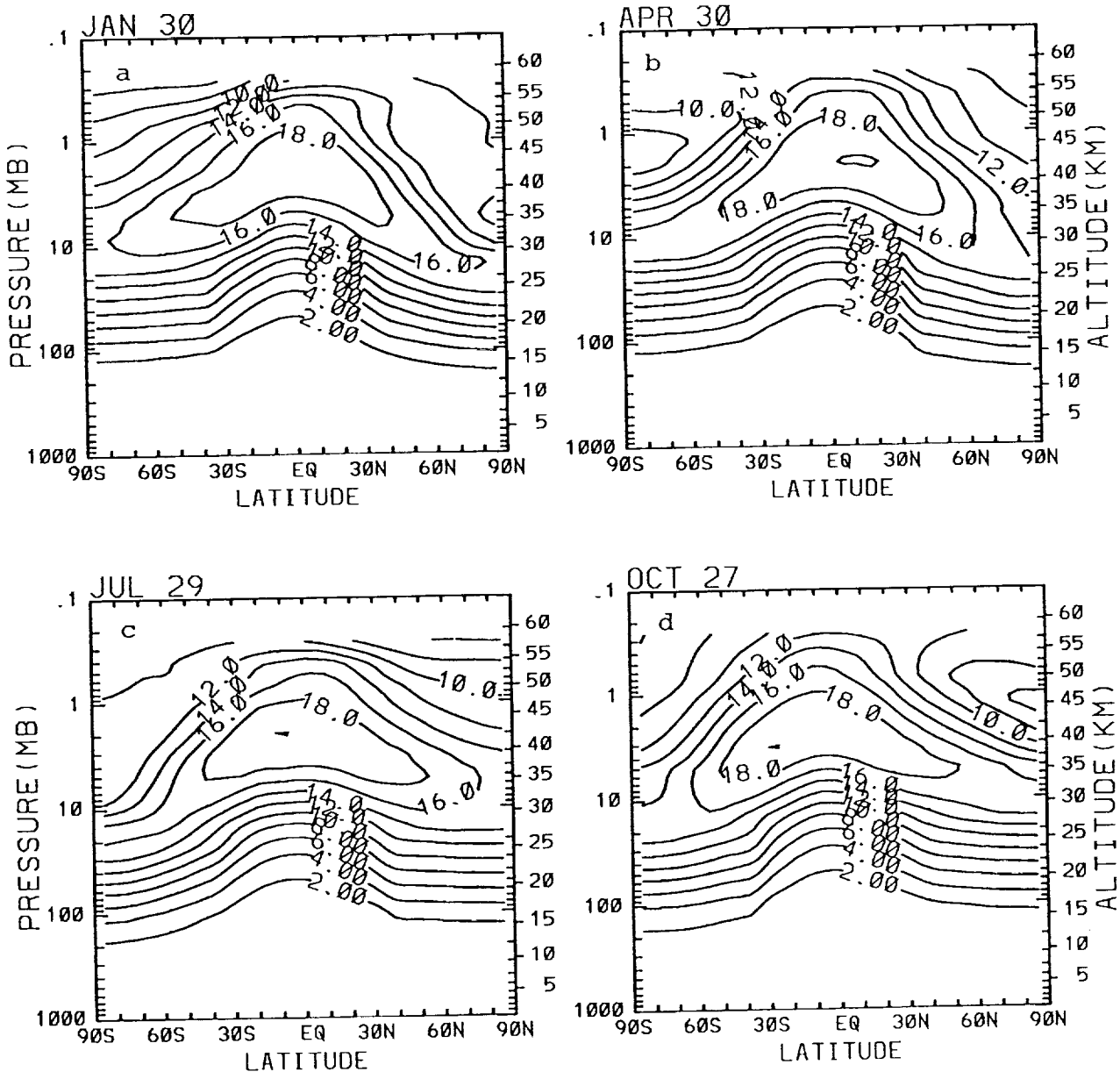

Figure A4. Model-calculated cross-sections of total odd nitrogen (NOY) in ppbv for present-day conditions as a function of latitude and height for (a) January, (b) April, (c) July, and (d) October. Contours are in 2 ppbv increments.

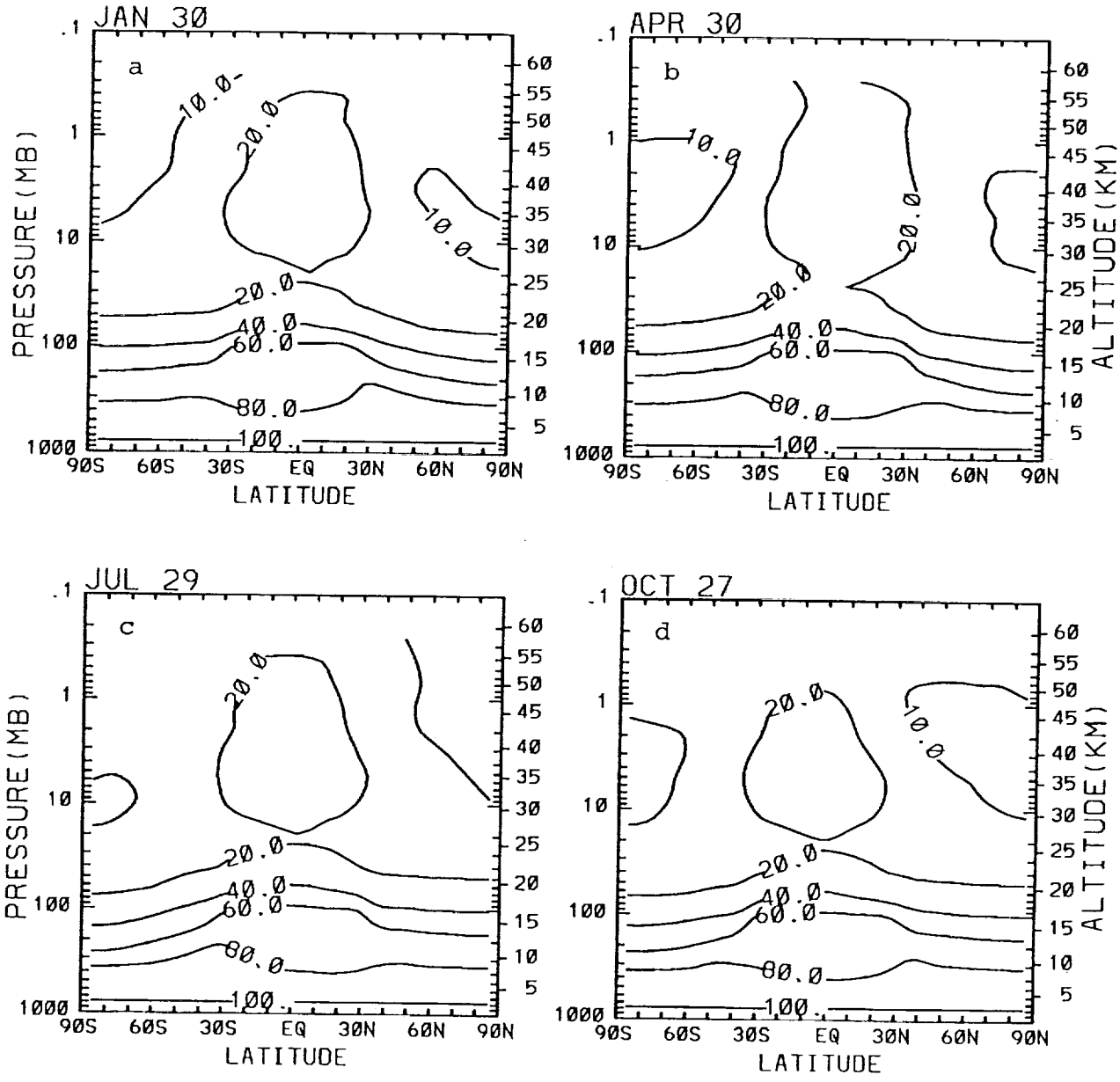

Figure A5. Model-calculated cross-sections of carbon monoxide (CO) in ppbv as a function of latitude and height for (a) January, (b) April, (c) July, and (d) October for present-day conditions. Contours are 10, 20, 40, 60, 80, 100 ppbv.

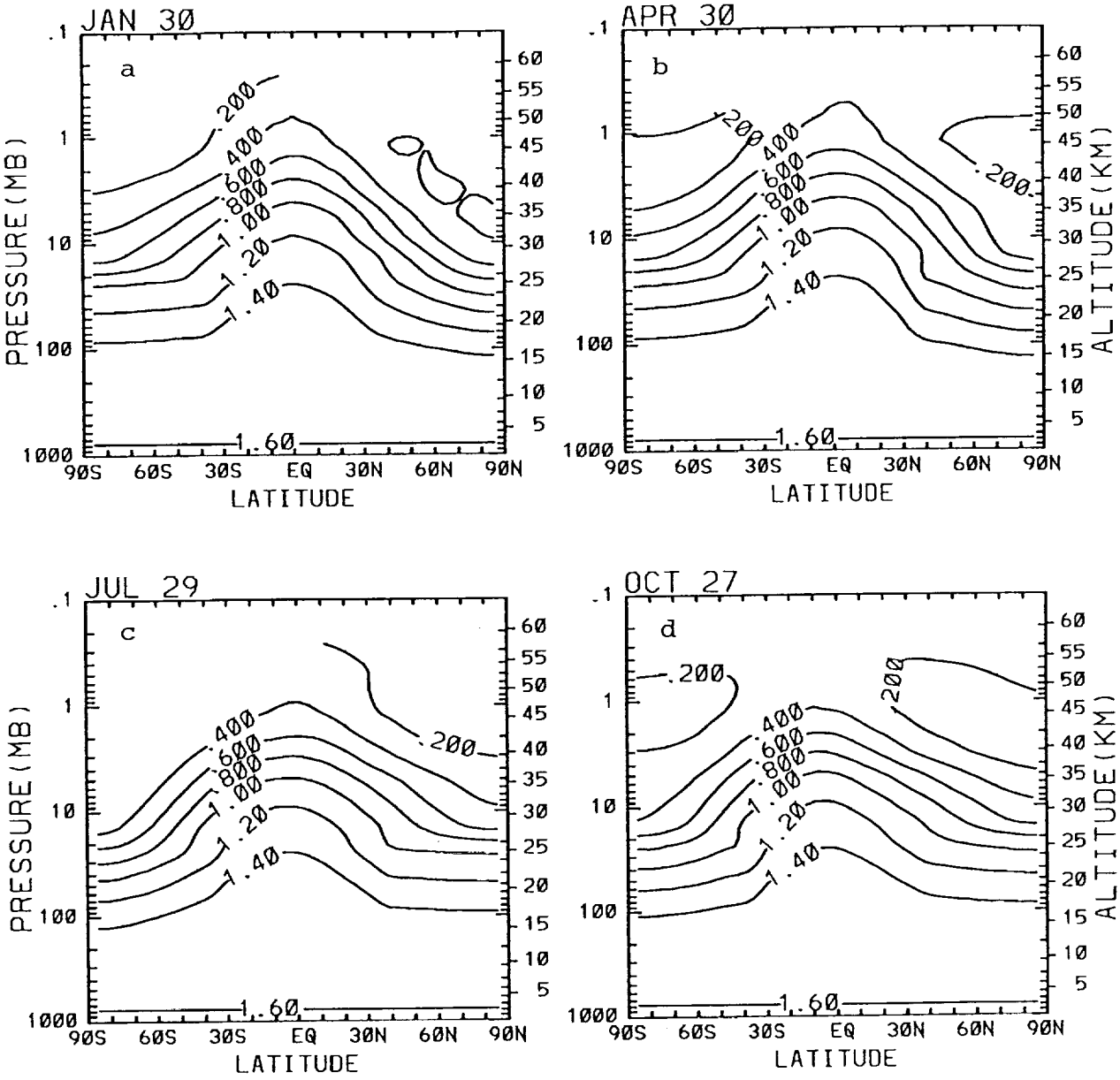

Figure A6. Model-calculated cross-sections of methane (CH_4) in ppmv as a function of latitude and height for (a) January, (b) April, (c) July, and (d) October for present-day conditions. Contours are 0.2, 0.4, 0.6, 0.8, 1.0, 1.2, 1.4, 1.6 ppmv.

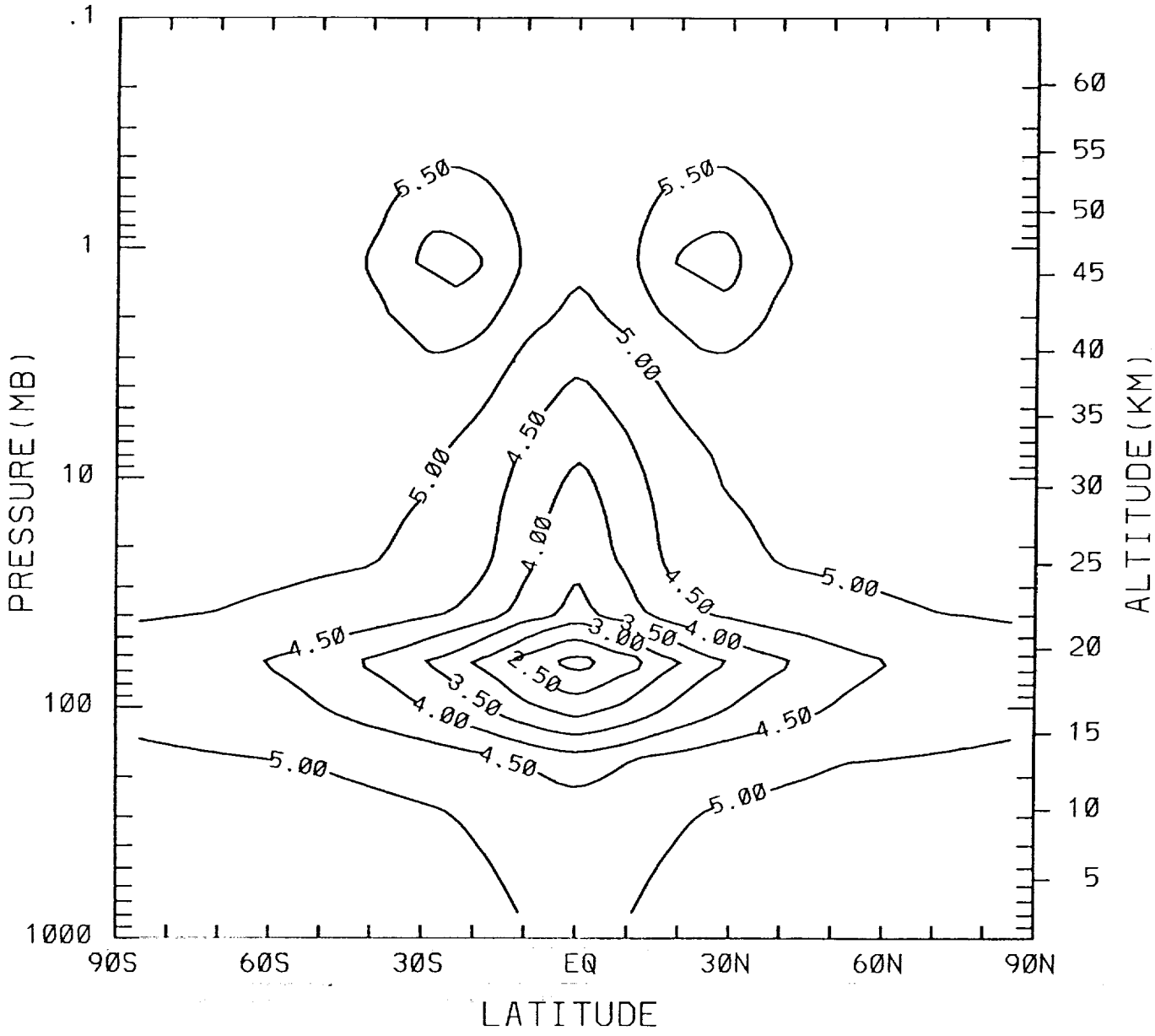

Figure A7. Water vapor concentration (H_2O) in ppmv as a function of latitude and height, derived from Remsberg, et. al. (1984), used for stratospheric H_2O concentration in the AER 2D model. Tropospheric water vapor is derived from relative humidity profiles. Contours are from 2.0 ppmv to 5.5 ppmv in increments of 0.5 ppmv.

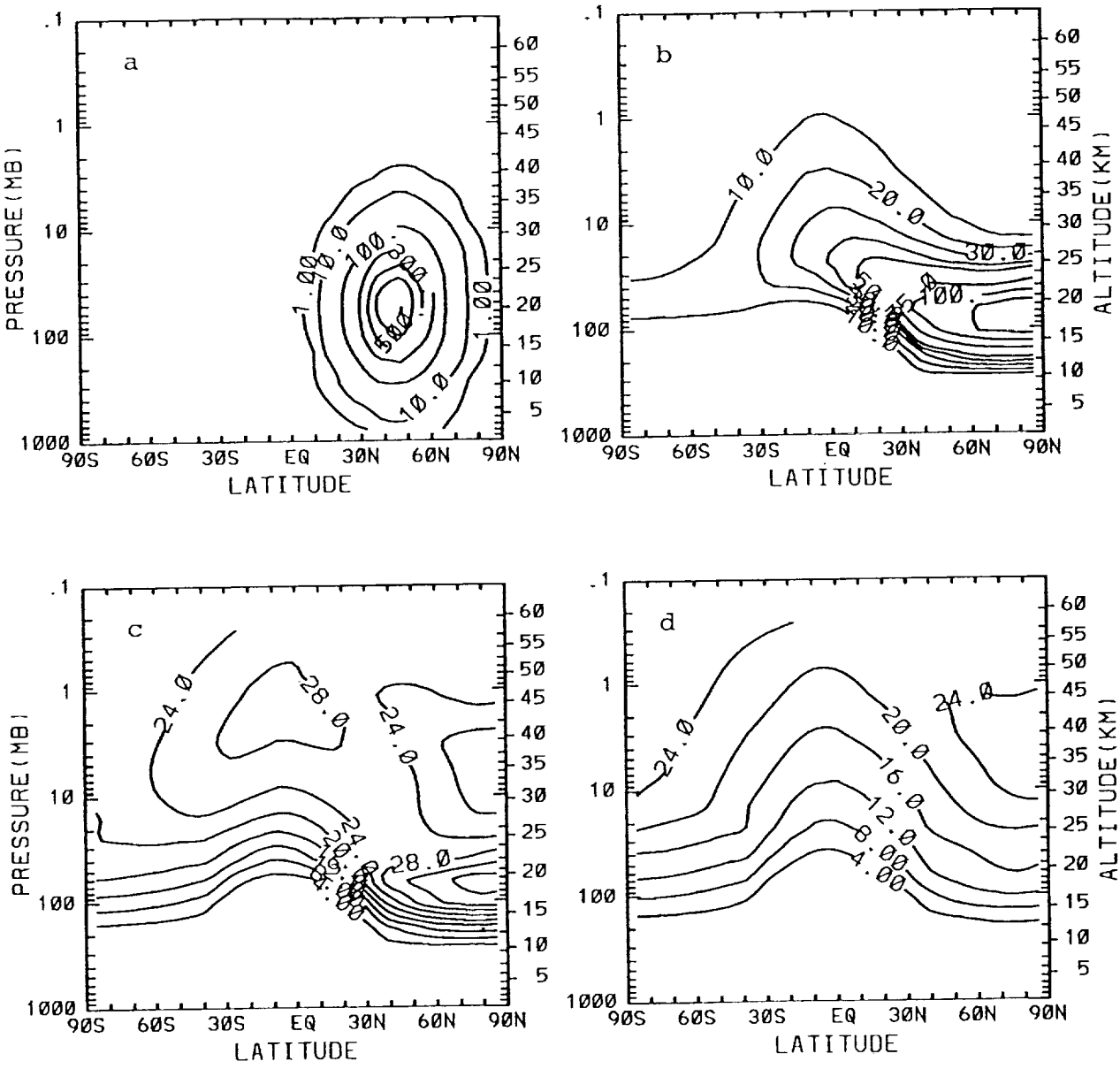

Figure A8. Results of a model experiment showing the dispersion of an inert tracer with initial distribution on January 1 shown in panel (a). Latitude-altitude cross-sections of the tracer are shown for January 1 after (b) 1 year of simulation, (c) 2 years of simulation, and (d) 3 years of simulation. Contours for (a) are 1.0, 10, 100, 300, 500, 700, 900 ppbv; contours for (b) are 10, 20, 30, 40, 50, 75, 100, 125 ppbv. Contour intervals for (c) and (d) are 4 ppbv.

NASA National Aeronautics and Space Administration

Report Documentation Page

1. Report No.	2. Government Accession No.	3. Recipient's Catalog No.
NASA CR-4346, Part I		

4. Title and Subtitle	5. Report Date
Effects of Engine Emissions From High-Speed Civil Transport Aircraft: A Two-Dimensional Modeling Study, Part I	March 1991
	6. Performing Organization Code

7. Author(s)	8. Performing Organization Report No.
Malcolm K. W. Ko, Debra K. Weisenstein, Nien Dak Sze, Jose M. Rodriguez, and Curtis Heisey	
	10. Work Unit No. 505-69-61-04

9. Performing Organization Name and Address	11. Contract or Grant No.
ST Systems Corporation Hampton, Virginia 23666	NAS1-18460
	13. Type of Report and Period Covered
12. Sponsoring Agency Name and Address	Contractor Report July 1988 - June 1989
NASA Langley Research Center Hampton, Virginia 23665-5225	14. Sponsoring Agency Code

15. Supplementary Notes

Malcolm K. W. Ko, Debra K. Weisenstein, Nien Dak Sze, Jose M. Rodriguez, Curtis Heisey: Atmospheric and Environmental Research, Inc., Cambridge, Massachusetts.
Langley Technical Monitor: Linwood Callis
Prepared by Atmospheric & Environmental Research, Inc., Cambridge, Massachusetts, under subcontract 88-6209-D1417 to ST Systems Corporation.

16. Abstract

The AER two-dimensional chemistry-transport model is used to study the effect on stratospheric ozone (O_3) from operations of supersonic and subsonic aircraft. The study is based on six emission scenarios provided to AER. Our study showed that:

- the O_3 response is dominated by the portion of the emitted nitrogen compounds that is entrained in the stratosphere. The entertainment is a sensitive function of the altitude at which the material is injected.
- the O_3 removal efficiency of the emitted material depends on the concentrations of trace gases in the background atmosphere. Evaluation of the impact of fleet operations in the future atmosphere must take into account the expected changes in trace gas concentrations from other activities.

Areas for model improvements for future studies are also discussed.

17. Key Words (Suggested by Author(s))	18. Distribution Statement
Ozone Civil Transport High Speed	Unclassified - Unlimited Subject Category 45

19. Security Classif. (of this report)	20. Security Classif. (of this page)	21. No. of pages	22. Price
Unclassified	Unclassified	100	A05

NASA FORM 1626 OCT 86

For sale by the National Technical Information Service, Springfield, Virginia 22161-2171

NASA-Langley, 1991